UNIVERSITÀ DEGLI STUDI DI PARMA
DIPARTIMENTO DI INGEGNERIA DELL'INFORMAZIONE

Dottorato di Ricerca in Tecnologie dell'Informazione
XXVII Ciclo

Niccolò Mora

BRAIN COMPUTER INTERFACES: AN ENGINEERING VIEW. DESIGN, IMPLEMENTATION AND TEST OF A SSVEP-BASED BCI

DISSERTAZIONE PRESENTATA PER IL CONSEGUIMENTO
DEL TITOLO DI DOTTORE DI RICERCA

GENNAIO 2015

UNIVERSITÀ DEGLI STUDI DI PARMA

Dottorato di Ricerca in Tecnologie dell'Informazione

XXVII Ciclo

BRAIN COMPUTER INTERFACES: AN ENGINEERING VIEW. DESIGN, IMPLEMENTATION AND TEST OF A SSVEP-BASED BCI

Coordinatore:

Chiar.mo Prof. Marco Locatelli

Tutor:

Chiar.ma Prof.ssa Ilaria De Munari

Dottorando: *Niccolò Mora*

Gennaio 2015

(da compilare a proprio gradimento)

A _____

- ☐ *Con affetto*
- ☐ *Con simpatia*
- ☐ *Con moderata molestia*
- ☐ *Con interismo*
- ☐ *Con tutto*

L'unico vero viaggio verso la scoperta
non consiste nella ricerca di nuovi paesaggi,
ma nell'avere nuovi occhi.
– Marcel Proust

Table of Contents

List of Figures

List of Tables

List of Abbreviations

AAL	Ambient Assisted Living
AC	Alternating Current
ADC	Analog to Digital Converter
AFE	Analog Front End
ALS	Amyotrophic Lateral Sclerosis
AMCC	Average Maximum Contrast Combination
AT	Assistive Technologies
BCI	Brain Computer Interface
BMI	Brain Machine Interface
BOLD	Blood Oxygen Level Dependent Response
BSS	Blind Source Separation
CCA	Canonical Correlation Analysis
CMRR	Common Mode Rejection Ratio
CSP	Common Spatial Patterns
DC	Direct Current
DUT	Device Under Test
ECG	ElectroCardioGraphy
ECoG	ElectroCorticoGram
EEG	ElectroEncephaloGraphy
EM	Expectation-Maximization (algorithm)
EMG	ElectroMyoGraphy
EOG	ElectroOculoGraphy

ERD	Event Related Desynchronization
ERP	Event-Related Potential
ErrPs	Error Related Potentials
ERS	Event Related Synchronization
fCCA	Frequency domain CCA
FES	Functional Electrical Stimulation
FFT	Fast Fourier Transform
fMRI	Functional Magnetic Resonance Imaging
GUI	Graphical User Interface
hBCI	Hybrid BCI
IC	Intentional Control (period)
ICA	Independent Component Analysis
ICT	Information and Communication Technologies
INA	INstrumentation Amplifier
LCD	Liquid Crystal Display
LED	Light Emitting Diode
MAP	Maximum A Posteriori
maxDeltaVar	Maximal Delta in Variance
MEC	Minimum Energy Combination
MEG	MagnetoEncephaloGraphy
MI	Motor Imagery (paradigm)
NIC	Non Intentional Control (periods)
NIRS	Near InfraRed Spectrography
PCA	Principal Component Analysis
PDF	Probability Density Function
PET	Positron Emission Tomography

pp	Peak-to-Peak
PSD	Power Spectral Density
QAD	Quadrature Amplitude Demodulation
RFI	Radio-Frequency Interference
RLD	Right Leg Driver
rms	Root Mean Square
RT	Real Time
RTI	Referred To Input
SCP	Slow Cortical Potentials
SGD	Stochastic Gradient Descent
SNR	Signal to Noise Ratio
SOM	Self-Organizing Map
SPI	Serial Peripheral Interface
SQUID	Superconductive QUantum Interference Devices
SSVEP	Steady State Visual Evoked Potential
tCCA	Time domain CCA
UI	User Interface

Introduction

Let me state from the beginning that this thesis is not a neuroscience thesis. Nor it is, in a strict-sense, an electronic design thesis. It is not even a signal-processing thesis. And, probably, it is not many other different things. This work is rather an attempt to synthesize, with engineering principles, all these different, but somehow related aspects, into a unique, convergent framework based on *Brain Computer Interface* (BCI) technology [1],[2]. As a matter of fact, BCI is a highly-multidisciplinary field, a human brain acting as an integral part of it being a tangible clue of such an argument.

A BCI (Figure 0.1) is an alternative, augmentative communication/control system that a person can use to directly communicate his/her intent to the external environment just by interpreting the brain activity, or, at least, specific patterns in it. In this sense, BCIs can also be regarded as *Assistive Technologies* (AT), i.e. tools conceived to assist and promote the person's autonomy; ATs are, in fact, focused on providing personal solutions, as much comfortable as possible, to overcome limitations in the possibility of interacting with the external environment and with other people.

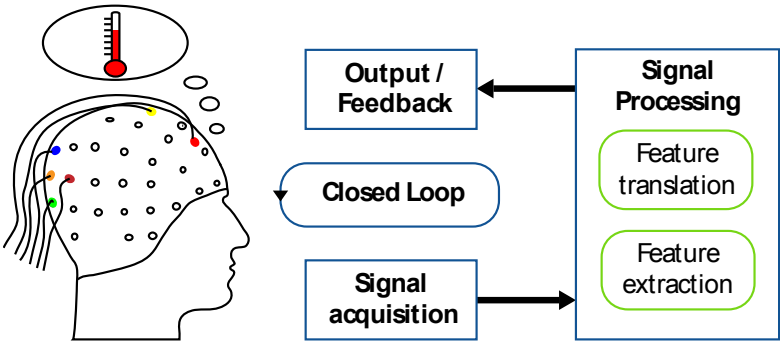

Figure 0.1 A BCI is an alternative/augmentative communication mean based on direct interpretation of the user's brain activity: user and computer can interact and form a closed loop, in which the user is both the source and the target of the processing.

The notion of "*assistive device*" is, indeed, a very old one: what today seems a simple, everyday object such as a pair of spectacles, in the past was considered as a special aid for people affected by visual impairments. Such "aids" were then realized to improve their quality of life, autonomy and independence. With time, then, more and more sophisticated assistive devices have been developed, and the quest for improving the quality and usability of services has also defined, in recent times, a methodology called *Design for all* (or *Universal Design*) [3]. Although initially referred to architectural contexts, to promote universal accessibility to public spaces, the theme of universal design is now being transposed to modern *Information and Communication Technologies* (ICT), such as, for example, in the design of accessible *User Interfaces* (UI). In this context, BCI could represent the technological bridge, for certain classes of users, to access e-services.

Nonetheless, the range of applications of BCI well extends beyond UI tasks (e.g. for spelling [4]). For instance, BCI-enabled orthoses were developed [5]-[7]; BCI was also successfully exploited, in conjunction with *Functional Electrical Stimulation* (FES), in studies on motor recovery after stroke [8]-[10]; finally, BCI technology was used to enable the control of electrical wheelchairs [11] and mobile robots [12],[13]. A complete list of all possible applications of BCI, though, would be too long to fit into the scope of an introductory chapter, and such a list, by the way, is growing as we write and read. For this reason we limit ourselves to just a few key points, to give an idea of the practical implications, even though the BCI approach is general. Furthermore, in order to demonstrate the proposed BCI device, we will use and focus on a real-world problem, namely the control of a home automation system or, to better state the context, an *Ambient Assisted Living* (AAL) system.

AAL systems are very heterogeneous both in terms of implementation and functionalities; in general, the goal of AAL systems is to make the home environment more intelligent and cooperative in accomplishing daily living activities. The key concept is to provide the technical and technological means to support, for as long as possible, people's independence and self-

reliance in the home environment they are accustomed to. With increasing and rapidly growing research activity in AAL, many innovative solutions have been developed, built on top of "traditional" home automation tasks (i.e. ambient light control, door and window automation, security, etc.). It is now possible, thanks to more and more "smart objects" in our homes, to provide "higher level" functionalities and feedbacks, as it is the case of *behavioural analysis* [14] (i.e. extracting a sort of "user digital footprint" through the ambient, analyzing his trends and behaviour, and highlighting relevant variations in such routines). Many other examples are possible, but the main point here is to underline the increasing importance that the AAL theme is acquiring, being an active research field, supported by the European Union within the *AAL Joint Programme* and *Horizon 2020* frameworks.

In our view, BCI technology can easily fit into such contexts, providing new and alternative ways of interfacing with a smart ambient, opening services and the entire ecosystem to a wider general public, including persons for whom interacting with the external environment may be troublesome, and sometimes even not possible (due to, for example, neurodegenerative diseases or severe motor impairments). Nonetheless, the module should be integrated into the already established system without impacting on its architecture. In other words, the BCI should act as a self-contained module, and interact with the system as a traditional and conventional user interface would do (be it a remote controller or a GUI on a smartphone). A pictorial representation of the application we want to target is shown in Figure 0.2, where the LAN-based AAL system, CARDEA [15],[16], is represented. CARDEA will be our gateway to home automation control, as it exposes a generic API for remote controllers to interact with.

Having AAL as "application target" in mind, however, calls for quite peculiar specifications with respect to most BCI designs.

In the first place, BCI technology must be considered no longer as a powerful lab research tool, but as a daily living device. In recent years, an increasing amount of work and efforts were put into turning BCI to "*outside the lab*" realities [17]-[19]. In fact, lab operating conditions are usually more

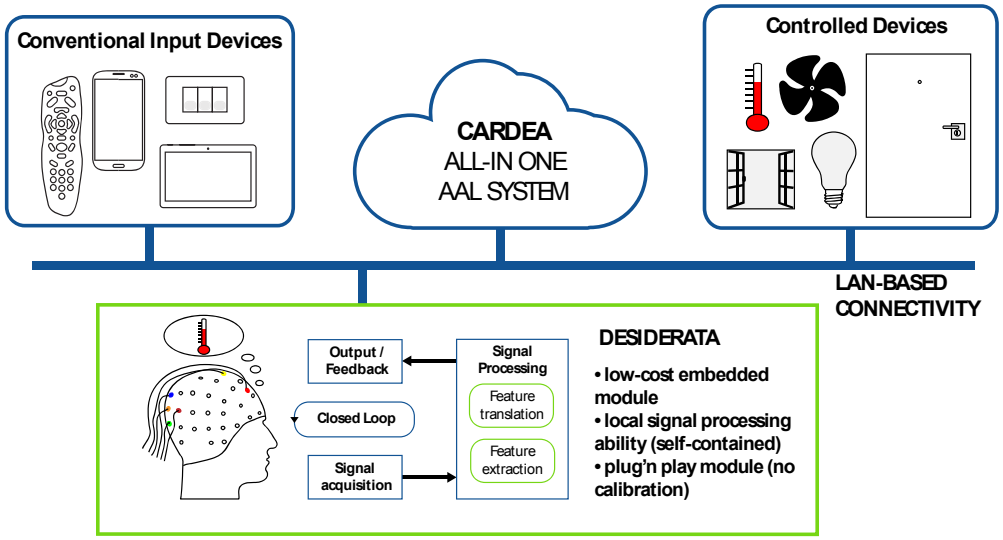

Figure 0.2 Application example for demonstrating the effectiveness of the proposed BCI platform. We will use BCI technology to control an Ambient Assisted Living system (CARDEA): for the system, the platform will be perceived just as a simple, conventional input interface.

controlled and predictable than those of the target environment, and this may lead to significant performance degradation when BCI are deployed in real scenarios. Just to give a few examples, background ambient luminosity could pose potential problems if the application makes use of visual stimuli, just as motion artifacts could hinder or compromise the BCI performance in mobility scenarios. Moreover, one should consider that the entire device setup and preparation should be performed by non-BCI experts, thus errors and non-optimal initial conditions could potentially arise. As a consequence, BCI hardware and software development for "out of the lab" scenarios should be carried out having practicality and robustness as primary goals.

Another general consideration for promoting BCI as daily living devices is related to its cost. In the commercial and consumer electronics realm a great deal of engineering work is absorbed by optimizing production costs, in order to offer competitive and lower prices (or the same prices with increased functionalities). Trying to lower the high costs of commercial-grade BCI setups (especially for the hardware equipment) does not merely means saving money, but rather broadening the spectrum of possible

applications for BCI-enabled devices, generating new concepts and ideas. The growth of mobile, low-cost platforms and the related applications and innovations are just examples supporting this argument. Close to this concept of costs optimization is the adoption of scalable, compact technological solutions; future BCI *embedded* implementations could potentially allow to discover new methods and applications, just as wearable devices are re-inventing the way we intend sensors.

Then, in order to further define the specifications, let us dive, in more depth, into the final target, i.e. AAL systems, which will allow us to demonstrate the effectiveness of our approach [20]-[24]. First of all, let us try to figure out the requirements for the interface; a typical home/environmental control case would require to control several appliances (e.g. lights, windows, shutters etc.), possibly organized in a menu that we would like to navigate through. However, we should also take into account the dynamics of such an interaction: this application, in particular, does not require a very high data throughput capability (low communication bandwidth), since the typical interaction paradigm consists only in issuing a few high-level commands. Moreover, user interactions are quite sparse in time. This last characteristic also unravels two other key aspects worth keeping in mind for practical BCI-enabled AAL control: *(i) false positives minimization*, and *(ii) a "Plug&Play" approach*.

The former key point, in particular, states that, given the reduced interaction periods (in the following we will call them *Intentional Control* periods, or IC, as opposed to *Non-IC* periods or NIC), it would be impractical to have a control device continuously triggering non intended commands; this could also raise security issues. Meanwhile, the ideal device should also exhibit a high sensitivity, making the control task easier and more prompt, from the user's point of view. However, usually these two "desiderata" (i.e. false positives minimization and high sensitivity) are not independent and cannot be addressed individually; thus a trade-off must be made, tailored to the specific application at hand.

The latter concept, the *Plug&Play* approach, is more related to the user experience side. With the interaction dynamics described as above, the user

could perceive undergoing an initial training period or periodic calibration phases as an excessive burden, given the final control purpose. It then becomes important to devise methods which do not rely on any calibration at all. Moreover, a closely related issue of such an approach is its generalizability to other users (*subject-independence*). In accordance with the calibration-free principle, we should develop methods which are highly interoperable between users; in addition, minor performance tuning should be controllable just by a few high-level parameters, directly accessible and editable by the user.

Another aspect which directly impacts on the user's experience and the device acceptability is the way the BCI allows interactions. Assuming the need to work *online* (i.e. continually and in Real-Time, RT), there basically exist two possibilities: *(i) cue-based* [25], i.e. when the BCI prompts the user each and every time it is ready to receive and interpret commands, and *(ii) self-paced* [26]-[29], where the BCI continuously scans the user's brain features and autonomously detect when the user is actually trying to control it (*IC* vs *NIC* periods); if this is the case, the BCI decodes which command he/she is issuing. It goes without saying that the latter method is more difficult and makes it harder to find a good trade-off between sensitivity and false positives minimization. On the other hand, though, the user-machine interaction would be perceived as more natural and acceptable. Thus, in order to develop "real-world" solutions, the self-paced operating principle must be assumed.

At the end of this brief discussion, a few points stand out and help us define the specifications for the system we intend to demonstrate:

- minimal, compact, easy experimental setup;
- at the same time the system should be flexible enough to allow studies of other bio-potentials (e.g. ElectroMyoGraphy, EMG, to be integrated as an additional channel in hybrid BCI, hBCI [30]-[32]);
- contained costs (e.g. < 1000 €);
- robust design, operation outside controlled lab environments;

- online, self-paced operation;
- calibration-free approach;
- subject-independence.

However, even though commercial, complete BCI solutions already exist, to the best of our knowledge no one could optimally meet the aforementioned criteria. In particular, with respect to the available hardware, either it exceeded the target price range, or no well-established, reliable or open solutions (i.e. with access to raw signals or even with the possibility to acquire other bio-potentials than EEG) exist.

Thus, our development flow started from the ground, electrical level with the realization of a suitable bio-potential acquisition platform. Then, we built our entire platform on top of it, addressing all the related aspects of storing the data, processing it in real-time, and delivering meaningful output. Such pervasive customization allowed us to fine-tune each step of this design, allowing us to craft each time the optimal solution for the specific needs, from the hardware level up to the software/processing one. (the term "optimal" is here used with reference to the whole aimed application; nonetheless, most of the used principles are, indeed, general).

The outline of this thesis work develops horizontally, encompassing all the sustained BCI design phases, from hardware and firmware, up to software and application. In *Chapter 1*, the state of the art and the general aspects of BCI technology will be covered, with a broad-band approach. Firstly, the principal brain activity monitoring and measurement techniques will be discussed. Then, focusing on ElectroEncephaloGraphy (EEG), the most commonly exploited brain signals will be presented. A brief survey of general BCI-related signal processing will follow, in order to complete the basic BCI building blocks. Finally, the architecture of the whole platform will be outlined. In *Chapter 2*, the realization of two custom EEG acquisition modules will be discussed, ranging from the electronic design specifications up to the implementation and production details. Both modules will be validated, and the newest one will also be compared against a commercial, high-end EEG device for BCI (*g.tec USBamp*), yielding very

good results. Also, the cap and materials choice will be briefly discussed. *Chapter 3* will present the offline signal processing research carried out for Steady State Visual Evoked Potentials (SSVEP) classification, reviewing state-of-the art methods, as well as introducing two novel algorithms. All these methods will be then compared; as it will be shown, the presented methods well behave in this offline classification context, improving over computational complexity, thus lending themselves better for future embedded implementations. *Chapter 4* will, instead, discuss how to adapt such methods to work more reliably in online, self-paced BCI sessions. A novel method for improving accuracy and minimizing False Positives will be presented, introducing a "prediction confidence indicator", which will also allow to discriminate between user's active, intentional control periods and inactive, non-intentional ones. A technique for dynamically choosing the EEG window length during the epoch-based signal processing will also be covered. In addition, the results achieved in lab experiments and in live demo sessions in the ("non-controlled", "harsh") context of the *Handimatica 2014* exhibition will be presented, highlighting the good performance in sensitivity and the improvement over the state of the art in terms of False Positive Rate. Finally, the *Conclusions and future developments chapter*, will review the main achieved results and explore the open questions and possibilities for the present work.

Chapter 1

BCI from multiple angles

This Chapter focuses on introducing the BCI context in more depth. In particular, all the principal, relevant concepts for the development of our system will be covered, namely: the techniques for measuring and monitoring the brain activity, the typical brain signals used in the BCI realm, and the signal processing techniques used for extracting information from such signals. This chapter is thought to provide a high-level, introductory view of such topics (far from being exhaustive); the interest reader can gain deeper information, for example, by looking at the references provided. Nonetheless, all these topics will allow us to place the whole presented work into a nicer context.

1.1 Various brain monitoring techniques in BCI

Brain Computer Interfaces directly interpret the brain's activity to extract meaningful information. However, many different brain parameters can be monitored, carrying different information. In the following, we address the principal techniques employed to gather data and information about the brain status. At the end, we will motivate our choice of relying on an EEG based approach.

1.1.1 ElectroEncephalography (EEG)

ElectroEncephaloGraphy (EEG) is the most widely used brain monitoring technique in non-invasive BCI. EEG measures neuronal electrical activity in terms of scalp potentials. It is worth remarking, though, that the electric potential generated by an individual neuron is far too small to be picked up by EEG; the recorded scalp potentials, therefore, always reflect the summation of the synchronous activity of thousands or millions of neurons that have similar spatial orientation. In fact, pyramidal neurons of the cortex are thought to produce most of EEG signal because they are well-aligned and fire together. However, with EEG it is not possible to acquire precise 3D information on neuronal activation, as opposed to other methods (e.g. fMRI), nor the spatial resolution is the best among all.
Nonetheless, the temporal resolution is very fine (~ ms), and EEG read-out circuitry is relatively inexpensive, when compared to other brain activity monitoring methods.
The typical EEG signals used in BCI lie in the [0-50] Hz band and have amplitudes in the range of a few μV; this poses quite tight constraints on the acquisition hardware, as it will be discussed in §2.1. In fact, SNR is not one of the key strengths of electroencephalography.
Still, as it will also be stressed later, EEG is currently recognized as the most versatile tool in BCI research, given its overall best tradeoff between spatio-temporal resolution, costs and setup complexity.
EEG electrodes are, usually, positioned over the scalp according to the International 10/20 system, or more dense variations of it (see Figure 1.1); the electrodes positions and names are standardized to facilitate comparisons and reproducibility of setups.
Commonly used materials for physical electrode realization are tin (Sn), gold (Au), silver (Ag) and silver/silver chloride (Ag/AgCl, also sintered). A thorough description of the physical properties of such different materials goes beyond the scope of this introduction; the interested reader could refer, for example, to [33]. Overall, sintered Ag/AgCl electrodes offer superior

performance in terms of reduced low-frequency noise and more contained offsets.

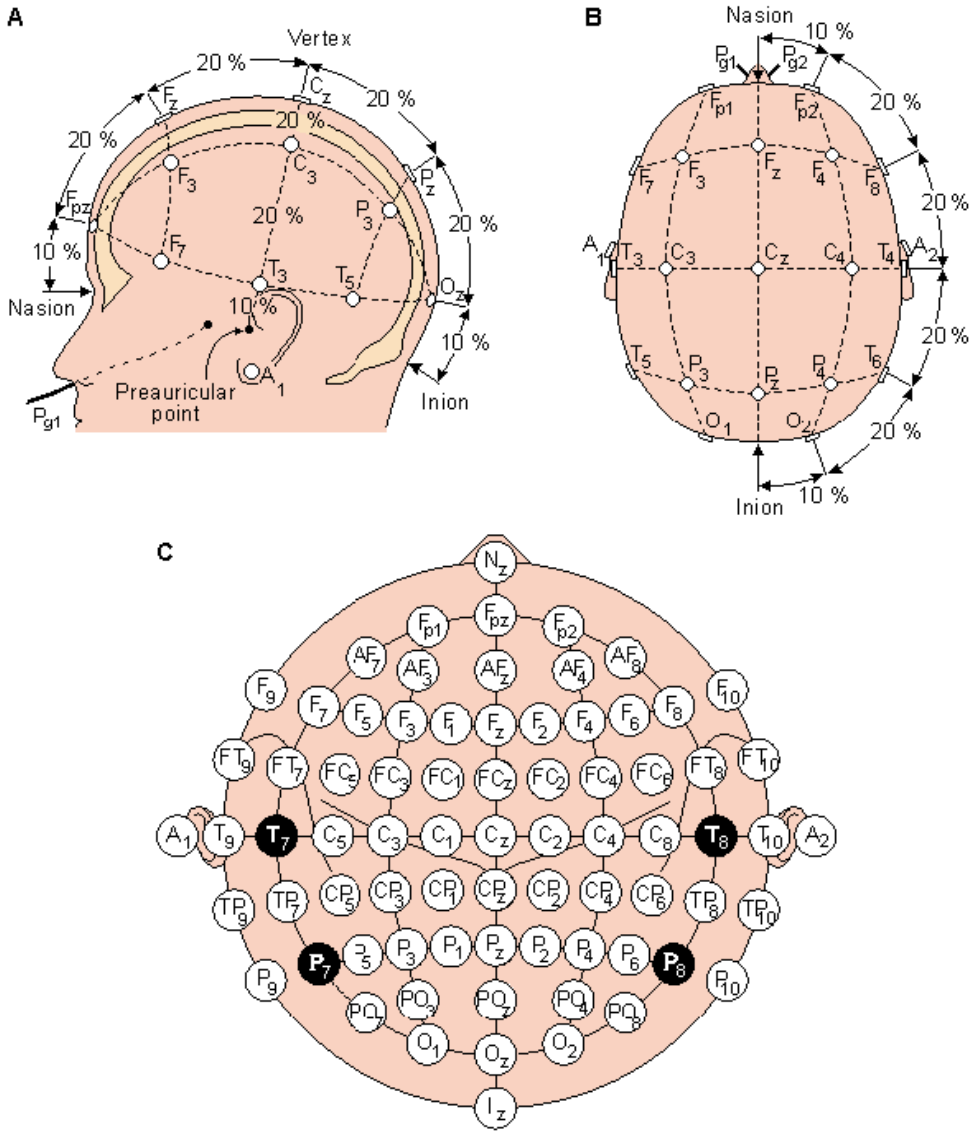

Figure 1.1 Electrode positioning and naming according to the International 10/20 system: (*A*) lateral view, (*B*) top view. More *dense* mountings are also possible, as shown in (*C*). Reference and ground electrodes are usually placed on earlobes or mastoids, sometimes even in frontal or central locations.

Electrodes can then be further divided into passive and active, the latter featuring a pre-amplification stage on top of the electrode (in order to reduce the artifacts and noise pickup along the cables).
Finally, electrodes can be used in conjunction with electroconductive gel, to reduce the signal source impedance, or in a dry-setup fashion (in this case exhibiting a higher impedance, thus being more susceptible to noise pickup, unless active electrodes are used).

1.1.2 MagnetoEncephaloGraphy (MEG)

Active bioelectric sources in the brain produce both electric and magnetic fields: *MagnetoEncephaloGraphy* (MEG) measures this latter quantity. However, typical neuro-magnetic fields in the brain are estimated to be in the order of 50-500 fT, about 10^8-10^9 times weaker than the earth's magnetic field. In order to measure such extremely small quantities, advanced technologies, based on Superconductive QUantum Interference Devices (SQUID), are used, which require sensor cooling by means of liquid helium circuits. Moreover, a large number of sensing elements is required, typically between 100 and 300, and measurements are usually taken in magnetically shielded environments.
These setups are, thus, incredibly sophisticated and bulky (and with high costs as well), limiting the application of MEG only to laboratory and clinical settings. However, the main advantages offered by MEG, with respect to, for example, EEG, are: *(i)* a much better spatial resolution, with 3D information, allowing to localize more precisely cortical activations related to task or sensory stimulations, and *(ii)* better Signal to Noise Ratio (SNR), especially at higher frequencies of interest like the gamma band (> 32 Hz) [34].
MEG is used for various BCI and rehabilitation tasks, including, for example, motor imagery [35],[36].

1.1.3 functional Magnetic Resonance Imaging (fMRI)

Lately, *functional Magnetic Resonance Imaging* (fMRI) has been used in BCI [37]-[38]; in this case, the input signal is the Blood Oxygen Level Dependent Response (BOLD), i.e. changes in the local concentration of deoxygenated hemoglobin in brain tissues, as a result of neuronal activity and metabolism.
Compared to EEG, fMRI yields a better space resolution (in the range of millimeters), and the analysis can also extend to deeper, subcortical areas, allowing 3D localization of neuronal activity . Advancements in technology and signal processing also allowed to reduce the delay of feedback down to below 2 s [39], thus enabling fMRI methods to be used in near real-time scenarios.
Once again, though, such technologies are bulky and expensive, thus better suited for laboratories and clinics, while their use in daily life is still impractical.

1.1.4 Near InfraRed Spectroscopy (NIRS)

Similarly to fMRI, *Near InfraRed Spectroscopy* (NIRS) can offer 3D brain imaging, even though at a shallower depth (typically, 1 to 3 cm). However, the whole signal acquisition system is much more compact (to the extent that it is even portable) and cheap, thus being more suitable to "outside the lab" contexts. NIRS, in fact, just uses pairs of light sources (lasers or LEDs, operating on two or more discrete wavelengths) and detectors. The measured physiological quantity is the ratio between oxygenated and deoxygenated hemoglobin, which cause different light absorption levels; such ratio varies between different brain areas, depending on their level of activation. Since NIRS is based on hemodynamic responses, though, changes in the brain activity are typically detected with delays of a few seconds [40].

The possibility of easily, simultaneously recording EEG and NIRS, makes it an attractive choice for *hybrid* BCI (hBCI): in [41] a NIRS-based "brain switch" is described, to switch on and off the EEG part of the hBCI. Authors report fewer false positives using this hybrid approach rather than one purely based on specific EEG features. NIRS BCI are quite often exploited also in mental state recognition [42] and motor imagery tasks [43].

1.1.5 ElectroCorticoGraphy (ECoG)

This method, reported for completeness, differs from the previous ones in that it is invasive. In fact, for *ElectroCorticoGraphy* (ECoG), the electrodes are placed directly over the cortical surface. Spatial resolution is very good (tenths of millimeters), and signal have broader bandwidth ([0-500] Hz), as well as larger amplitudes (50-100 μV), thus exhibiting higher SNR, with respect to EEG.
ECoG, traditionally used in clinical applications such as localizing the source of epileptic seizures, also finds multiple applications in BCI, from studies of the sensorimotor cortex [44] to direct speech recognition [45]-[47].

1.1.6 A final word about our choice for EEG-based BCI

We briefly reviewed several brain activity monitoring techniques and the related measurement instrumentation. From the discussion about the requirements for our project in the introductory chapter, we conclude that the technology which could better suit our needs is EEG. In fact, EEG can be acquired noninvasively from surface electrodes, and offers a good tradeoff between performance and cost/compactness. Moreover, experimental setup is relatively easy and compatible with home deployment.

From the sensors point of view, we decided to rely on passive Ag/AgCl electrode technology (making use of electro-conductive gel, in order to lower the source impedance and partially counter the increased noise and motion artifacts problems). Given our analysis we find that, overall, passive electrodes are the most compact and accessible solution for our custom BCI. In fact, active electrodes are not, usually, sold as standalone devices (nor they come at a low price), and their development would impact quite severely on budget (not the electronics *per se*, but rather the whole product engineering and manufacturing).
The complete EEG module electrical specifications and a discussion about possible sources of interference and non-idealities will be discussed in §2.1.

1.2 Typical BCI brain signals from EEG

During a BCI session, the user is typically required to perform different mental tasks, or he/she could be presented with some stimuli. In response to those actions, some characteristic patterns arise in the EEG, and such features are used to decode the user's intent. In this brief paragraph we review some of the most commonly encountered "patterns" (at least in "traditional" BCI-enabled control/spell applications), explaining how these potentials are typically elicited/regulated and what their most distinctive features are. As in the previous paragraph, at the end we will motivate our final choice of relying on a SSVEP-based paradigm for operating our BCI.

1.2.1 Slow Cortical Potentials (SCP)

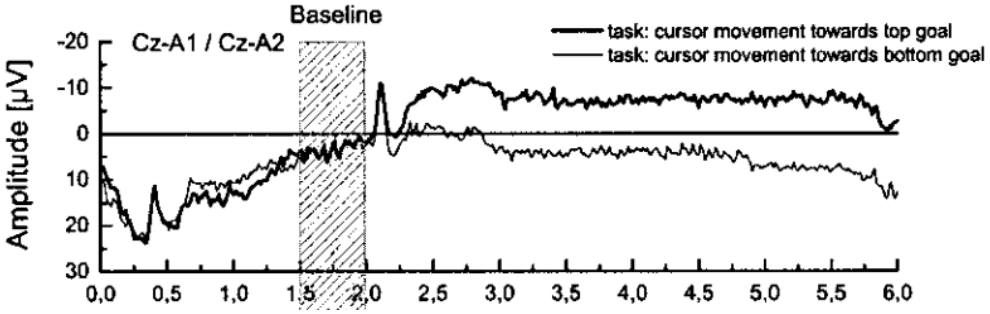

Figure 1.2 Examples of regulation of SCP to accomplish a binary task. At the beginning of a trial, the task is presented, accompanied by a high-pitch warning tone (S1), signaling that, after 2 s, the active phase will begin, providing SCP feedback; such active phase is introduced by a low-pitched tone (S2).

Slow Cortical Potentials (SCP) [48],[49] are slow voltage changes generated in cortex that users can learn to self-regulate. With training, user can either produce cortical positivity or negativity, according to the task requirement; negative SCPs are typically associated with movement and other functions involving cortical activation, while positive SCPs are usually associated with reduced cortical activation.

A typical paradigm presented to SCP-BCI users is the so-called "S1-S2" paradigm: a high-pitched tone (S1) signals the user that two seconds later, simultaneously with a low-pitched tone (S2), feedback of SCP will start. Such feedback could be, for example, a cursor movement on a monitor, and two different tasks control the upward or downward direction of such movement. To perform the task, users have to produce either positive or negative SCPs. The amplitude of such SCP is required to exceed a predefined threshold before being ruled as a positive or negative SCP, and feedback is intended to help the user produce larger amplitude shifts. This S1-S2 paradigm is reported in Figure 1.2, where the amplitude of the SCP is measured relatively to a short baseline period preceding the S2 tone.

SCP-BCI were also successfully controlled by users affected by severe paralysis [50],[51].

1.2.2 SensoriMotor Rhythms (SMR)

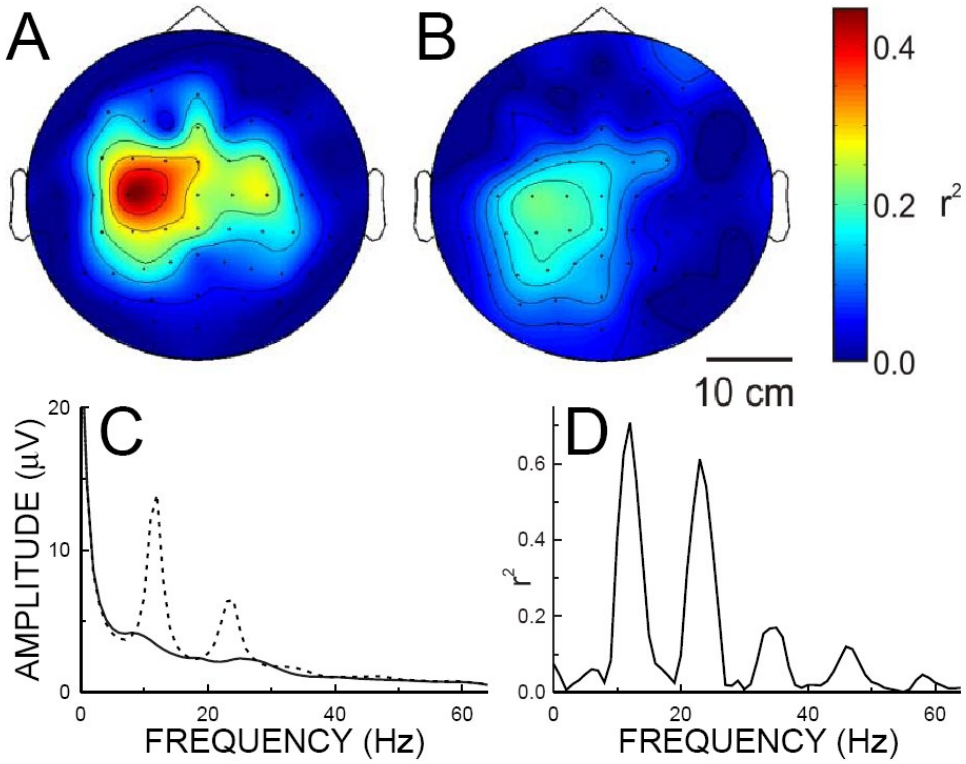

Figure 1.3 (*A*,*B*) Topographical scalp distribution of the difference between actual (*A*) or imagined (*B*) right-hand movements vs the rest case (r^2 score) in a [10.5-13.5] Hz band; (*C*) spectra relative to motor imagery (solid line) and rest (dashed line) acquired from the sensorimotor cortex; (*D*) r^2 score of picture (*C*).

The act of performing actual movements, manifesting motor intention or even imagining a movement is able to modulate the neurophysiological rhythmic activities recorded over the sensorimotor cortex. Such modulation appears as amplitude decrease in the [8-13] Hz band (also known as mu band) and in the [14-26] Hz one (beta band). Meanwhile, such decrease is accompanied by an increase in gamma frequency band ($f > 32$ Hz), as studies on ECoG and brain implants confirm.

All these rhythms are collectively referred to as *SensoriMotor Rhythms* (SMR). In particular, the amplitude decrease in the lower frequency bands (mu and beta) due to task-related modulation is called *Event-Related Desynchronization* (ERD) [52]. After motor completion, mu and beta band experience a positive amplitude rebound, a phenomenon referred to as *Event-Related Synchronization* (ERS) [52]. Figure 1.3 shows an example of the ERD phenomenon. The uppermost figures depict topographical distribution of the difference between rest and right-hand motor task (actual movement, *(A)*, and imagined movement *(B)*, for the [10.5-13.5] Hz band); such difference is plotted in terms of r^2 score, i.e. the proportion of the single-trial variance that is due to the motor task. In picture (*C*), instead, the spectra of rest (dashed line) and motor imagery task (solid line) are compared, and picture (*D*) plots the difference between such tasks in terms of r^2 score, highlighting that mu, beta and gamma are the most affected frequency bands for motor imaging tasks.
Thus, motor intention or motor imagery induce SMR modulation, and this feature can be exploited by the user to encode his intent and, consequently, for operating a BCI [53]-[55]. Example applications include the control of a virtual pointer with as much as 3 *Degrees of Freedom* (DOF) [54].

1.2.3 P300

The *P300* response is an evoked potential which is elicited when the user recognizes an event he/she considers important; in this sense, P300 is an *Event-Related Potential* (ERP). For example, in the case of a visual evoked P300, the user can be asked to attend and silently count each presentation of a rare, target stimulus between a stream of frequent, non-target stimuli (this is the so-called *oddball* paradigm) [56]. The P300 response can be then observed in the EEG as a positive deflection, time-locked to the attended stimuli (typically delayed by 300 ms), as exemplified in Figure 1.4 (*B*, *C*). The amplitude of such pattern is largest at the parietal site, and gets

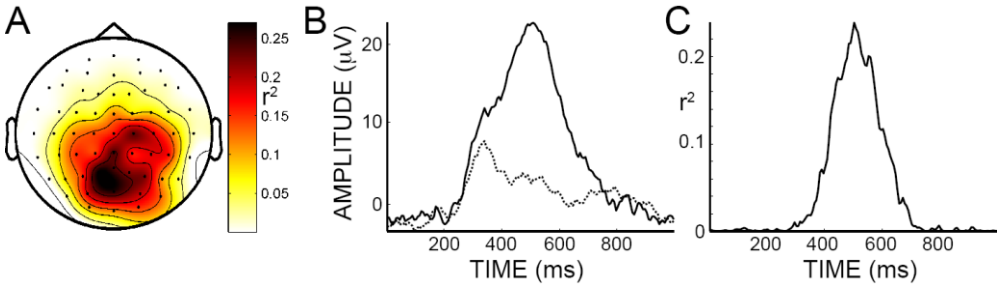

Figure 1.4 (*A*) Topographical distribution of the P300 potential at the peak time instant (r^2 score calculated between target and non-target stimuli); (*B*) time series of EEG recorded from electrode Pz (International 10/20 System), for target (solid line) vs. non-target (dashed line) stimuli; (*C*) r^2 score plot of (B).

attenuated as it spreads towards central and frontal locations (Figure 1.4 (*A*)).

Studies demonstrated that it is possible to modulate the P300 amplitude with visual attention: this was successfully exploited to design *covert* attention paradigms [57],[58] (as opposed to the classical *overt* approach, in which the user is still able to shift attention by means of gaze direction). Some research also focused on visual stimuli optimization in order to obtain larger ERPs, and it was shown that, beyond the classic matrix-arranged flashing characters [56], stimuli can also be presented in forms of emotional faces [59],[60].

P300 has received a lot of attention as a BCI control signal, as it is a "highly parallel" paradigm, in which a high number of choices is available to the user. The high variability of such temporal features, though, requires periodic recalibration of the system in order to achieve better performance [61]. Nonetheless, a large number of studies report successful P300-based control by users affected by severe pathologies, such as ALS (*Amyotrophic Lateral Sclerosis*), e.g. [62].

1.2.4 Steady State Visual Evoked Potentials (SSVEP)

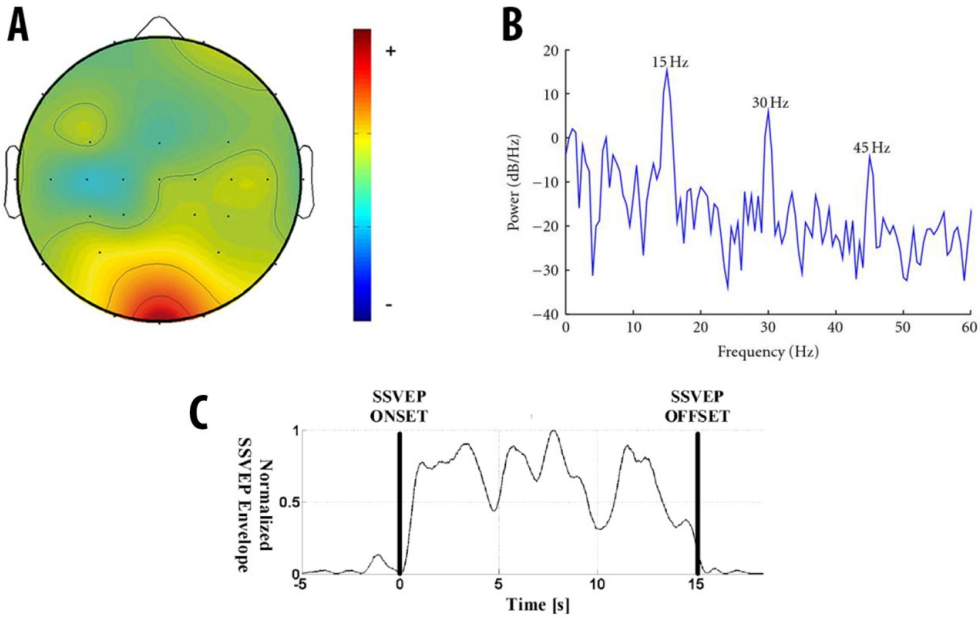

Figure 1.5 (*A*) Topographical distribution of a SSVEP response; (*B*) an example power spectrum of a 15 Hz SSVEP recorded over the occipital area: the fundamental frequency and its second and third harmonic are clearly visible; (*C*) temporal evolution of a 14 Hz SSVEP (its normalized Quadrature Amplitude Modulation envelope): onset is about 700 ms delayed, first peak is after 1.52 s of stimulation, and the response is suppressed after 15 s.

A *Steady State Visual Evoked Potential* (SSVEP) is a periodic brain response elicited by a visual stimulus, flickering at a constant frequency: a peak in the brain power spectrum, synchronous with such frequency (Figure 1.5 *B*), can be produced just by looking at the visual stimulus. SSVEPs are mainly elicited in the occipital and parieto-occipital area, although some activity can also be detected in the parieto-temporal and frontal areas (as shown in Figure 1.5 *A*). Moreover, analysis on the temporal evolution of the response ([63] extract this information using a modified *Quadrature Amplitude Demodulation* – QAD – scheme, as in communication engineering) highlight a non-stationary behaviour, as depicted in Figure 1.5 *C*: the SSVEP onset is typically delayed (from 700 ms up to 1.3 s,

depending on the frequency) from stimulus application, and the first peaks in SSVEP intensity typically requires a couple of seconds to build up. Then, about after 15 s of continuous visual stimulation, the SSVEP response is completely suppressed.
Practical SSVEP stimulation frequencies can be divided into three sub-bands [64]: Low-Frequency (LF, [5-13] Hz), Medium-Frequency (MF, [13-30] Hz), High-Frequency (HF, [30-60] Hz). Highest SSVEP amplitudes are usually achieved in the LF range, since, typically, the brain power spectrum exhibit a $1/f$ behaviour; however, even in the MF range it is possible to achieve good detectability. In [63], the most discriminative frequencies were found to be 5.6 Hz, 8 Hz, 12 Hz (best one) for the LF range, 15.3 Hz for the MF, and, to a minor extent, 28 Hz in the HF one.
Traditionally, different commands are mapped to different stimuli frequency, in SSVEP-based BCIs. Nonetheless, many studies pointed out that it is also possible to code the commands as phases of SSVEP responses [65]-[67], or to have a hybrid frequency-phase coding [68].
Stimulus size and type also impacts on the SSVEP amplitude: for a review, [69] provides a good starting point. Here we just point out three main protocols: light (e.g. flashing LEDs [70]), pattern reversal (e.g. checkerboards on LCD screens [71]) and graphical objects. As far as the latter technique is concerned, presentation of emotional faces resulted in an improvement in SSVEP classification [72]. Finally, SSVEP amplitude is also modulated by visual attention; as in the P300 case, *covert* attention SSVEP-based BCI can be developed [73]-[75].

1.2.5 Error Related Potentials (ErrPs)

Error Related Potentials (ErrPs) are not a BCI paradigm *per se*, but are useful brain features that can be used, in conjunction with other paradigms, to improve the BCI performance. Moreover, such potentials are generated naturally by the user, and no training is thus required to produce them.

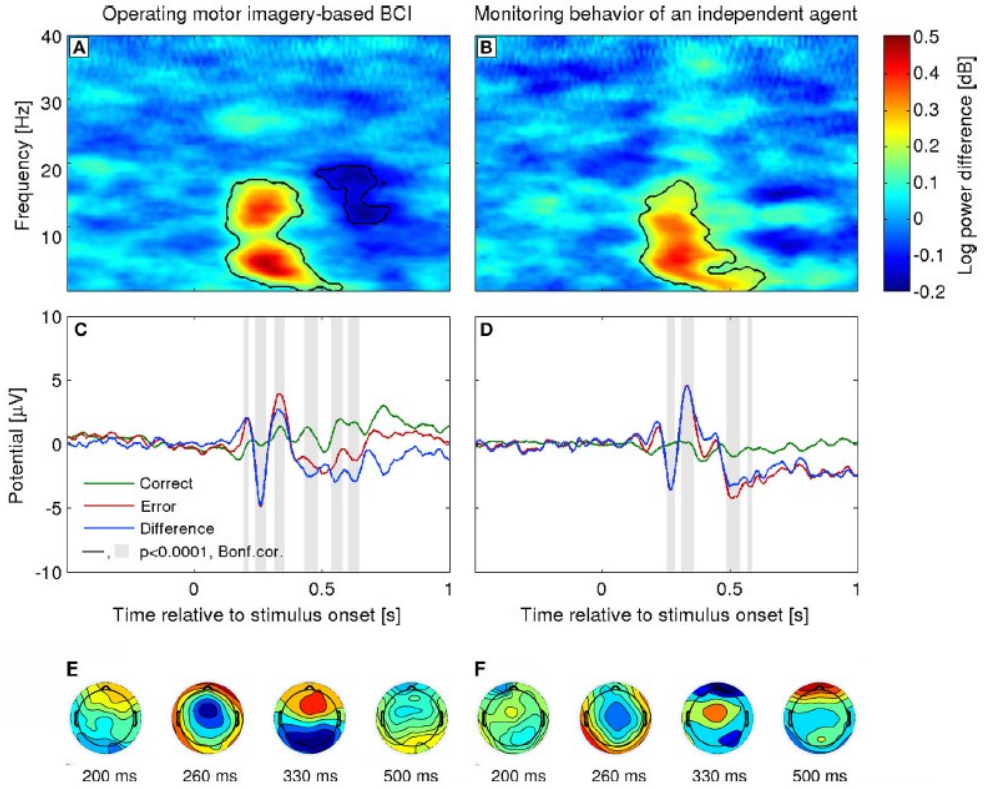

Figure 1.6 Error related potentials by interaction (cursor controlled by user with a 2 task MI-BCI, left column) and monitoring (cursor moves automatically and induces ErrPs in wrong movements)[76]. (*A*, *B*) Event-related spectral perturbation; (*C*, *D*) Grand-average ERP at electrode FCz (*difference* is defined between correct and error). (*E*, *F*) Corresponding topographical distribution.

Various kinds of ErrPs exist, depending on the context/protocols which generates them. ErrPs were observed in [77] by pressuring users to perform fast decisions: recognized errors would manifest as negative potential deflections in the fronto-central area (*Event-Related Negativity*, ERN) about 50-100 ms after wrong decisions, followed by a centro-parietal positive deflection. Similar patterns were observed in [78], when users were presented with feedback (in the form of a delayed result of their choice), with a 200-300 ms temporal delay. In addition, ErrPs were generated also by observing errors committed by another person/agent [79].

An important result for BCI application was achieved when ErrPs were observed in the EEG as a response to a BCI wrongly-interpreted command [80]. Figure 1.6 depicts this scenario: the difference between correct responses and errors manifests as an initial positive peak delayed, approximately, by 200 ms, followed by a large negative deflection at about 250 ms, and a third, positive, peak at about 320 ms.
ErrPs represent a great potential for BCI: they can be used, for example, to prevent the execution of an incorrectly classified command (e.g. [81]), or they can be even exploited as real-time feedback for online, adaptive calibration of the classifier (e.g. [82]). Finally, a very nice property of ErrPs was shown in [79]: a classifier trained for recognizing such potential maintained the same performance even months after initial calibration.

1.2.6 Our paradigm choice

Having reviewed the most commonly encountered BCI signals, and considering the preliminary requirements, as indicated in the introduction, we chose to rely on SSVEP as our BCI operating paradigm. In fact, SSVEP has the following key characteristics, which meets our desiderata:

- it allows, in principle, to avoid training and calibration phases: responses are elicited naturally, and the characteristics are quite repeatable and predictable. This also holds true across different users, thus allowing to adopt a *subject-independent* approach and move closer to a *Plug&Play* behaviour;
- SSVEP are regarded as reliable features for BCI [83], given their inherently higher SNR, when compared to other paradigms. This means that it is possible to achieve higher accuracies and, typically, fewer false positives;
- it allows for multiple, parallel commands;
- the protocol used to elicit and detect SSVEP does not require, in general, any synchronization between the stimuli unit and the EEG

acquisition one (unless phase features are being used). This allows to simplify the overall setup.

However, SSVEP also comes with several restrictions/drawbacks, such as: *(i)* user must focus on the visual stimuli in order to elicit the response: thus, while controlling the BCI, the user cannot be engaged in other tasks; *(ii)* in overt operation, user still must be capable of small eye movements; *(iii)* long stimulation periods can induce visual fatigue, especially at lower flickering frequencies; *(iv)* given the temporal evolution of a SSVEP, delays between 1-3 s are to be expected.
Nonetheless, considering the target application we intend to pursue, those points are well compensated by the advantages. In particular, with respect to *(i)* and *(iv)* we can state that, given the limited and sparse interaction with the BCI, having to focus on the visual stimuli for a short amount of time and experiencing contained delays do not impact significantly on the usability of the device, for its purposes. Moreover, in order to counter point *(iii)* we will attempt to user MF flickering frequencies, namely, 16, 18, 20, 22 Hz: this particular choice will be guaranteed by exploiting LEDs as stimuli. While, on the one hand, larger SSVEP responses are typically obtained in the LF band, on the other hand such frequency range overlaps, for example, with the alpha rhythms; this, in turn, can cause a higher false positive rate, thus limiting the effectiveness of the control. We will then try to contrast weaker SSVEP response with dedicated signal processing, as it will be shown in Chapter 3 and 4.

1.3 BCI signal processing

Signal processing in BCI can be viewed as a multi-stage process, which we can conveniently break up as composed of:

- pre-processing and signal cleaning;
- feature extraction;
- classification or regression;

- post-processing, output, feedback.

Not always this distinction is rigidly respected. For example, *Common Spatial Patterns* (CSP) filters collapse the pre-processing stage and the feature extraction into one step. Nonetheless, the processing flow is quite always performed in those steps.
Pre-processing is typically performed to clean data from artifacts and useless information. Feature extraction, then, takes the whole (multivariate) input signal and computes just a few relevant, representative characteristics (*feature vector*), which will then be used in the following classification/regression step. These, in turn, can be performed by exploiting general *machine learning* algorithms or just by *ad-hoc* procedures. Finally, post-processing can be used to improve/further process classification/regression results and, then, to display the output/feedback to the user.
A thorough review of signal processing methods goes beyond the scope of this paragraph, since particular solutions and implementations strongly depend on the type of paradigm used and many more other variables; we will briefly review the most common processing steps/techniques encountered in BCI contexts. Also, a detailed description of calibration-less, SSVEP processing techniques will be reviewed in Chapter 3.

1.3.1 Pre-processing

(a) Temporal/Spectral filtering

Depending on the EEG signals of interest (e.g. SMR, SCP etc.) and on the analysis one wishes to carry out, it can be useful to restrict, for example, the bandwidth of such signals (e.g. low-pass, band-pass, high-pass). This can be easily accomplished by designing FIR (*Finite Impulse Response*) or IIR (*Infinite Impulse Response*) filters, or even by transforming via FFT (*Fast Fourier Transform*) in the frequency domain, apply some filtering functions, and then transforming back to time domain via IFFT (*Inverse FFT*).

Moreover, sometimes it is useful to downsample the signals, just to reduce their dimensionality and speed up further processing.

Other encountered filtering methods for cleaning/smoothing data are, for example, moving averaging or de-noising via *Wavelet Transform* (WT). WTs were also used as techniques to extract features for classification (e.g. [84],[85] used wavelet features for ERP classification).

(b) Spatial filtering

While temporal/spectral filters are typically performed on a per-channel basis (i.e. each input channel is considered and treated separately), spatial filtering combines the information from multiple sources. Signals are mixed, i.e. a weight is assigned to them, and a spatial filter maps the input space (called *sensor space*) to a new space, called *signal space*, in which the desired features are more easily or meaningfully extracted.

One of the simplest spatial filters is the *bipolar* filter: the potential reading of one electrode site is simply subtracted from another one. Such a simple procedure allows to put more focus on local activity, as it cancels out the common mode (defined as the average potential between the two electrodes).

A variation, yet very simple to implement, is the *Common Average Reference* (CAR) filter. It consists in subtracting the average potential of all electrodes to each one of them. CAR filtering has the effect of getting rid of common mode activity; however, it can also introduce spatial smearing in the channels.

Similar to CAR is the *Laplacian* filter, in which the average of surrounding electrodes is subtracted from the one of interest. The Laplacian filter tends to cancel-out common mode activity as the CAR, yet it retains more local information since this averaging is limited only to neighboring electrodes.

Spatial filters can also be used to decompose multivariate signals into components and to reduce data dimensionality. For example, *Principal Component Analysis* (PCA) decomposes the signals into uncorrelated

components which are ordered according to decreasing variance. It does so by finding an orthonormal basis in which each uncorrelated component explains a certain percentage of the total input variance, with decreasing explanatory power.

Mathematically, if $\mathbf{X} \in R^{n \times m}$ is an EEG record of m time points from n channels, with zero mean, PCA will find a projection matrix $\mathbf{W}=[\mathbf{w_1},\ldots,\mathbf{w_n}] \in R^{n \times n}$ to transform the data into uncorrelated components by performing a *generalized eigenvalue decomposition* of the sample covariance matrix $\mathbf{R}=\mathbf{X}\mathbf{X}^{\mathbf{T}}$. The vectors $[\mathbf{w_1},\ldots,\mathbf{w_n}]$ are the n normalized orthogonal eigenvectors of $\mathbf{R}$, corresponding to the eigenvalues $\lambda_1,\ldots, \lambda_n$, sorted in descending order. The components are then found applying the transformation to the input data:

$$\mathbf{Y} = \mathbf{W}^T\mathbf{X}\,, \tag{1.1}$$

where the rows of $\mathbf{Y}$ (i.e. the components), are uncorrelated. If every component is considered, then perfect reconstruction of the original signal $\mathbf{X}$ is possible; otherwise, one finds an approximation $\tilde{\mathbf{Y}}$, in a lower dimension (i.e. considering only the first p components, called *principal components*), which accounts for as much data variance as needed.

When we apply PCA, we must keep in mind the main underlying assumptions, namely: *(i)* linearity, *(ii)* mean and variance are sufficient statistics, *(iii)* large variances have important dynamics (outliers could compromise this assumption). In order to account for non-linearity, and achieve more meaningful capturing of non-linear process, *kernelization* methods can be applied [86]. More on *kernels* and the *kernel trick* will be presented in §1.3.3.

Independent Component Analysis (ICA) is another spatial filtering technique which aims at separating the original input signal into components which are maximally statistically independent: it is, in this sense, a solution for *Blind Source Separation* (BSS) problems.

ICA works as follows: given n observed signals $\mathbf{X}=[\mathbf{x_1},\ldots,\mathbf{x_n}]^{\mathrm{T}}$, we assume that they originated from n unknown source signals $\mathbf{S}=[\mathbf{s_1},\ldots,\mathbf{s_n}]^{\mathrm{T}}$, which are linearly superimposed:

$$\mathbf{X} = \mathbf{AS}\,, \tag{1.2}$$

where **A**, the mixing matrix (assumed full-rank, with *n* linearly independent columns, therefore invertible), is a *n*x*n* time-invariant matrix whose elements are estimated from the data. Both **A** and **S** are unknown, and further assumptions are needed in order to solve the de-mixing problem. ICA, in particular, assumes that the source signals $[\mathbf{s_1},\ldots,\mathbf{s_n}]^T$ are mutually independent. Then, the de-mixing matrix **W** is computed: it allows to separate the observed signals **X** into maximally statistically independent components **Y**:

$$\mathbf{Y} = \mathbf{WX}\,. \tag{1.3}$$

Having decomposed the input signal, one can choose which components are not relevant to the study or contain noise/artifacts, and usually discards them ($\tilde{\mathbf{Y}}$). Then an approximation of the input signal $\tilde{\mathbf{X}}$, cleaned of the unwanted components, can be reconstructed back-projecting into the original electrode space:

$$\tilde{\mathbf{X}} = \mathbf{W^{-1}}\tilde{\mathbf{Y}}\,. \tag{1.4}$$

Many algorithms exist to compute the de-mixing matrix [87], such as Infomax, Second Order Blind Identification (SOBI), Joint Approximation Diagonalization of Eigen matrices (JADE). In general, ICA is used in BCI as a pre-processing step for getting rid of artifacts and unwanted signal components.

Common Spatial Patterns (CSP) [88]-[90] is a *supervised* technique which allows to maximize the variance-to-variance ratio of two conditions or classes: i.e., CSP will attempt to maximize the variance of the samples relative to one condition, while simultaneously minimizing the variance of the samples of the other condition. Being a supervised method, CSP requires class labels in order to learn the optimal spatial filter weights.
If changes in variance encode the actual difference between classes, this pre-processing technique also extracts the features for the subsequent classification stage. For its properties, CSP is often used in *Motor Imagery* (MI)-based BCIs [91],[92].

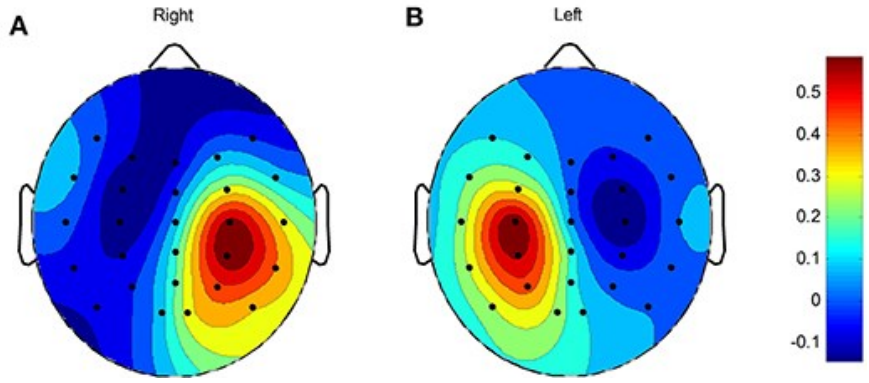

Figure 1.7 Example of common spatial patterns extracted from a two-class, left vs. right motor imagery task.

In order to better understand CSP, let us consider the transformation matrix $\mathbf{W} \in M^{n_x n}$. As in equation (1.3), the transformed data are obtained by matrix multiplication $\mathbf{WX_i}$, $i \in \{1,2\}$, where $\mathbf{X_i} \in R^{n_x m}$ represents the input signal matrix, in both condition 1 and 2, in which each row is an electrode reading. With CSP, the first row will contain most of the variance of, say, the class 1 (and the least variance of class 2), while the last row will explain most of the variance of class 2 (and the least of class 1). **W** is calculated as the result of a simultaneous diagonalization of the two sample covariance matrices $\mathbf{R_1}$ and $\mathbf{R_2}$, with the additional constraint that diagonalization of $\mathbf{R_1}+\mathbf{R_2}$ must yield the identity matrix, **I** (to guarantee that maximization of variance for class 1 results in minimization of variance in class 2)

$$\mathbf{WR_1W^T = D} \text{ and } \mathbf{WR_2W^T = I - D}\,, \tag{1.5}$$

where **D** is a diagonal matrix.

The columns of $\mathbf{W^{-1}}$ are called *common spatial patterns* (an example of CSPs extracted for a two-class, left vs. right motor imagery task is shown in Figure 1.7).

Various extension of the basic CSP technique have been proposed, such as, for example, *Common Spatio-Spectral Patterns* (CSSP) [93], which attempts to optimize spatial features, as CSP, in conjunction with spectral

ones (by additionally feeding the algorithm with time-lagged copies of the original signals). Also, multi-class extensions have been proposed [94].

1.3.2 Feature extraction and selection

Feature extraction involves finding characteristic quantities and attributes which help in defining the object of a classification/regression problem: they are the input to the learning/prediction stage. Of course, which feature best describe the problem heavily depends on the nature of it.
For example, in MI tasks, the input features could be the power of a specific/several specific frequency sub-bands; maybe this power can be extracted after the application of a CSP filter. Another possibility is to estimate power spectra with *AutoRegressive* (AR) models, and use the coefficients of such model as input features [95].
For a P300 setup, time domain features can be exploited. The signals can be cleaned of artifacts with ICA, band-pass filtered and downsampled (to reduce dimensionality); then, the samples in an interval around the expected P300 response can be selected as features. We will discuss in Chapter 3 and 4 the features we used for SSVEP detection and classification.

Other than extracting features, it is also important to select the most relevant/discriminative ones. It is a known issue that classification and regression problems may suffer the so-called *curse of dimensionality*, i.e. when the problem we intend to solve is too high-dimensional (in the number of features) for the too-few examples we have in order to learn an effective and generalized representation of the data. In these cases, selecting just a subset of features which contain the most discriminative power can significantly improve the performance of the subsequent stage.
We can think, for example, of a procedure to select the best channels based on the optimization of statistical measures such as *Fisher* score, r^2 score or *Student*'s *t-statistics*. It is also possible to implement *genetic algorithms* for automatic feature selection [96], or to adopt *information-theoretic*

approaches (e.g. based on *Mutual Information*) in feature evaluation [97],[98].

1.3.3 Classification and regression

A classification problem entails predicting the membership of an item given its descriptive features; a regression problem, instead, will try to predict a quantity, relative to an item, given the input features.
Although *unsupervised* methods (i.e. methods that learn on examples without the need of any labeling) exist, here we just pick a few, representative *supervised* learning algorithms, which are commonly used in BCI experiments.
In general, those methods will learn, from the given examples, the weights to be assigned to each feature in order to minimize a loss function (which quantifies the model *fitness* to solve the given problem). For a binary classification problem, the loss function *J(w)* is, generally, composed of two terms, i.e. a loss term *L(w)*, and a regularization term *R(w)*:

$$J(w) = \sum_i L\left(y^{(i)} f_w\left(x^{(i)}\right)\right) + \lambda R(w)\,, \tag{1.6}$$

$$f_w\left(x^{(i)}\right) = w^T x^{(i)} \tag{1.7}$$

Where $y^{(i)} \in \{-1,1\}$ is the class label, $x^{(i)}$ a sample, w the feature weights, λ an hyper-parameter which controls the relative strength of the regularization term.

As far as the loss term *L(w)* is concerned, many functions exist, depending on the learning algorithm. Examples are:

- *Squared loss*

$$L_{square} = \frac{1}{2}\left(f_w\left(x^{(i)}\right) - y^{(i)}\right)^2\,. \tag{1.8}$$

- *Log loss*

$$L_{log} = y^{(i)} \log\left(g_w\left(x^{(i)}\right)\right) + \left(1 - y^{(i)}\right) \log\left(1 - g_w\left(x^{(i)}\right)\right), \tag{1.9}$$

$$g_w\left(x^{(i)}\right) = \frac{1}{1 + e^{-f_w\left(x^{(i)}\right)}} . \tag{1.10}$$

- *Hinge loss*

$$L_{hinge} = \max\left(0, 1 - y^{(i)} f_w\left(x^{(i)}\right)\right) . \tag{1.11}$$

The first one is the most used in regression problems, while log loss is used for classification problems, e.g. in *Logistic Regression*. Hinge Loss, on the other hand, is used in *Support Vector Machines* (SVM), which have application in both regression and classification tasks.

As previously stated, loss functions *J(w)* usually include a regularization term, *R(w)*, which is particularly important to contrast an effect called *overfitting*. Overfitting happens when a model is excessively complex, such as having too many parameters relative to the number of observations available. By introducing a penalty term for excessively complex solutions, the model may perform better in terms of generalization.
Examples of penalty terms are:

- *L_2 norm (Tichonov)*

$$R_2 = \frac{1}{2} \|w\|_2^2 . \tag{1.12}$$

- *L_1 norm (Lasso)*

$$R_1 = \|w\|_1 . \tag{1.13}$$

- *Elastic net*

$$R_{elastic} = \lambda_1 \|w\|_2^2 + \lambda_2 \|w\|_1 . \tag{1.14}$$

Moreover, the choice of the regularization parameter(s) is critical: too high parameters will lead to excessively simple model, with low prediction

power; on the other hand, too few regularization may not effectively counter the overfitting effect.
Usually, in order to choose the best value, data are split into *train*, *validation* and *test* set: model is trained on the first split, and *cross-validation* is used to find the best hyper-parameter; finally, the test set is used to assess the performance on unseen data [2]. When data is not very large, *k-fold cross-validation* can optimize data usage, as explained in [2].

Examples of machine learning algorithms commonly found in BCI are:

- *Linear Discriminant Analysis* (LDA)

  In a binary problem, assuming normally distributed data, with equal covariance matrices $\Sigma_1 = \Sigma_{-1} = \Sigma$ (*homoscedasticity* assumption), the optimal separating function is given by

$$\hat{f}(\mathrm{x}) = \Big(\big(\mu_1 - \mu_{-1}\big)^T \Sigma^{-1} x - \frac{1}{2} \big(\mu_1 - \mu_{-1}\big)^T \Sigma^{-1} \big(\mu_1 - \mu_{-1}\big) + \log \frac{P(Y=1)}{P(Y=-1)} \Big) , \tag{1.15}$$

  where μ_i is the mean for the two class clusters. LDA can be made more robust in many ways. First we can drop the homoscedasticity assumption by assuming different covariance matrices Σ_1, Σ_{-1}; then we correct the covariance matrix estimation as follows:

$$\hat{\Sigma}_i = (1-\lambda)\Sigma_i + \lambda\Sigma , \tag{1.16}$$

  where $i \in \{-1,1\}$, $\Sigma = (\Sigma_1 + \Sigma_{-1})/2$. For $\lambda=0$ we have a *Quadratic Discriminant Analysis* (QDA).
  Furthermore, we can regularize the improved LDA via regularization; in particular, *spectral regularization* can be achieved by shrinking the covariance matrix's eigenvalues as follows:

$$\bar{\Sigma}_i = (1-\gamma)\hat{\Sigma}_i + \frac{\gamma}{m} \mathrm{tr}(\hat{\Sigma}_i)\mathrm{I} , \tag{1.17}$$

  where *tr(·)* is the trace operator, *m* the dimensionality of the data, and γ the *shrinkage* parameter, which controls spectral regularization.

- *Fisher Discriminant Analysis* (FDA)

  FDA attempts to project high-dimensional features into a lower dimensional space in which the two classes are more easily separable. It does so by maximizing the ratio of between-class scatter (S_B) to within class scatter (S_W):

$$J(w) = \frac{w^T S_B w}{w^T S_W w}, \tag{1.18}$$

$$S_B = \left(\mu_1 - \mu_{-1}\right)^T \left(\mu_1 - \mu_{-1}\right), \tag{1.19}$$

$$S_W = S_1 + S_2, \tag{1.20}$$

$$S_i = \sum_{j \in \{Class\ i\}} (x_j - \mu_j)^T (x_j - \mu_j). \tag{1.21}$$

- *Gaussian Mixture Model* (GMM)

  A GMM is a probabilistic model that assumes all the data points are generated from a mixture of a finite number of Gaussian distributions (prototypes) with unknown parameters ($\lambda=\{w_k, \mu_k, \Sigma_k\}$). The data is then modeled as a *Probability Density Function* (PDF):

$$P(x|\lambda) = \sum_{k=1}^{N_g} w_k N(x|\mu_k, \Sigma_k), \tag{1.22}$$

  Such parameters can be estimated in many different modes, e.g. with the *Expectation-Maximization* (EM) algorithm [99] or *Maximum A Posteriori* (MAP) [100].

  In [101], a two-step procedure is used for fitting the model parameters, assuming equal diagonal covariance matrices for each class: at first, the centroids of the prototypes are estimated with a clustering algorithm, such as *Self-Organizing Maps* (SOM) [102]. Then, diagonal covariance matrices are initialized in their elements as follows:

$$(\Sigma_C)_{mm} = \frac{1}{N_C} \sum_{n \epsilon C} \left(x^{(n)} - \mu_k{}^{nearest(n)} \right)_m^2 , \quad (1.23)$$

where $\mu_k{}^{nearest(n)}$ represents the nearest prototype centroid to point $x^{(n)}$, N_C is the number of elements in class C, m is the vector element and mm the matrix diagonal element. Then, estimates of μ_k and Σ_k are further refined by performing *Stochastic Gradient Descent* (SGD) [103] to minimize the mean square error between the output of the classifier (the posterior class probability distribution), and the target vector.

- *Support Vector Machine* (SVM)

  An SVM [104] constructs a hyper-plane, in a high-dimensional space, which can be used for classification, regression, or other tasks (such as novelty detection [105]). Intuitively, a good separation is achieved by the hyper-plane that has the largest distance to the nearest training data point of any class. In practice, there are situations in which data cannot be linearly separated by means of an hyper-plane. In this case, it is possible to allow for non-optimal separation by introducing slack variables $\xi_1,\ldots,\xi_n$ and solve the following optimization problem:

$$J(w, \xi) = \frac{1}{2} \|w\|^2 + C \sum_{i=1}^{n} \xi_i , \quad (1.24)$$

$$\text{subject to: } y^{(i)} \left(w^T x^{(i)} + b \right) \geq 1 - \xi_i ,\ \xi_i \geq 0 , \quad (1.25)$$

  where C is the regularization parameter that controls the trade-off between the complexity and the number of non-separable data points, w are the feature weights and b is the bias.

Methods like LDA, FDA, and SVM are linear in the implementation, and therefore cannot capture potential nonlinear structures in the data. However, it is possible to modify such behaviour by mapping features into a higher-dimensional space in which they are more separable. A simple example of such situation is shown in Figure 1.8.

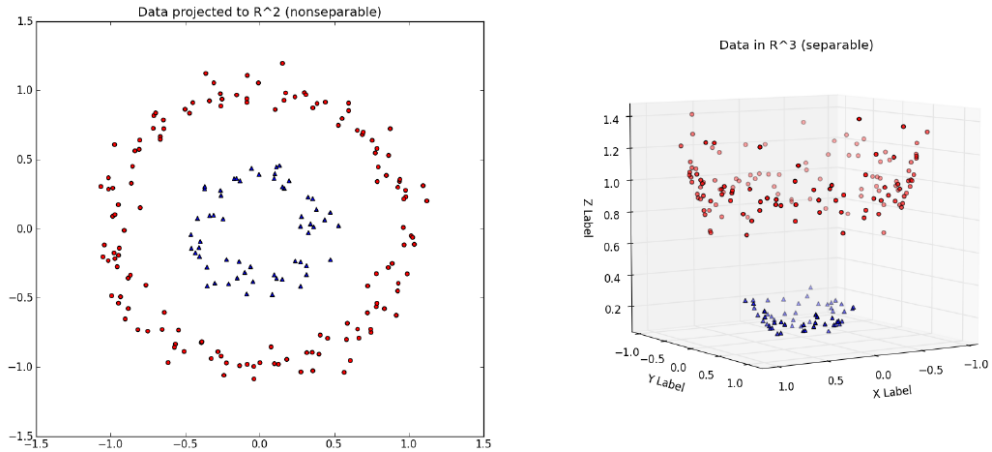

Figure 1.8 Example of a non-linearly-separable dataset (*left*). The introduction of nonlinear mapping into a higher dimensional space can make the data separable by a hyper-plane (*right*).

However, explicit feature mapping $\Phi(\cdot)$ to higher dimensional spaces can quickly turn the considered problem into a non-manageable one, in terms of data dimension. Nonetheless, things can be greatly simplified by observing that feature mapping can be formulated just in terms of dot products.
The so-called *kernel trick* consists in replacing these dot products with an equivalent kernel function

$$k(\mathrm{x}, \mathrm{x}') = \Phi(\mathrm{x})^T \, \Phi(\mathrm{x}'). \tag{1.26}$$

Thus, one can calculate dot products of higher-dimensional (potentially infinite) spaces without explicitly transforming x and x' to the higher-dimensional space. This allows to scale to higher-dimensional spaces using no extra memory, and with a minimal impact on computation time, thus allowing to scale this procedure to high-dimensional data. Popular kernel choices are:

- *Polynomial kernel*

$$k(x, x') = (x^T x' + c)^d \,, \tag{1.27}$$

  where c and d are parameters.

- *Gaussian RBF (Radial Basis Function) kernel*

$$k(x, x') = \exp\left(-\frac{\|x - x'\|^2}{2\sigma^2}\right), \tag{1.28}$$

  where σ is the bandwidth parameter.

- *Sigmoid kernel*

$$k(x, x') = \tanh(x^T x' + r)\,. \tag{1.29}$$

  where r is a parameter.

All the kernel parameters above impact on the performance of the classifier. Therefore, accurate parameter selection is important: such choice is usually performed via cross-validation optimizations.

1.4 Proposed platform architecture

So far, we reviewed BCIs under different lenses: from the physical signal acquisition side, through several commonly exploited brain signals, to the processing methods which are commonly used to extract information from such signals. Now, we collect the ideas and lay down the basic architecture of our platform. Once again, even though we will demonstrate, in practice, the effectiveness of the system with a SSVEP operating protocol, the approach is general and scalable: different protocols can be investigated just by adding plugins and functions to the signal processing block.

Referring to Figure 1.9, our platform will be coordinating and integrating three major blocks:

- the Analog Front End (AFE), which will be designed *ad-hoc* to meet the main requirements discussed in the introductory chapter;
- the real-time signal processing block, which will also take care of storing the whole EEG data to disk during an experiment;

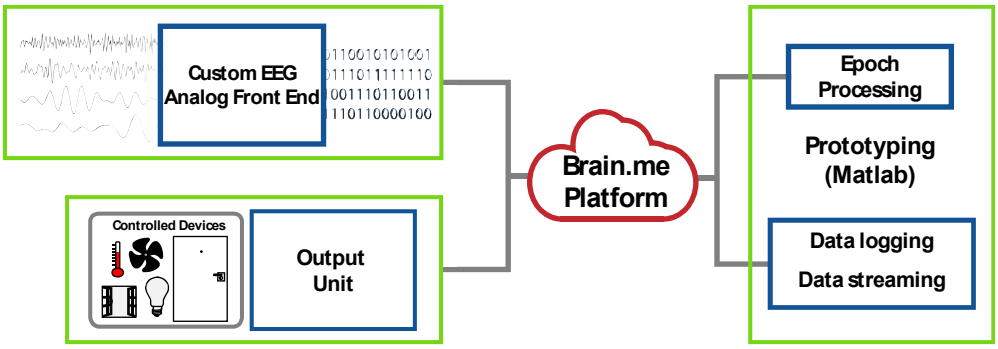

Figure 1.9 System architecture for the proposed BCI platform.

- the output/feedback unit, in charge of data display and interaction with the external environment;

Communication between the AFE and the platform will be based on a wired, high-speed connection, in order to minimize RF interference with the sensible analog section: this link will be established via USB 2.0, operating at full-speed (12 Mbps).

The AFE will be equipped with a control unit (based on an ARM® Cortex®-M4[1] microcontroller), which will manage both the data streaming and the proper control and initialization of the AFE. In this sense, this logic will provide a first level of *Hardware Abstraction Layer* (HAL), and provide a more abstract interface to the upper layers. This interface will be maintained even in case of hardware upgrades, in order to ensure compatibility with the software.

As of now, the platform is based on MATLAB®[2], a powerful computing environment optimized for numerical and statistical analysis. MATLAB offers a large number of modules and plugins, which makes it highly interoperable, as well as a useful tool for rapid prototyping. The signal processing module, in this state of the research, will be thus based on this environment, running on a commercial laptop, aiming at developing

[1] http://www.arm.com/products/processors/cortex-m/cortex-m4-processor.php
[2] www.mathworks.com

efficient methods and algorithm for future implementation in more compact hardware, such as on embedded computers (e.g. Raspberry Pi[3], BeagleBone[4]).

The module will be in charge of the full-chain, real-time signal processing (exploiting calibration-less methods, as per our requirements), as well as the data storing. It is, in fact, very important to collect data also from online experiments, in order to further process it offline and test/develop new algorithms. In addition, a plugin will make the platform compatible with the TOBI [106] input interface, in order to access all the functionalities offered by such platform. Interfacing will be possible via TCP/IP sockets exchanging data with the TOBI acquisition client.

Finally, the output/feedback module will handle two main task: *(i)* providing a GUI for the experimenter/user, displaying input waveforms, the result of classification and possible feedbacks; *(ii)* issuing high-level commands to the CARDEA system. This latter interaction will be based on TCP/IP protocol as well.

[3] http://www.raspberrypi.org
[4] http://beagleboard.org

Chapter 2

Building the BCI: the EEG module

Acquiring EEG signals, whose amplitude can be as low as a few μV, poses tight constraints on the electrical specifications of the acquisition system. However, high-end, clinical grade EEG equipment making use of a large number of electrodes are scarcely suitable for the aimed application: lower costs, smaller size devices are to be designed, suitable for extracting basic information on brain activity. This section deals with the physical realization of two EEG modules, covering analog signal conditioning aspects, signal digitalization, and the dedicated control and communication electronics. Both modules will be validated, and the newest one will be compared against a commercial, high-end EEG device for BCI. In the Appendix, complete schematics and layout files of the newest EEG module will be reported. Also, the cap and materials choice will be briefly discussed. Finally, a possible future development with active electrodes will also be sketched.

2.1 A closer look to the electrical specifications for the EEG module

As previously stated, typical EEG signals of interest in BCI applications have amplitudes as low as a couple of μV, in a bandwidth that, most commonly, lies within [0-50] Hz. SNR is typically low in EEG, and it is not uncommon to find, in measurement devices, *Referred To Input* (RTI) noise

specifications in the range of 1 μV_{rms}[5] ($\approx$ 6.6 μV_{pp} if we apply the 6.6 standard deviation rule, also known as 99.9% rule), over the full bandwidth.

Most of the commercial *Analog to Digital Converters* (ADC) chips are not able either to achieve a sufficiently low *Least Significant Bit* (LSB), i.e. sufficient resolution, or the RTI noise level may degrade the performance at lower scales. This is commonly dealt with by means of low-noise pre-amplification stages.

However, instrumentation noise is not the only contribution to the total measurement noise. In fact, we can identify several other factors, including:

- Mains (50 or 60 Hz, depending on the country) and *Radio-Frequency Interference* (RFI). The latter one cannot be, in general, directly observed at carrier frequency (due to the limited bandwidth of the acquisition hardware). It can, however, leak into the signal bandwidth due to radio-frequency rectification [107] inside the input *INstrumentation Amplifier* (INA). A strong RF signal may become rectified and appear as a DC offset error. Once rectified, no amount of low-pass filtering at the in-amp output will remove the error. If the RF interference is of an intermittent nature, this can lead to measurement errors that go undetected. As far as mains interference is concerned, [33] and [108] show a technique, based on a feedback loop (*Right Leg Driver*, RLD), which actively biases the user and attempts to minimize the error introduced by common mode noise. Battery-operated devices, in turn, exhibit lower mains interference, which would otherwise leak through the mains-supplied power converter (safety isolation does not imply optimal noise suppression).
- Electrode impedance. High-impedance voltage readings are known to be sensible to capacitively-coupled interference. In fact, current injected capacitively flows across the source impedance (electrode + cable), resulting in voltage noise. Usually, two

[5] E.g. http://www.biosemi.com/activetwo_full_specs.htm

strategies are exploited to counter this problem: *(i)* shielding, either passively or actively, or *(ii)* by lowering the source impedance with the use of active electrodes. In the latter case, if pre- amplification occurs near the surface electrode, noise pickup will see, as source impedance, the output impedance of the amplifier, which is typically low. Moreover, noise would corrupt a stronger signal, with respect to a passive electrode. In any case, the use of electroconductive gels and careful skin preparation (i.e. degreasing and scrubbing) lowers the electrode-skin impedance.

- Electrode material. While, for example, tin electrodes have the advantage of being cheap, they introduce a large amount of low-frequency noise, below 1 Hz. For low-frequency recordings, Ag/AgCl electrodes are typically used, and sintered Ag/AgCl offer the best solution in terms of noise and stability of characteristics.
- Artifacts form the motion of cables and electrodes. For the latter, the use of electro-conductive gel in mechanically improves the skin-electrode contact. For cable motion artifacts, the use of active electrodes improves the immunity, since higher level signals are transmitted through such cables.
- Artifacts from other bio-potentials, such as EMG (originating from the muscles of the face, neck and years), EOG (from eye blinks or eye movements), or ECG. Depending on the kind of protocol being used, if left unhandled, those artifact may hinder subsequent classification performance.

From the discussion above we draw the following conclusions regarding the implementation of the AFE module and its specifications:

- At least 6 EEG channels are desired for a SSVEP-based BCI. More channels can be useful in terms of flexibility towards other protocols.
- Signal bandwidth should extend, on the high-frequency side, at least to 60 Hz, while low-frequency corner should, at least, capture

frequencies as low as 0.1 Hz. DC-handling capability should be considered in, e.g., SCP studies.

- Noise level contributed by the electronics should be kept below 0.3 μV_{rms} RTI (i.e. less than 2 μV_{pp}). In case the ADC chip itself is not able to meet this requirement, a low-noise pre-amplification stage will be necessary. Noise level must, in any case, account for all possible EM noise sources over the whole PCB (*Printed Circuit Board*); i.e., in the noise measurement, the input short-circuiting will occur at the board connector level, using jumper cables.
- Although active electrodes may improve the performance of an EEG module (depending, of course, on the good design of this stage), the increased costs and complexity (in terms of driving circuits) made us opt, at least in this stage, for the worst-case scenario, i.e. passive electrodes. Furthermore, no shielding will be implemented. Of course, form the BCI point of view, signals are more likely to be affected by noise and artifacts in this way; nonetheless, we aim at recovering additional information with signal processing and we rely on the robustness of the SSVEP protocol. On the other hand, should artifacts overwhelm the recorded signals, realization of such active devices will be taken into consideration; a concept schematic for that stage will be explained in §2.6.
- The EEG module should be battery operated, mainly for two reasons: *(i)* improved electrical safety, and *(ii)* better rejection of mains noise.
- Communication with the platform will be implemented as wired, namely via USB 2.0. This is to reduce EM interference on the analog section and to guarantee higher bandwidth. Anyway, all the inputs will be RFI protected.

2.2 EEG module: release 1

In this paragraph, the first prototype EEG module [21] is presented. Some of the features include:

- 6 dedicated (pre-amplified EEG channels) plus 2 spare, fully-differential channels to be used as auxiliary inputs or for other bio-potential recordings. All the channels are simultaneously sampled, in order to maintain alignment between records. PCB dimensions are 21x16 cm.
- Pre- amplification stage. In fact, at the time of the prototype production (early 2012), no commercially-available ADC chips exhibited sufficient noise performance, thus a pre-amplifier was added to contain the contributed noise. Our ADC choice was the *Texas Instruments ADS1298*[6], which features, at maximum input gain ($G = 12$), an RTI noise of 0.4 μV_{rms}, which is larger than we said we should tolerate (namely, 0.3 μV_{rms}). With the addition of the custom pre-amplifier, noise performance was kept within the specifications ($\leq 1.8\ \mu V_{pp}$).
- The module is battery operated (2xAA alkaline batteries for each analog supply, 3xAA alkaline batteries for the digital supply), with two different supply option: *(i)* symmetrical (±2.5 V), as in most devices (even though lower voltages are used, in this case), or *(ii)* unipolar (0-5 V). Consequently, in both modalities, the RLD/GND electrode will deliver the appropriate bias voltage, namely, 0 V in the first case, 2.5 V in the second one.
- Power consumption (including efficiency of the LDO-regulated power section): 134 mW.

[6] http://www.ti.com/product/ads1298

- Board control and interfacing is handled by a very compact ARM Cortex-M4 based development board (Teensy[7] 3.x), which can handle full speed USB 2.0 communication as a CDC (*Communication Device Class*).

Figure 2.1 shows a high-level schematic of the EEG module, while Figure 2.2 shows photographs of the analog module and the interface/control board.

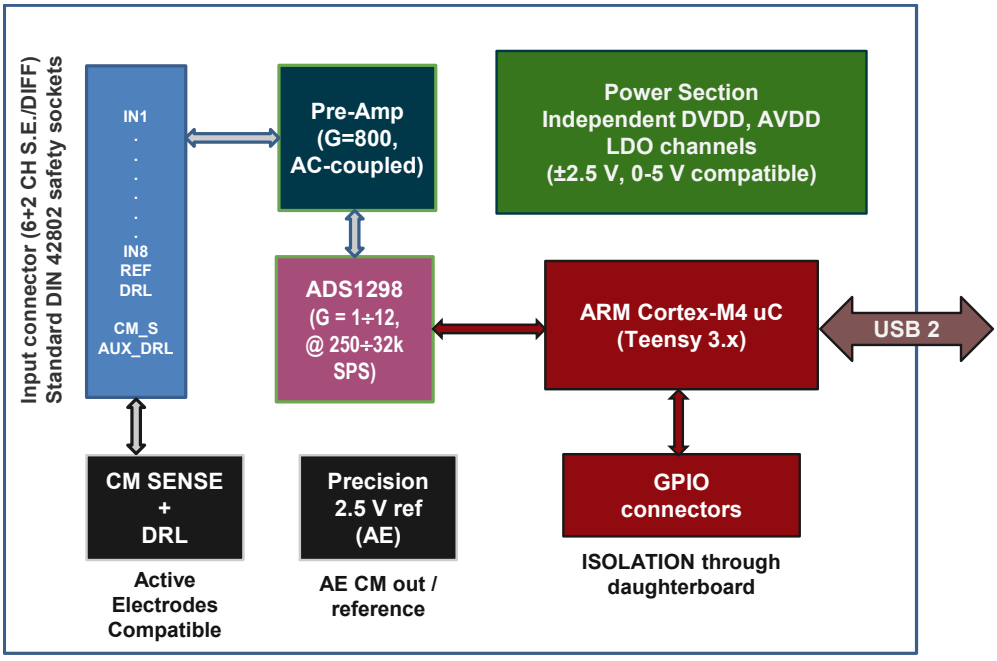

Figure 2.1 High-level schematic of the EEG module – release 1.

[7] https://www.pjrc.com/teensy

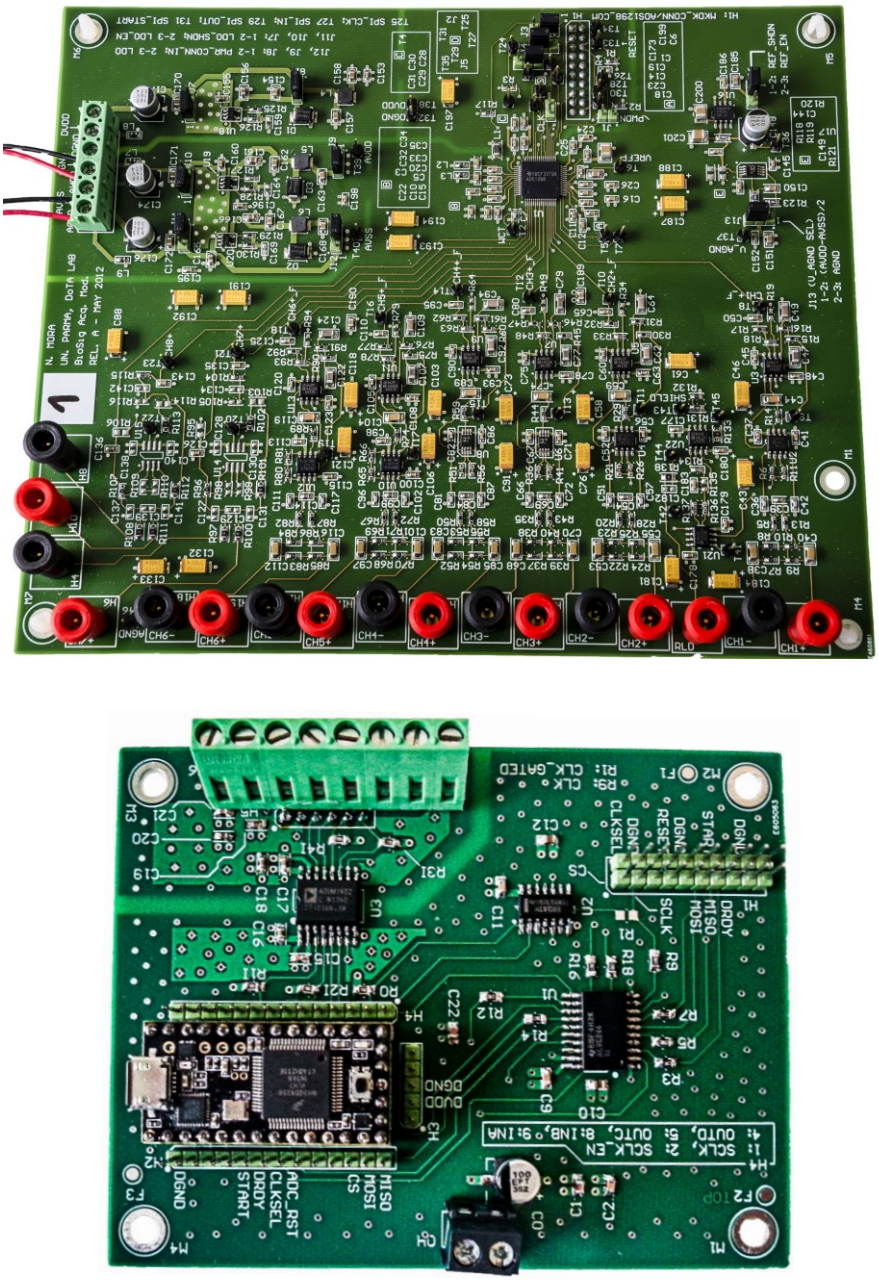

Figure 2.2 Photos of the EEG module – release 1: amplifier and ADC (*top*), isolated microcontroller unit (*bottom*).

2.2.1 Schematic of a dedicated EEG channel

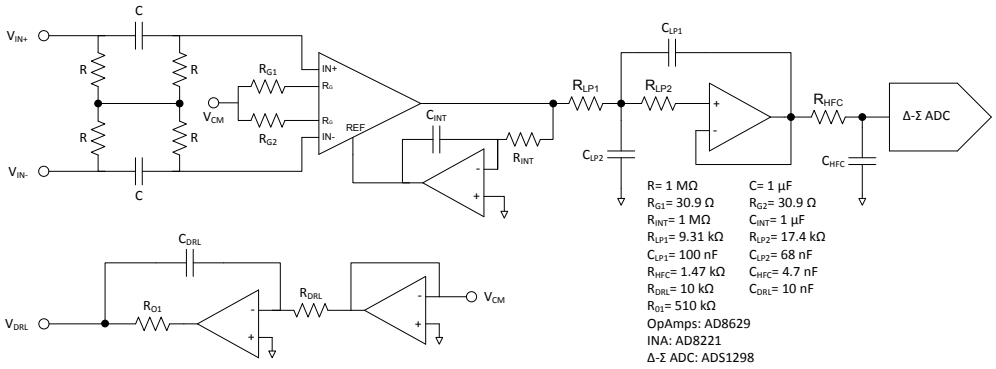

Figure 2.3 Schematic of a dedicated EEG channel.

Figure 2.3 shows the schematic of a single, dedicated EEG channel, along with the *Right Leg Driver* (RLD) circuitry.

A common approach for bio-potential measurements exploits DC-coupled Instrumentation Amplifiers (INA) or equivalent circuits; operating such devices at a high gain would maximize the Common Mode Rejection Ratio (CMRR), while minimizing the equivalent input referred noise. However, due to electrode offset voltages, the overall gain in this configuration is limited to moderate values. This situation is more critical for low-voltage, battery powered applications. Therefore, in order to obtain high gain from the first stage of the bio-potential amplifier, AC-coupling is needed.

In [109], a simple, passive AC-coupling network is presented (the *RC* input network shown in Figure 2.3, before the *Analog Devices AD8221*[8] INA), which provides input differential signals with AC-coupling, while maintaining a DC path for bias currents (draining to ground through the amplifier's common electrode). Since the coupling network is ungrounded, if a common mode input voltage is applied, no current flows through the

[8] http://www.analog.com/en/specialty-amplifiers/instrumentation-amplifiers/ad8221/products/product.html

network (there is no common-mode current path), keeping all nodes at the same potential and thus ideally yielding an infinite CMRR. In practice, however, several factors actually limit the total CMRR, such as grounded impedances (e.g. the INA's input capacitance), or unbalanced electrode impedances. Considering the differential mode, and assuming $\tau_1=RC$, the transfer function of the network is:

$$G_D(\mathrm{s}) = \frac{s\tau_1}{1+s\tau_1}\,. \tag{2.1}$$

As discussed in [110], the noise contributed by the circuit, integrated over the EEG band is, approximately:

$$e_{n0}{}^2(\mathrm{s}) = \frac{4kT}{\pi C}\ [\mathrm{V}^2]. \tag{2.2}$$

From equation (2.2), in which k is the Boltzmann constant and T is the temperature (in Kelvin), it follows that minimizing the noise implies maximizing C, compatibly with practical implementation constraints.

While such input coupling network effectively gets rid of differential DC voltages, originating from the electrodes, the op-amps (or INA's) input common mode voltages are still present, and can significantly reduce the output dynamic range. Moreover, the thermal noise of input resistors (from DC up to the corner frequency $f_{c1}=1/(2\pi\tau_1)$) and the INA's input voltage noise are amplified as well. Since the input network itself exhibits a high-pass behaviour, excluding any information below f_{c1}, it is thus convenient to suppress the INA's low frequency gain; this can be easily accomplished by putting an integrator in the INA's feedback loop, driving the reference pin (REF) [111]. The resulting transfer function, accounting for the input coupling network and the AC-coupled INA, becomes:

$$H_{INA}(\mathrm{s}) = A_{V0}\,\frac{s\tau_1}{1+s\tau_1}\,\frac{s\tau_2}{1+s\tau_2}, \tag{2.3}$$

where A_{V0} is the amplifier's gain, set by resistors R_{G1}, R_{G2}, as specified in [111], $\tau_2=R_{INT}C_{INT}$ is the time constant introduced by the feedback integrator. In our design, the INA's gain, A_{V0}, was set to 800.

Also, not shown in Figure 2.3, for image clarity purposes, a passive RFI protection filter is placed at the INA's inputs, as in [111].

After amplification by the INA, the signal is low-pass filtered by a second-order, unit-gain Sallen-Key filter [112] with a cutoff frequency of 250 Hz: this value was chosen in order to keep the board suitable for a wider range of bio-potentials, including, for instance, ECG. A Bessel response was selected, maximizing phase response linearity, in order to better preserve the wave shape.

The RLD circuit is introduced to improve common mode noise rejection [33],[108],[113]. The input common mode voltage is sensed at node V_{CM} connecting gain-setting resistors R_{G1} and R_{G2}, it is buffered and then fed to an integrator, which gains and invert the signal, feeding it back to the patient's body as a reference voltage. This feedback, which attempts to minimize the error between a reference, fixed voltage, and the measured, noise-corrupted common mode voltage, is also exploited to generate a virtual ground for single supply operating mode (in this case the reference voltage is set at mid supply). Otherwise, reference voltage is set to ground.

Digitalization is performed at the end of the analog signal chain by a 24-bit ADC (the aforementioned *TI ADS1298*). Without any of the pre-amplification stage, the noise contributed by the sole ADC (0.4 μV_{rms}) would have violated the specifications we set; with the implemented solution, noise measured at board level (i.e. with contributes of active components and layout non-idealities) was found to be less than 1.8 μV_{pp}, which falls within the desired specifications.

Examples of acquired waveforms (FFT of alpha rhythms with eyes open/closed comparison and PSD estimate of a SSVEP response) are reported in Figure 2.4.

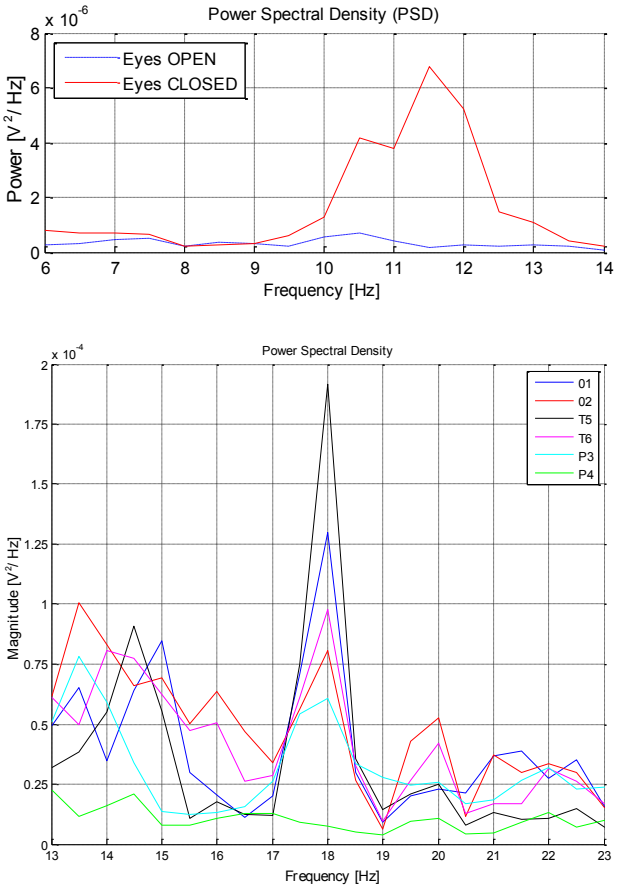

Figure 2.4 (*top*) PSD comparison of EEG acquired from location Fp1 with eyes open (*blue*) and closed (*red*): the alpha band has significantly more power in the latter case (due to alpha rhythms); (*bottom*) example of a PSD estimate of an 18 Hz SSVEP

2.2.2 Layout and general considerations

When designing low-noise PCBs, careful layout planning is essential for guaranteeing optimal performance. For this reason, digital and analog domains were partitioned, thus avoiding mutual interference between return

currents. Split planes are tied and referenced to the same potential in a single point, near the ADC, by means of a ferrite filter.

The board was manufactured with a standard 4-layer PCB process, and solid ground/power planes were used to ensure the lowest possible impedance and voltage uniformity. A similar technique was used for the reference voltage.

A stable supply and reference voltage is capital in high-precision, low-noise analog circuitry; therefore careful supply and reference filtering and bypassing techniques were applied. Noise and transients coupled on these voltages can, in fact, leak from the supply into the active components. Even though attenuated by the device's *Power Supply Rejection Ratio* (PSRR), noise in supply can still affect the performance of analog circuitry for high-precision and high-resolution sensing. For this reason, power from the batteries is filtered through a series, low-noise, *Low DropOut* (LDO) regulator. Moreover, in order to improve filtering and stability of the supply and reference voltage across the whole PCB, careful bypassing techniques were implemented [114], both at the local level, as well as at the global one.

2.3 Digital domain

2.3.1 Hardware control and interfacing

As mentioned in the introductory chapter, digital signal processing is currently carried out by a MATLAB-based platform, running on a personal computer, thus allowing faster design and tuning of algorithms, suitable for subsequent embedded implementation. To complete the test environment, we hence needed to connect the AFE and the PC. A Teensy 3.x development board, based on an ARM Cortex-M4 micro-controller, is

exploited for managing and supervising communication. Main tasks of such board include:

- Communication: data coming from the ADS1298 are acquired through a SPI (*Serial Peripheral Interface*) port and routed to the PC through a high speed (12 Mbps) virtual COM port, emulated over USB. Furthermore, USB is isolated via an external dedicated module, in order to effectively untie the user from the PC ground.
- Power-Up sequencing of the converter, needed to guarantee proper initialization.
- Conversion stream management: data must be read from the ADS1298 after each conversion is completed. Conversion results are then encapsulated into structured data packets (containing a given number of conversions, in order to maximally exploit the communication bandwidth), allowing some sort of flow-control on the MATLAB side.
- On-the-fly AFE parameter management: the user can specify several AFE parameter directly from MATLAB, such as, for example, ADC's gain or data rate, initial state and many others.
- Management of GPIO (*General Purpose I/O*) pins; 8 digital pins are exposed to the user, in order to capture asynchronous triggers and events, allowing for synchronization of EEG waveforms and user markers.

The microcontroller was programmed with the C++ programming language, using the *Object-Oriented Programming* paradigm. The code is broken into elementary blocks, implemented as classes, in order to allow maximal interoperability and scalability.
In particular, one class provides the abstraction of the physical ADC chip (e.g. the *ADS 1298* or, as in the second hardware release, the dual *ADS1299* solution), implementing methods for proper device setup and handling. A generic ADC class provides the abstract interface to which the underlying ADC class should comply; this class is, in turn, controlled by another one,

called *scheduler*, which constantly waits for user commands and calls the *data streaming* class whenever data are ready to be transmitted. This last class implements the data transmission; in order to guarantee high-bandwidth, a double-buffering scheme is implemented, and conversion results are transmitted in groups to maximize efficiency.

2.3.2 Handling and displaying the data stream in Matlab

Data from the USB comes into a twos complement, 24-bit format (the ADC native one); as soon as a data block transfer is completed, it is converted to a voltage reading via the following formula:

$$v_{sample} = \frac{ADC_{code}}{2^{(ADC_{res}-1)} - 1} ADC_{ref} \text{ [V]}, \tag{2.4}$$

where ADC_{res} is the resolution of the ADC (24-bit), and ADC_{ref} is the reference voltage. During this phase, data are vectorized and organized into matrices, in order to speed up further processing. From now on, columns will represent electrodes and rows their temporal evolution.

After vectorization, data can be processed in real-time and, in parallel, stored. In order to maximize the efficiency of disk access, data are dumped in larger blocks, and the flexible *HDF5* data format is used. Double buffering is implemented in this case as well.

Without going into the details of the signal processing, which will be covered in Chapter 3 and 4, data are pre-processed and fed to the GUI, where they are displayed as real-time temporal waveforms, as well as PSD estimates, as shown in Figure 2.5. Here, the output of the classification is also displayed, and several interface buttons allow the user to manually trigger software markers, as well as to stop the ongoing signal acquisition.

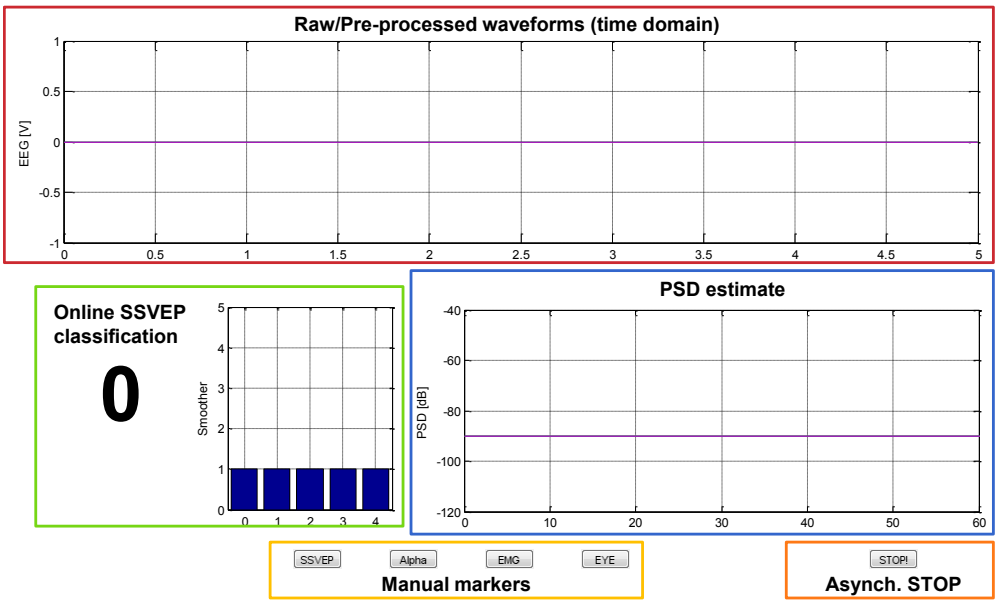

Figure 2.5 Snapshot of the Matlab-based GUI.

2.4 Cap and materials choice

Various commercial, pre-cabled caps exist, which can be purchased independently of the EEG hardware. However, the cost of such solutions, even in minimal 21 lead setups, is quite high (typically greater than 350 $), especially if compared to the targeted hardware costs.

We thus decided to build an elastic electrode support, as shown in Figure 2.6. Disposable Ag/AgCl disk electrodes (approximate price: 0.10 $, each) are held in place by this cap (a plastic ring cup surrounds the electrode, for gel containment), and they are attached to cables by means of snap clips. The cap is modeled, as far as the transverse bands are concerned, on a standard 10/20 electrode montage.

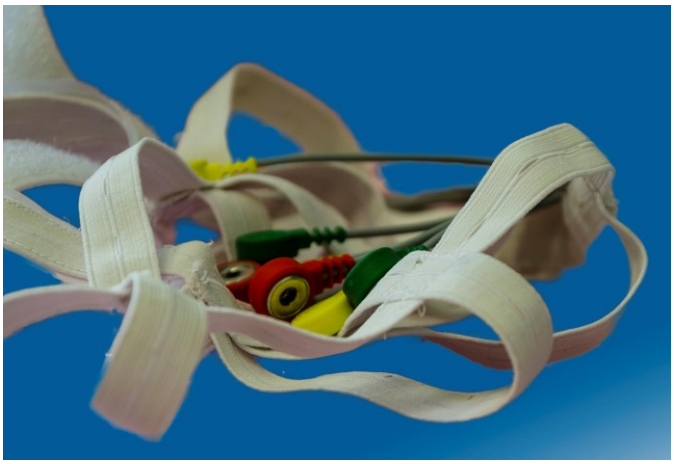

Figure 2.6 Photo of the elastic cap, along with the snap leads.

Electrode cables (approximate price: 10 $, each) depart from the cable, grouped together, and bring the signal to the EEG module. Male (cable) and female (board) connectors are based on standard DIN 42802 (1.5 mm) safety connectors, a format commonly encountered in EEG hardware.

2.5 Improving the EEG module: release 2

2.5.1 What needed to change… and how it changed

The first release of the EEG module was used, as we will see, to collect most of the data for the offline analysis. However, experience suggested some improvements could be made, such as:

- More EEG input channels, in order to pursue a more general purpose approach.

- Dimension shrinking. This could mean opening to portable and mobility scenarios, where bulky equipment could represent an obstacle to practical use of BCI.
- Technological improvement. Texas Instruments released a newer high-precision ADC (*ADS1299*[9]) in late 2012: this chip dramatically improves RTI noise, to the extent that it can, in principle, be used without any external pre-amplification stage (using just the low-gain, built-in one), thus saving space on the PCB and allowing to design more compact AFEs.
- More reliability. High-gain stage could quickly saturate in case of artifacts or deteriorating contacts. Using a lower gain could improve this situation, since a wider dynamic range would be possible. This is possible via the *ADS1299* technological improvement introduced above.

Considering all these aspects, a new release of the EEG module was realized, with the following results:

- 16 input channels, achieved by paralleling of two *ADS1299* ADCs (a master, who sets the sampling clock, and a slave). This channel number (or multiples of it) is commonly encountered in commercial EEG devices. Having 16 channels available, with respect to just 6, allows to study and exploit a wider spectrum of possible BCI protocols.
- Reduced dimensions: 13x10 cm. This was possible thanks to two main factors: *(i)* elimination of the pre-amplification stage, thanks to the new *ADS1299* chip; *(ii)* adoption of a unipolar supply scheme (0-5 V). This latter point allowed to remove the negative power section, saving space and improving energy efficiency. It also greatly simplified the power bypassing scheme, cutting the required capacitor number by half. Moreover, power for the analog and digital (3.3 V) part is now drawn from a single battery pack (4x AA

[9] http://www.ti.com/product/ads1299

alkaline batteries), thus allowing a more compact module, also in terms of enclosing package.

- Production costs, in large scale, are in the range of 300 €.
- Power consumption (including efficiency of the power section): 162 mW. With respect to the previous release, this results in approximately 45% less power per EEG channel.
- Superior noise performance (< 1.3 μV_{pp}), as it will be shown next.
- Improved input dynamic range. With a maximum applied gain of 24, the input range is now wider, allowing to record more consistently the EEG in the presence of artifacts. In particular, the full-scale differential input range is given by:

$$v_{d,max} = \frac{\pm V_{REF}}{G} \text{ [V]}, \tag{2.1}$$

where V_{REF} is the ADC reference voltage (4.5 V, in our case), and G is the applied input PGA (*Programmable Gain Amplifier*) gain (typically, 24 or 12). Setting $G = 24$, for example, yields, approximately, a ±188 mV input dynamic range.

As far as layout is involved, the general considerations about power supply bypassing in §2.2.2 still apply. However, this time a different technique was exploited for internal planes design. Since, in this case, there is more than one mixed-signal device (i.e., the two parallel ADCs), it would not be possible to adopt the split ground planes approach, as it would not be possible to place the common reference point close to both devices. This problem is even more evident with a higher number of devices. In these cases, following the approach in [115], a solid, continuous ground plane is kept below such devices, shared with the analog section. The important factor is to try to keep digital and analog return currents well separated by avoiding crossings over different planes, and by carefully designing the bypass scheme to reduce the return current loop areas (and consequent overlaps). For the supply planes, instead, the same internal layer was used, splitting between digital and analog supply isles.

A high-level scheme of the new module is reported in Figure 2.7, while Figure 2.8 shows a picture of the realized PCB. Complete schematics and production files are reported in the Appendix.

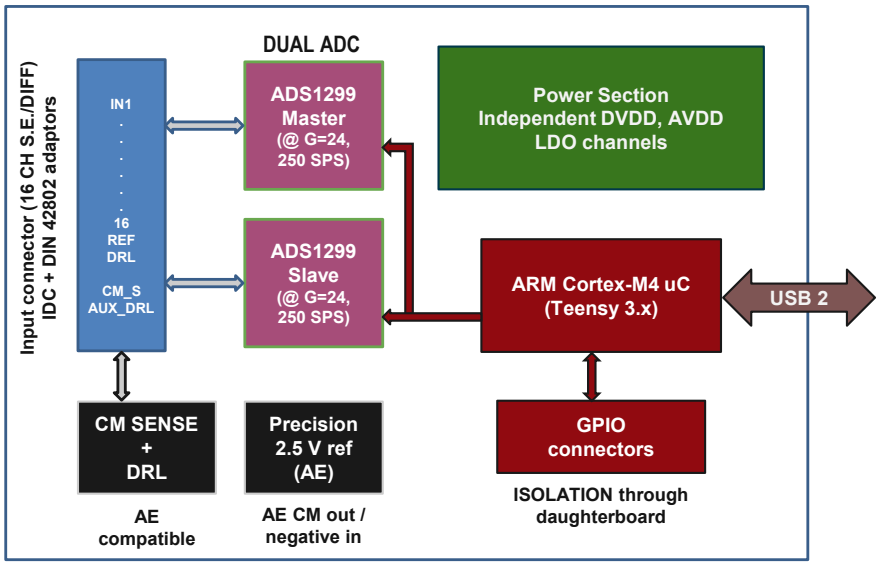

Figure 2.7 High-level schematic of the EEG module – release 2.

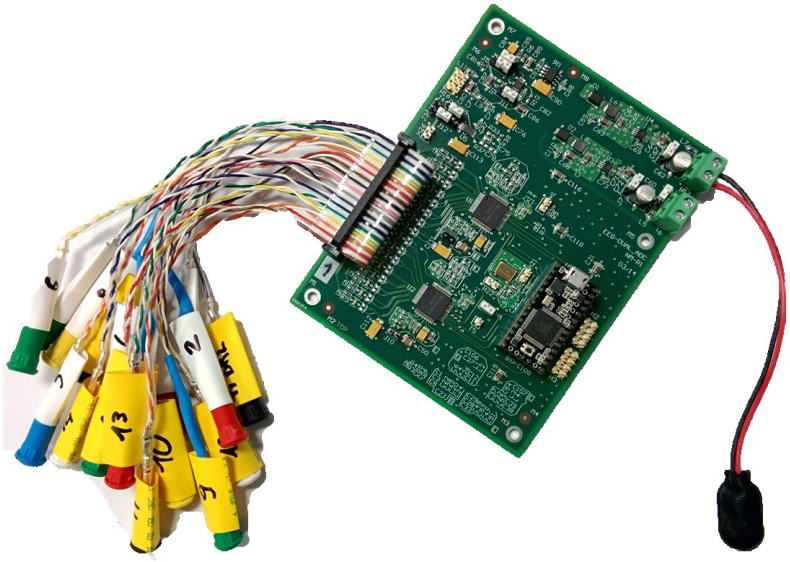

Figure 2.8 Photo of the EEG module – release 2, along with DIN 42802 input connectors.

2.5.2 Validation and comparison with a high-end EEG unit for BCI

In order to validate the new EEG module, and assess its performance, several tests were performed. At first, "static" performance was checked, characterizing input noise, and observing signals from a deterministic source. Then, "dynamic" tests were performed, checking for biological artifacts and reproducing a simple P300 experiment. Such results were compared with a commercial, high-end device (*g.tec*[10] *USBamp*[11]).

(a)"Static" performance

The first test consisted in, simply, reading a known, deterministic signal, namely, a 10 Hz sinusoidal waveform, generated with a g.tec test signal generator. However, this was more of a qualitative test, since a precise characterization of the generator was not available. We could think of this test as a sanity-check for the device; nonetheless, signals were recorded with the *USBamp* as well. The experiment parameters are the following, where *DUT* (*Device Under Test*) indicates the realized EEG module:

- $20\mu V_{pp}$, 10 Hz sinusoid (actually, 10.1 Hz from measurements with both devices).
- At least 120 s records.
- PSD resolution: 0.1 Hz.
- g.tec: 512 SPS, analog 50 Hz notch.
- DUT: 250 SPS, no filtering applied.

As it can be seen in Figure 2.9, both devices effectively capture the 10 Hz tone. The *USBamp* exhibits a sharp tone at 150 Hz, almost 14 dBm lower than the carrier. On the other hand, *DUT* is affected by 50 Hz noise (approximately -32 dBm lower than the carrier), as well as 10 Hz harmonic

[10] http://www.gtec.at/
[11] http://www.gtec.at/Products/Hardware-and-Accessories/g.USBamp-Specs-Features

noise (≈-31 dBm below the carrier), which is probably due to noise generated by USB data packet bursts. In future implementations, to correct this effect, the digital isolation stage will be inserted between the ADC and the microcontroller, instead of only on the USB side. Nonetheless, signal quality appears good, as shown next with the noise test.

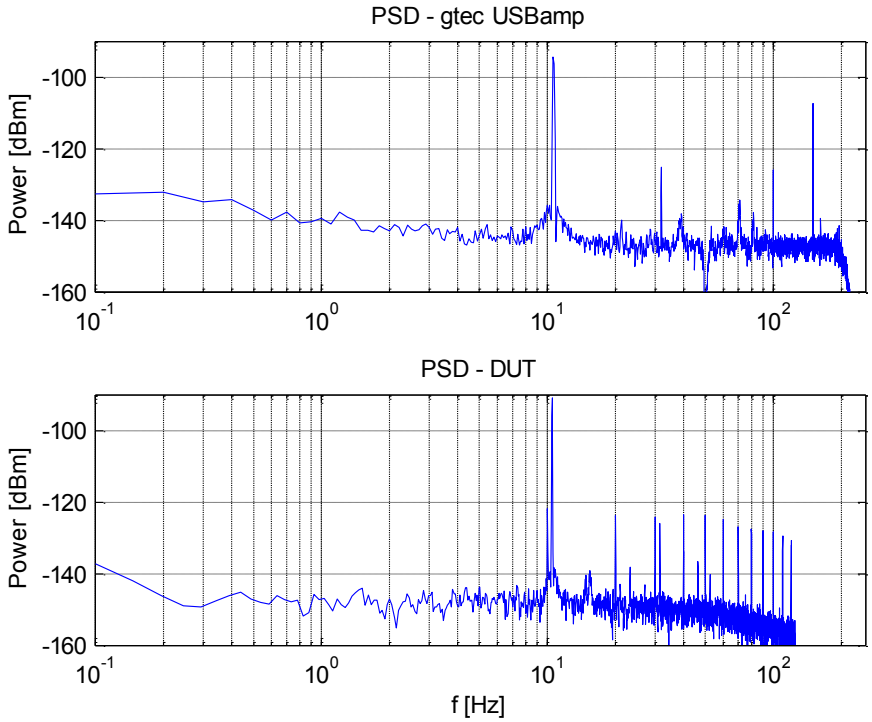

Figure 2.9 PSD comparison of g.tec USBamp (*top*) and the EEG module (*DUT, bottom*) when a 10 μV_{pp}, 10 Hz is applied.

The second test which was performed in "static" condition is a noise test. In order to account for all sources of noise within the PCB (e.g. ADC, layout non-idealities), the measurement is taken as follows:

- Input terminals (the exposed board connectors for the electrode cables) are short-circuited with jumper cables.

- Input waveforms are acquired for at least 120 s, with the same device settings in the previous test.
- Once the mean is removed (offset), any non-zero value is due to noise.

Characterization of such noise can then be performed, e.g. by extracting a PSD estimate (Figure 2.10), or by comparing RTI peak-to-peak/rms values. In addition, in order to make a fair comparison, noise integrated over the [0-40] Hz was extracted for both devices, from their PSD. Such comparisons are summarized in Table 2.1.

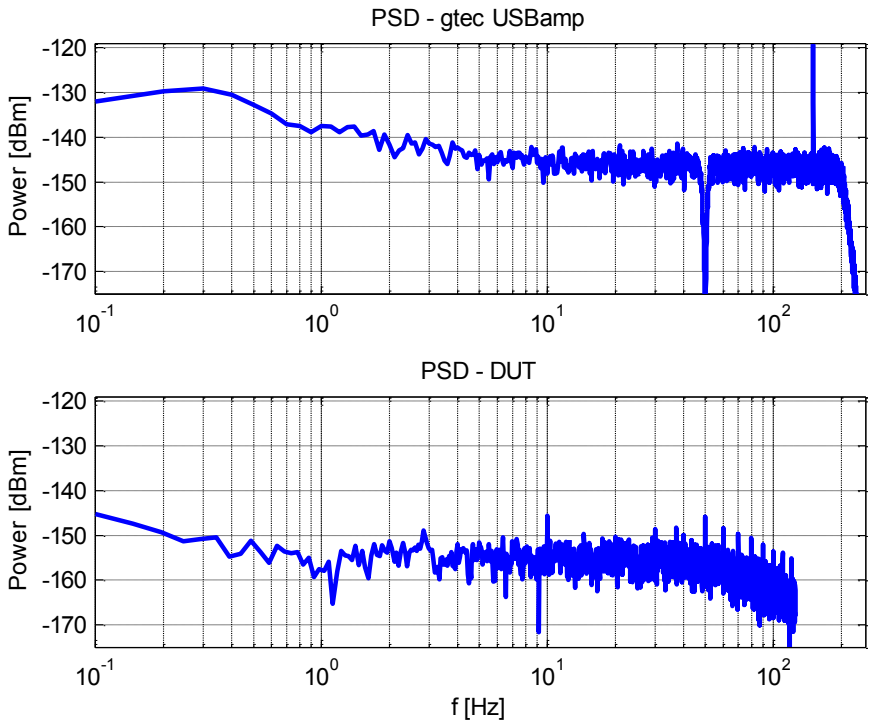

Figure 2.10 PSD comparison of noise acquired with a g.tec USBamp (*top*) and the EEG module (*DUT, bottom*).

Table 2.1 Summary of noise test comparisons (all values are RTI)

	rms [μV_{rms}]	**peak-to-peak [μV_{pp}]**	**[0-40] Hz [μV_{rms}]**
USBamp	0.87	7.16	0.42
DUT	0.17	1.27	0.09

As it can be seen, the *DUT* performs very well in terms of electrical noise specification, meeting all the requirements. In particular, referring to Figure 2.10, the trends found in the 10 Hz test are confirmed. Noise performance of the *DUT* is remarkable, even better, to some extent, than the reference device. The new EEG module also improves over the previous release, achieving a maximum 1.27 μV_{pp} vs. 1.8 μV_{pp} RTI noise. Overall, the *DUT* proves to be a valuable tool for low-level signal studies.

(b)"Dynamic" performance

All previous tests were done with a very controlled procedure: no user was, in fact, connected to the EEG, thus all noise sources other than electrical were not being considered. The following tests are aimed at assessing the usability of the EEG module as a tool for physiological investigation.
The first "dynamic" test we performed (only on the *DUT*) is, again, comparable to a sanity-check: 6 electrodes were connected in FP1, FP2, P3, P4, O1, O2 locations. Standard artifact-checking tasks were accomplished by asking the users to blink or to grind (for generating EMG artifacts); example waveforms are reported in Figure 2.11. Also, alpha burst rhythms were generated by asking the users to close their eyes: oscillations start to build up in the [8-13] Hz band, and are clearly visible, for example, in Figure 2.12. These sanity-checks allow to confirm that the *DUT* is actually recording physiological data.

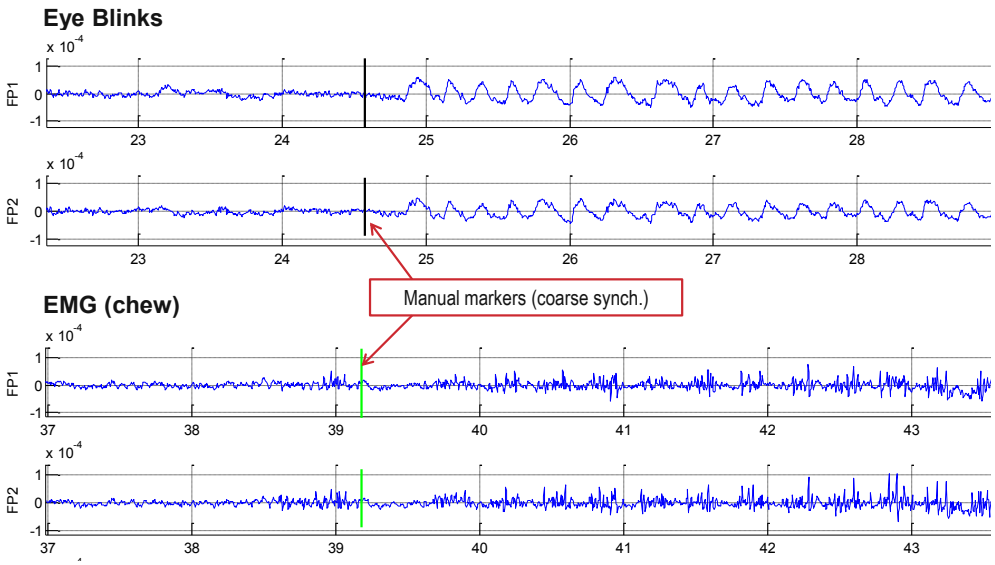

Figure 2.11 EEG waveforms acquired from FP1 and FP2 locations in presence of eye-blinking artifacts (*top*) and EMG artifacts generated by grinding (*bottom*). Manual markers very coarsely indicate when the user was instructed to perform those actions.

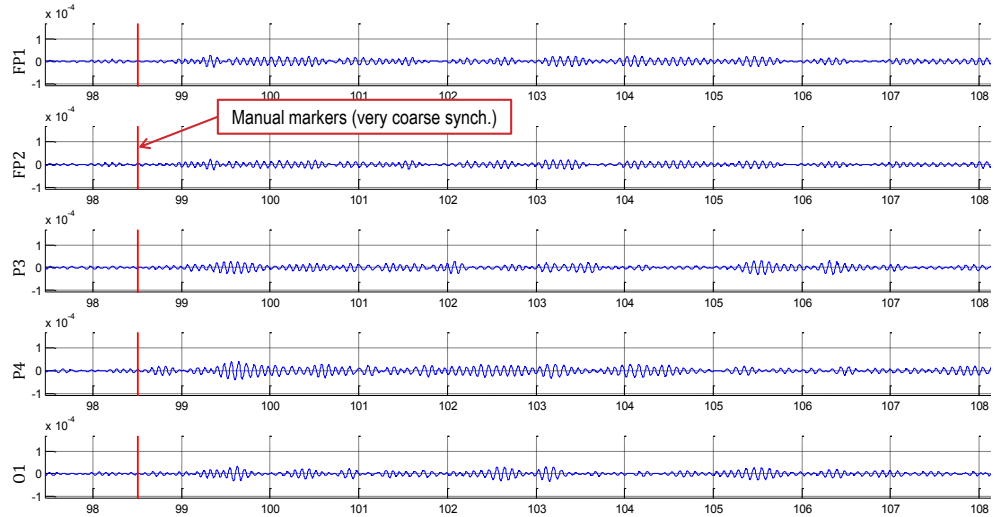

Figure 2.12 EEG waveforms acquired from FP1, FP2, P3, P4, O1 locations in presence alpha burst ([8-13] Hz band-pass filtered). Manual markers very coarsely indicate when the user was instructed to perform those actions.

A more quantitative test, comparing the *DUT* and the *USBamp* was performed using a *P300*-based protocol. The procedure aims at assessing if the waveforms acquired with the *DUT* and the *USBamp* are consistent one-another. In particular, it was devised as follows:

- Two subjects participated to this test, totaling 12 runs
- P300 responses are elicited by asking the users to silently count how many green squares (*target*) appeared within a stream of red squares (*non-target*).
- Each run consisted of 10 series of 23 flashes of target ($p_{target}\approx 0.13$) and non-target stimuli.
- In order to make a comparison, EEG was recorded using the same electrode set and cap, alternating the recordings by simply switching the connectors in an interleaved scheme (e.g.: run1 *USBamp*, run2 *DUT*, etc.). Direct, parallel acquisition was not possible due to different device bias, which would have interfered.
- Acquisition parameters are similar to the previous "static" tests.
- EEG data are pre-processed by band-pass filtering in the [1-16] Hz band and by applying a CAR filter.
- Analysis of the waveforms, assessing the statistical significance of the difference between target vs. non target waveforms, was carried out for both the *USBamp* and the DUT.

An example of such comparison, representative of the many others, is shown in Figure 2.13. As it can be seen, both devices are consistent, predicting good separability between *P300* and *null* response in similar time intervals.

This allowed us to conclude that the realized AFE does not introduce significant noise or bias, when compared with a high-end, reference device, and can, therefore, be equivalently used in BCI experiments.

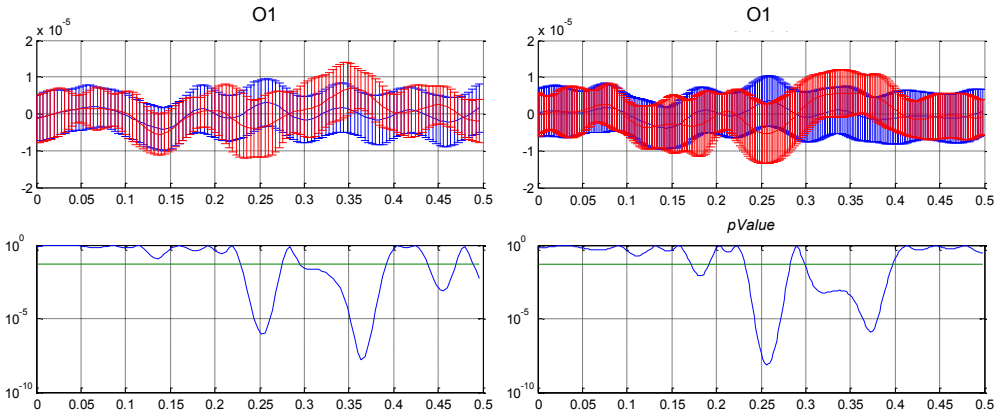

Figure 2.13 P300 test comparison: *USBamp* (*left*) and *DUT* (*right*). In the *top* figures, mean time domain waveforms are displayed (*solid line*), along with their standard deviations (*bars*). P300 responses are drawn in *red*, non-target responses in *blue*. In the *bottom* figures, the logarithms of *p-values* (extracted with a two-sample *t-test*) relative to difference between target and non-target distributions are reported; the *green* line represent the 5% significance level

2.6 Future development: active electrodes

It is possible to introduce an improvement in our design, should the passive electrode technology not fit a particular application (e.g. where noise pickup or mechanical artifacts are expected to be higher). This can be achieved via an active electrode pre-amplification. A possible scheme for this purpose is shown in Figure 2.14.

This circuit is designed to yield a differential output ,achieved with a second INA as a feedback driver for the first INA's reference pin; this differential output can be directly fed to the EEG module. The advantage of such a mechanism is that differential signaling is more robust to noise. However, we still need to bring the negative input voltage to each active electrode: any imbalance or differentially coupled noise would not be rejected by such differential mechanism. Nonetheless, this consideration still applies to

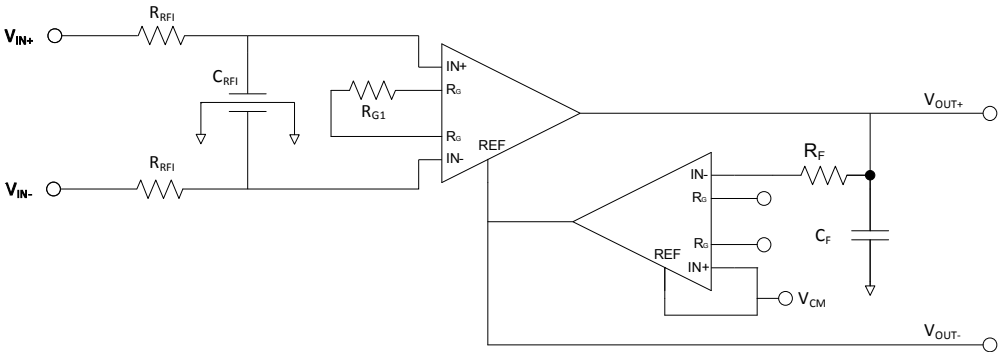

Figure 2.14 Possible schematic of an active electrode (just the pre-amplifier; boundary, passive components are not shown for image clarity purpose).

unipolar leads: in the end, all measurements are differential, and differentially coupled noise poses equal problems.

Also shown in the picture are the input RFI filter (resistors R_{RFI} and the "X2Y capacitor" C_{RFI}), and a compensation network for the stability of the feedback loop (R_F and C_F). This design requires that a supply, ground, reference and a common mode voltage (these last two can coincide) be brought to the active electrode.

Many other examples of active electrode circuits are found in literature. In particular, in [116], a two-wire active electrode is presented. A constant supply-current feedback is established for signaling, and the resulting differential voltage for keeping such constant supply is read by an INA in the ADC module.

Chapter 3

Building the BCI: offline signal processing

In Chapter 2 we covered the realization of the hardware infrastructure for the BCI. Now, the signal processing will be analyzed. In particular, in this chapter, the initial *offline* studies will be presented, which will serve as a starting base for the development of the *online* part, presented in Chapter 4.
At first, a naïve approach for SSVEP classification, based on PSD analysis, is presented. Then, in order to improve performance, methods from the literature are presented, namely: MEC (*Minimum Energy Combination*), AMCC (*Average Maximum Contrast Combination*) and CCA (*Canonical Correlation Analysis*). In addition, two methods we developed will be presented, aiming at improving the computational efficiency. Finally, the performance of each method will be compared.
One thing, indeed, is in common to all these methods: the calibration-free operation. As a consequence, such methods must adapt to all users; their performance will be, thus, evaluated on the whole sample population basis rather than on a per-user basis.

3.1 A naïve approach based on PSD analysis

The very first approach towards a calibration-less SSVEP classification algorithm was based on a simple PSD analysis, adding *ad hoc* heuristics to improve accuracy.

As a first step, a preliminary screening session was conducted to determine the most detectable frequencies on average, by analyzing the PSD estimated of the EEG raw channels (O1, O2, P3, P4, P5, P6). Volunteers were shown one stimulus frequency at a time, selected in the range [16-30] Hz in steps of 2 Hz. By visual inspection of the waveforms and by subsequent automated classification, based on the algorithm introduced above, the best frequency range was selected [16-22] Hz. Actually, even larger SSVEP peak amplitudes were observed at lower frequencies, in the alpha band region. However, if other frequencies were to be considered, the alpha rhythm could mislead the classification algorithm and produce high false positives occurrences, due to its relatively large amplitudes. Moreover, exploiting higher frequency flickering stimuli turned out to be more comfortable for the user, resulting in less visual fatigue. At the high end of the inspected range, [26-28] Hz stimuli were not clearly discriminable in every subject, resulting in generally lower amplitudes.

Subsequently, a four-choice classifier was set up as follows. Data are pre-processed by a [14-24] Hz band-pass filter. Then, PSD features are extracted for each channel. Before classification, such features undergo a further transformation, aimed at improving the classification algorithm's robustness with respect to inter-channel variations, for instance due to impedance imbalance. To this purpose, the estimated channel power spectrum is integrated over a given frequency interval, depending on the actual frequency range of the SSVEP stimuli (for example, 1 Hz below and above the considered SSVEP frequency range) and the channel powers are then equalized over this bandwidth. Such normalization improves the classification robustness by somehow self-adapting to variable scenarios. The classification algorithm, then, exploits the a priori knowledge of the actual set of stimulation frequencies, checking the conditions only on such set: the channel powers are summed at each target frequency. Candidate targets are selected whenever a given fraction (e.g., at least 50%) of the channels exhibit a local maximum in the PSD at the target frequency. Then, candidates are compared; a two-step procedure has been devised: if a single candidate exists, the power of which exceeds all the remaining ones by a

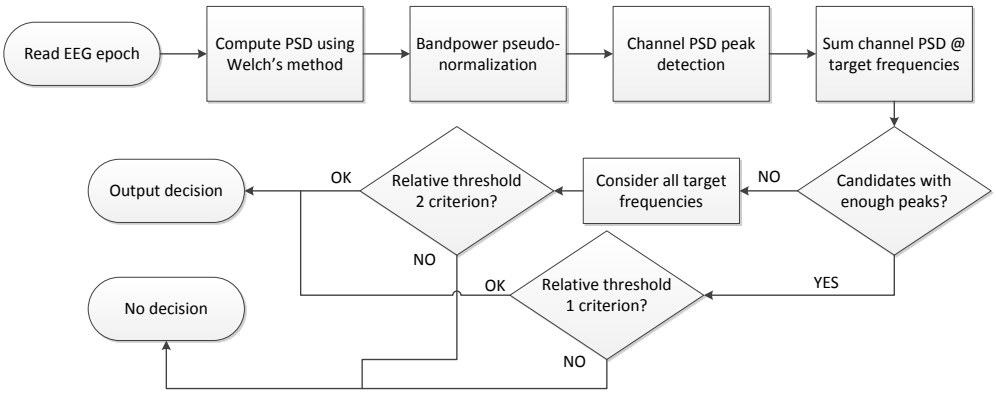

Figure 3.1 Workflow of the PSD-based classification algorithm.

given threshold, the decision is made. Otherwise, a more selective comparison is carried out, considering all the target frequencies as candidates and raising the threshold. The described algorithm is summarized in Figure 3.1.

The aforementioned algorithm was tested in a 4-class choice scenario: 4 simultaneously flickering LEDs were shown, each one at a different frequency in the {16, 18, 20, 22} Hz set. EEG was acquired for 6 s; the algorithm was then run on each epoch, to classify the attended frequency. The observed EEG window was varied between 3 s, up to the whole 6 s, and the Welch's window for PSD estimation was set to 2 s, with a 50% overlap factor. Accuracy and theoretical ITR (*Information Transfer Rate*) were then calculated, the latter according to the definition in [1]:

$$\begin{aligned} \text{ITR} &= \\ &= M\left[\log_2 N + P\log_2 P + (1-P)\log_2\left(\frac{1-P}{N-1}\right)\right] \text{[bit/min]}, \end{aligned} \tag{3.1}$$

where M is the number of trials per minute, N the number of possible choices, and P the classification accuracy. Table 3.1 lists the average accuracy and ITR that were achieved over the 4 users. As it can be seen,

Table 3.1 Average accuracy and ITR for the naïve PSD-based algorithm.

	3 s	4 s	5 s	6 s
Accuracy	90.8	91.0	93.3	94.7
ITR	28.35	21.59	18.91	16.49

accuracy improves with increasing observed windows; on the other hand, spending more time in taking a decision implies less choices per minute, i.e. lower *M*, thus lower ITR. Nonetheless, accuracy is high, which is very important, considering the targeted application

3.2 Improving signal processing: methods from literature

The aforementioned method works fine in terms of accuracy; still, some improvements can be made, especially in terms of responsiveness. This could improve the user's comfort: less time in making a decision means less time spent observing a flickering stimulus, thus lowering eye fatigue.

We started from studying popular SSVEP processing methods from literature, all calibration-less, namely: MEC (*Minimum Energy Combination*), AMCC (*Average Maximum Contrast Combination*) and CCA (*Canonical Correlation Analysis*).

Minimum Energy Combination [117] attempts to find an optimal spatial filter from minimizing an estimate of the noise. In particular, the voltage time series of a single electrode $y_i(t)$, can be modeled as:

$$y_i(t) = \sum_{k=1}^{N_h} \left(a_{i,k} \sin 2\pi k f t + b_{i,k} \cos 2\pi k f t\right) + E_i(t)\,, \qquad (3.2)$$

where the first term is the model of a SSVEP response corresponding to a stimulus frequency f (considering up to N_h harmonics), and $E_i(t)$ is a noise and nuisance signal. Given an EEG epoch of N_t samples, the input signals from the N_y electrodes can be represented as a matrix $\boldsymbol{Y}$ of size $N_t \times N_y$, whose columns are the potential readings from each electrode site. In the same way, we can represent the SSVEP term in equation (3.2) as a multiplication between a SSVEP information matrix $\boldsymbol{X}$ having size $N_t \times 2\,N_h$, containing N_h (*sin*, *cos*) column pairs, and a weight matrix G of size $2\,N_h \times N_y$, containing all the $a_{i,k}$, $b_{i,k}$ coefficients. Equation (3.2) then becomes:

$$Y = XG + E\,. \tag{3.3}$$

To extract discriminant information, signals from the electrodes are combined with appropriate weight vectors $\mathbf{w}=[w_1, \ldots, w_{Ny}]^T$. New channel vectors $\mathbf{s}$ of length N_t are then obtained as:

$$s = \sum_{i=1}^{N_y} w_i\, y_i = Yw\,, \tag{3.4}$$

which generalizes to N_s channels as follows:

$$S = YW\,, \tag{3.5}$$

where $\boldsymbol{S}=[\mathbf{s_1}, \ldots, \mathbf{s_{Ns}}]$ represents the set of channels and $\boldsymbol{W}=[\mathbf{w_1}, \ldots, \mathbf{w_{Ns}}]$ is the corresponding weight matrix.
Then, MEC proceeds as follows: at first, an orthogonal projection is used to remove any potential SSVEP activity from the recorded signal:

$$\tilde{Y} = Y - X(X^TX)^{-1}X^TY\,. \tag{3.6}$$

$\tilde{\boldsymbol{Y}}$ then approximately contains only noise, artifacts and background brain activity. An optimal set of N_s weight vectors $\hat{\mathbf{w}}$ must be then chosen such that the energy of the signal $\tilde{\boldsymbol{Y}}$ is minimized:

$$\min_{\hat{w}} \left\| \tilde{Y}\hat{w} \right\|^2 = \min_{\hat{w}} \hat{w}^T \tilde{Y}^T \tilde{Y}\, \hat{w} \,. \tag{3.7}$$

As shown in [117], the optimal solution is the eigenvector $\boldsymbol{v_1}$ that corresponds to the smallest eigenvalue λ_1 of the matrix $[\tilde{\boldsymbol{Y}}^T\tilde{\boldsymbol{Y}}]$. The weight matrix is then composed using the eigenvectors, corresponding to the N_s smallest eigenvalues, sorted in ascending order:

$$W = \left[\frac{v_1}{\sqrt{\lambda_1}} \cdots \frac{v_{N_s}}{\sqrt{\lambda_{N_s}}} \right]. \tag{3.8}$$

N_s is selected by finding the smallest number k which makes the sum of the k smallest eigenvalues greater than 10% of the sum of all the eigenvalues. This can be interpreted as selecting the number of channels in such a way as to discard as close to 90% of the nuisance signal energy as possible.
Finally, features are extracted according to the following equation:

$$\hat{P} = \frac{1}{N_s N_h} \sum_{l=1}^{N_s} \sum_{k=1}^{N_h} \left\| {X_k}^T s_l \right\|^2 . \tag{3.9}$$

The process described so far is repeated for each stimulus frequency *f*, and a classifier picks the attended stimulus frequency.

Average Maximum Contrast Combination [118] is similar to MEC up to equation (3.6). It then attempts to maximize the SNR by optimizing the following equation:

$$\min_{\hat{w}} \frac{\hat{w}^T C_Y \hat{w}}{\hat{w}^T C_{\tilde{Y}} \hat{w}} \,, \tag{3.10}$$

where $\boldsymbol{C_Y}$ and $\boldsymbol{C_{\tilde{Y}}}$ are the covariance matrices of signals $\boldsymbol{Y}$ and $\tilde{\boldsymbol{Y}}$, respectively. Again, minimization of the generalized Rayleigh quotient in (3.10) yields optimal weight vectors which can be used to construct the weight matrix $\boldsymbol{W}$ accordingly.

Canonical Correlation Analysis [119] is a statistical method, generally used for finding the correlations between two sets of multi-dimensional variables. It seeks a pair of linear combinations (canonical variables, characterized by

weight vectors $\mathbf{w_x}$, $\mathbf{w_y}$) for the two sets, such that the correlation between the two linear combinations $\mathbf{x_L}=\mathbf{w_x}^T\boldsymbol{X}$ and $\mathbf{y_L}=\mathbf{w_y}^T\boldsymbol{Y}$ is maximized.

$$\max_{w_x, w_y} \rho = \frac{\mathrm{E}[x_L {y_L}^T]}{\sqrt{\mathrm{E}[x_L {x_L}^T]\,\mathrm{E}[y_L {y_L}^T]}} = \frac{{w_x}^T X Y^T w_y}{\sqrt{{w_x}^T X X^T w_x \; {w_y}^T Y Y^T w_y}}, \tag{3.11}$$

Then it finds a second pair, uncorrelated with the first one, that has the second highest correlation. The process continues until the number of pairs of canonical variables equals the number of variables in the smallest set.
CCA can be applied to SSVEP detection by attempting to maximize the correlation between the input signals $\boldsymbol{Y}$ and the SSVEP information matrix $\boldsymbol{X}$, for each stimulus frequency: As features for classification, the maximum CCA score of each stimulus frequency are used.

3.3 Two novel algorithms for SSVEP processing

Having reviewed the most popular algorithms in literature, on which several variants are developed, we now introduce two specific SSVEP processing methods we developed for our platform. Both are calibration-free.

(a) fCCA

The first method, called *fCCA* (*frequency-domain CCA*, to distinguish it from the CCA introduced above, which will be referred to as *tCCA* from here on), shares the same principle of tCCA, except that here we attempt to maximize correlations in the frequency domain.

It can be viewed as a merge of the PSDA and CCA methods. The main objective, as it will be explained later, is to improve the efficiency of the algorithm, while retaining the high accuracy featured by the tCCA method.

The algorithm works as follows. At first, the PSD of each EEG channel is estimated via Welch's method, as in a conventional PSDA; then, we attempt to maximize the correlation between the estimated PSDs and reference spectra via CCA. Such reference spectra are designed as sets of Kronecker delta functions, exhibiting a peak at either the stimulus frequency ($\delta(f_{stim})$) or its harmonics ($\delta(kf_{stim})$, $k = 2 \dots n$, n being the number of considered harmonics).

This also fosters the sparsity in the first canonical variable obtained from the input channels. The first, highest canonical correlation is taken as feature. Such procedure is carried out for all possible stimulus frequencies, and the one with the highest correlation coefficient is classified as the one eliciting the SSVEP.

It is important to remark that fCCA is performed on a fixed number of samples, defined by the frequency resolution of the PSD estimator. The preliminary PSD evaluation thus reduces the complexity of the CCA calculation, also helping in improving processing speed, since DFT (Discrete Fourier Transform) can be calculated in a very efficient way.

Since the classification is based on relative comparisons only, it is virtually independent of training and calibration procedures.

(b) maxDeltaVar

The second method, called *maxDeltaVar* [20],[22],[23], [120] is a simplified approach, aiming at efficiency, in terms of speed and memory usage. The basic idea is quite simple and stems from the first part of MEC and AMCC methods; first, a SSVEP information matrix $\boldsymbol{X}$ of size $N_t \times 2N_h$ is built for each stimulus frequency

$$X = = \begin{bmatrix} \sin 2\pi f t_1 & \cos 2\pi f t_1 & \cdots & \sin 2\pi N_h f t_1 & \cos 2\pi N_h f t_1 \\ \vdots & \vdots & \ddots & \vdots & \vdots \\ \sin 2\pi f t_{N_t} & \cos 2\pi f t_{N_t} & \cdots & \sin 2\pi N_h f t_{N_t} & \cos 2\pi N_h f t_{N_t} \end{bmatrix} \quad (3.1)$$

Then, input channels are normalized, in order to have the same variance. Projection on the space spanned by the sinusoidal components of $\boldsymbol{X}$ is performed to remove any potential SSVEP activity from the recorded signal, as in equation (3.6). The differences in variance before and after each projection, summed along all channels, are taken as features.

Such simplified feature extraction procedure involves fewer steps than previously mentioned methods; thus, it better suits future implementation on small embedded devices.

Classification identifies the stimulus frequency by looking for the $\boldsymbol{X}$ matrix which induces the larger decrease in the overall variance. As in the previous algorithms, the method uses relative comparisons, and no calibration phase is required.

3.4 Results: comparison of methods

In the following, the presented algorithms are compared. Comparison is, again, oriented to the specific aimed application, and based on *offline* classification accuracy (much relevant for control applications) and computational demand (in view of future embedded implementations). Computational performance is estimated, in the following, by looking at the mean algorithm execution times.

All the EEG waveforms were acquired in the context of a 4 class SSVEP experiment as follows: four healthy volunteers (age 22-27, with normal or corrected to normal vision) were asked to stare at one of the four simultaneous flickering LED while resting on an armchair at approximately 1 m from the visual stimulus. Each trial lasted for 6 seconds, and each LED presented a different stimulation frequency (16, 18, 20, 22 Hz); EEG was acquired at 250 SPS with our custom hardware unit (as per release 1, [21]) from 6 scalp locations (namely, position O1, O2, P3, P4, P5, P6 of the International 10-20 system), using standard 10 mm Ag/AgCl disk electrodes

with conductive paste (no particular skin preparation was performed, though).

All the algorithms were tested on the same EEG epochs. It is worth remarking that, since no user-specific calibration procedure is required, all of the EEG waveforms from different users were considered as a whole, seeking for a method suitable for general use, regardless of specific user's waveform features. This view is consistent with the goal of developing "Plug&Play" devices, suitable for basic AAL control purposes, and featuring ease of use and simple setup procedures.

Table 3.2 reports the average accuracies (and standard deviations) obtained with the presented methods. Results show that both our methods perform close to (or better than) reference methods. In particular, with respect to fCCA, maxDeltaVar seems to achieve higher accuracy over shorter EEG epochs ($p<0.02$), while fCCA needs longer time segments but is able to achieve better accuracy performance. In fact, fCCA performs better than all the other methods at the longest EEG windows ($p<0.05$), and behaves comparably with the best at 3 s segments (no statistically significant difference with respect to AMCC and tCCA). This is related to the fact that fCCA relies on PSD estimation via Welch's method, and the more sub-windows are averaged, the better the estimate is. The method maxDeltaVar, on the other hand, exhibits a more constant behaviour over varying window lengths, and performs very close to tCCA (no statistically significant difference in performance is noticeable up to the 4 s window length), or AMCC (no statistical significance up to 3 s windows, but better on the 4 s case, $p<0.01$).

It is also worth noting, though, that neither tCCA, fCCA, nor maxDeltaVar do perform any dimensionality reduction as MEC or AMCC do; however, in our scenario, where the number of electrodes is intentionally low for cost and comfort constraints, such step in processing does not appear as a large gain.

An indirect estimate of computational performance is given in Table 3.3 which reports the average execution time of the algorithms, when running

Table 3.2 Average accuracy (and std. deviation) vs. EEG window length for each algorithm.

	1.5 s	2 s	3 s	4 s
MEC	75.94 % (1.24 %)	78.02 % (2.63 %)	77.23 % (2.91 %)	73.76 % (2.92 %)
AMCC	88.02 % (1.89 %)	88.51 % (1.63 %)	91.09 % (1.04 %)	85.15 % (1.75 %)
tCCA	88.71 % (2.56 %)	90.30 % (1.86 %)	90.69 % (1.49 %)	90.20 % (2.11 %)
fCCA	81.39 % (2.18 %)	86.53 % (2.43 %)	89.50 (2.56 %)	91.49 % (1.56 %)
maxDeltaVar	87.33 % (3.02 %)	89.31% (1.53 %)	88.22 % (2.82 %)	87.72 % (1.42 %)

Table 3.3 Average (and std. deviation) execution time [ms] vs. EEG window length for each algorithm.

	1.5 s	2 s	3 s	4 s
MEC	3.18 (0.32)	4.72 (0.86)	11.00 (0.81)	23.09 (0.89)
AMCC	3.24 (0.28)	4.82 (0.79)	11.28 (0.85)	23.26 (0.81)
tCCA	2.37 (0.20)	2.54 (0.21)	2.68 (0.29)	2.85 (0.26)
fCCA	2.21 (0.27)	2.30 (0.28)	2.24 (0.27)	2.26 (0.29)
maxDeltaVar	0.62 (0.08)	1.64 (0.08)	2.90 (0.24)	4.38 (0.37)

Table 3.4 Cost/Performance index [ms] vs. EEG window length for each algorithm.

	1.5 s	2 s	3 s	4 s
MEC	4.19	6.05	14.24	31.30
AMCC	3.68	5.45	12.38	27.32
tCCA	2.67	2.81	2.96	3.16
fCCA	2.72	2.66	**2.50**	**2.47**
maxDeltaVar	**0.71**	**1.84**	3.29	4.99

on a commercial laptop (Intel® Core™ i7 @ 2.20 GHz, 6 GB RAM). As it can be observed, both proposed methods always execute faster than MEC or AMCC. In particular, maxDeltaVar is the fastest algorithm on shorter EEG segments (up to 2 s), while tCCA and fCCA show a much slower increase in execution time over the whole window length span. Also, fCCA always executes faster than tCCA, and is the fastest algorithm from 2 s windows up.

It is to be stressed again that the main goal here was low computational demand: both proposed algorithm well behave with this respect, still providing comparable accuracy with respect to reference methods.

Table 3.4 gives illustrates such statement at a glance, by introducing a simple cost/performance index, i.e., the ratio between computational effort and attained accuracy for all mentioned cases, showing that proposed methods, in the cases at hand, always provide better indexes than other methods.

Chapter 4

Building the BCI: online, self-paced operation

In the last chapter, the focus was on presenting SSVEP classification algorithms, and two novel signal processing methods were proposed. All these algorithms were then tested and compared in an *offline* fashion.

In this chapter, we take a step further and adapt those concepts to *online*, self-paced operation. A key concept which will allow such an improvement is the addition of another classification problem: i.e., recognizing uncertain/non informative (for SSVEP-based BCI purposes) EEG periods.

This will allow to continuously analyze the EEG, rejecting epochs in which the user does not appear to be controlling the device (*Non-Intentional Control*, or NIC, periods). On the other hand, when an *Intentional Control* (IC) period is recognized, classification can be attempted as explained in the previous chapter.

First, a strategy for improving accuracy is presented, based on the notion of a "prediction confidence index". This will allow us to distinguish between NIC and IC periods, performing classification in the latter case. Building on top of this, an adaptive method for choosing EEG window length will be presented, for improving performance.

Finally, results of an online, self-paced operating scenario will be discussed, pointing out the generality of the method, to the extent that many users can operate the BCI with the same parametric setup, thus avoiding initial calibrations.

4.1 Re-thinking previous algorithms

4.1.1 A strategy for improving accuracy

In order to increase the accuracy of the classification stage, one can decide not to make a decision whenever the level of confidence in it is not high enough [101],[121]. We call this "no-reliable-decision" state a *neutral* state, not to be confused with idle conditions, in which the user does not intend to make any choice.

Such a "confidence indicator" can be defined in many different ways. A possible solution is to check for the difference in scores between the selected stimulus frequency and the second best. For instance, in the case of CCA-based methods, the difference between the correlation coefficients could be assumed as indicator; maxDeltaVar method could instead take the relative ratio between the maximum variance drop and the second largest drop; finally, MEC and AMCC could exploit relative ratios between estimated powers. We will call this indicator d. Distribution of both correct and mistaken SSVEP classifications with respect to d value is illustrated in Figure 4.1, by means of a histogram approximation.

In order to assume d as a confidence qualifier, ideal behavior should associate all errors (red bars) to low values of d, with correct classification (blue bars) associated to largest values instead. Then, one could choose a suitable threshold value for d^* to allow for decision: whenever $d \leq d^*$ we assume a neutral condition, otherwise a decision is made.

Again, it is desirable that the threshold does not vary with subjects, so we characterized the method on the whole population of the test, instead of relying on a per-user basis analysis.

Histograms in Figure 4.1 show that actual distributions (although far from matching the ideal case) exhibit, indeed, a qualitatively sound dependence on parameter d.

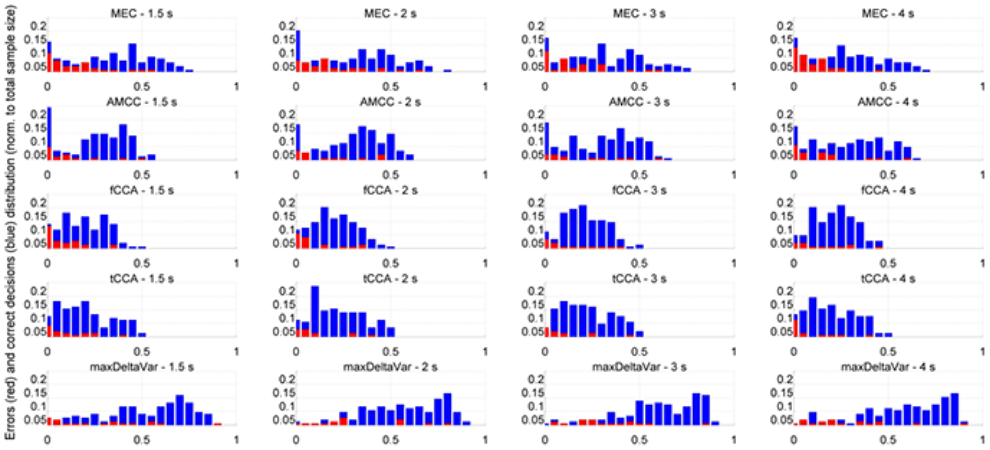

Figure 4.1 Distribution of wrongly (red) and correctly (blue) classified epochs (normalized to the sample size) as a function of the parameter *d*. The distributions are also plotted for different EEG window lengths, and for different algorithms.

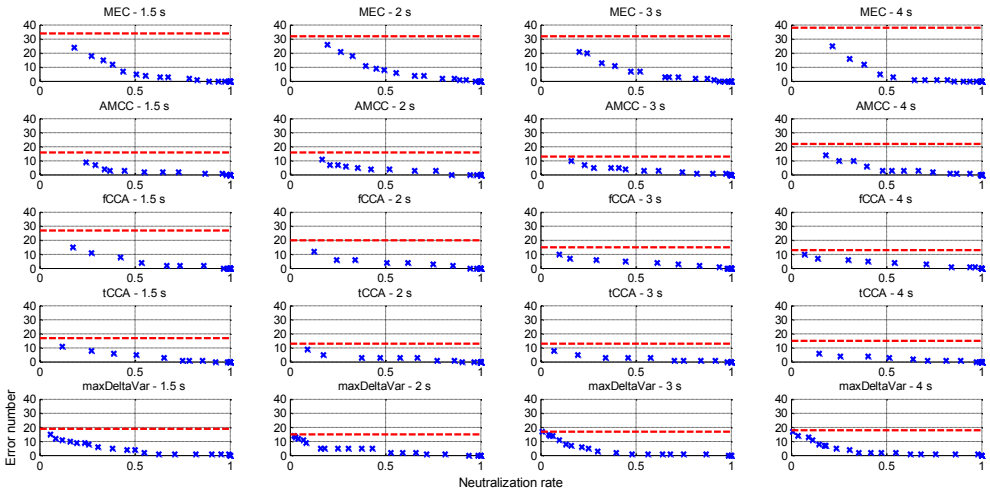

Figure 4.2 Error occurrence as a function of neutralization rate, at different values of threshold *d. In red, the original, "raw" error level, without neutralization (i.e., *d** = 0). The graphs are plotted for different EEG window lengths.**

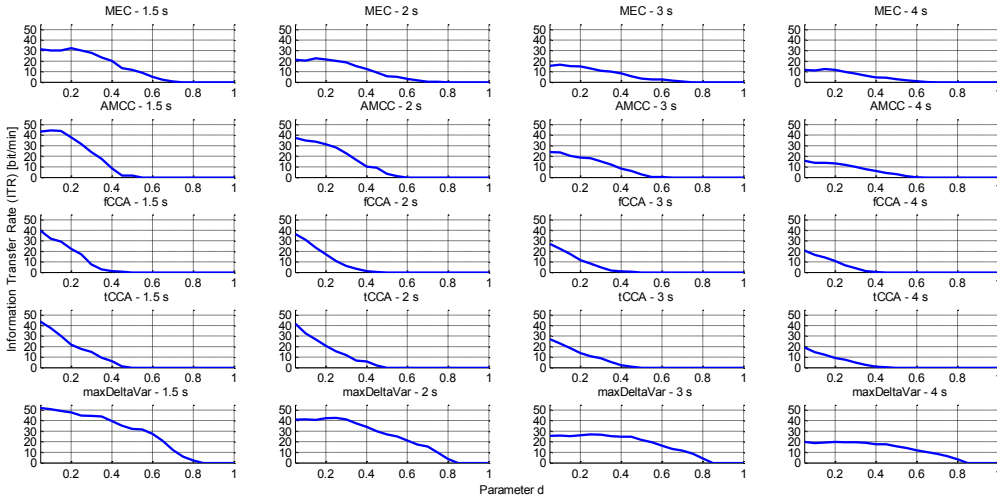

Figure 4.3 Information Transfer Rate (ITR) as a function of the parameter *d*. The distributions are plotted for different EEG window lengths.

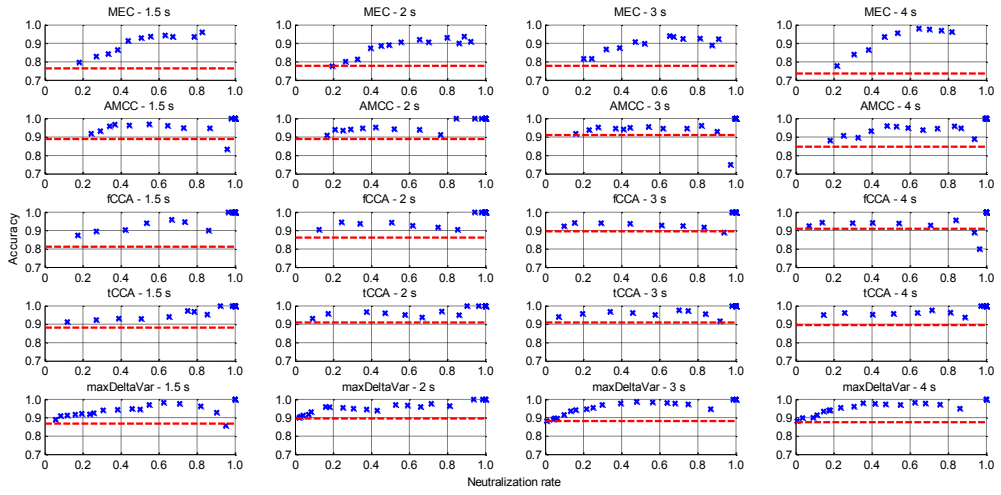

Figure 4.4 Accuracy as a function of neutralization rate, at different values of threshold *d. The red dashed line represents the original, "raw" accuracy level, without neutralization (i.e., *d** = 0). The graphs are plotted for different EEG window lengths.**

A more quantitative assessment of algorithms behavior upon introduction of neutral condition is given in Figure 4.2**,** Figure 4.3**,** and Figure 4.4: here errors, ITR and accuracy are correlated to the actual fraction of neutralized epochs. To this purpose, for a given value of the threshold *d*,* a subset of epochs is selected, fulfilling the condition $d \geq d^*$; then wrong and correct classification are counted within the subset.

The error number monotonically decreases with neutralization rate, as shown in Fig. 3: the red dashed lines there refer to the error count, when no neutralization is accounted for; ideal behavior here should consist of a sharp error reduction in the leftmost part of the graph (i.e., at low neutralization rates, thus rejecting the smallest fraction of epochs). As shown, tCCA and maxDeltaVar exhibit the best behavior with this approach, especially at shorter EEG time segments.

Also, neutralization is more effective on fCCA too, with respect to AMCC and MEC. I.e., given a fixed budget of epochs we can afford to reject, better error rejection is attained.

Overall, we observed that a threshold value of $d^* = 0.3$ for the maxDeltaVar algorithm, and $d^* = 0.1$ for all the other ones, leads to a good trade-off between error rejection and percentage of neutralized epochs.

ITR can be calculated as well [12]:

$$ITR = (1 - p_n)\left[\log_2 N + (1 - p_e)\log_2(1 - p_e) + \right. \\ \left. + p_e \log_2\left(\frac{p_e}{N-1}\right)\right] \cdot \frac{60}{T_w} \ \text{[bit/min]}, \tag{3.1}$$

where N is the number of classes (4 in this case), p_n is the probability of the neutralization state, p_e the probability of error, T_w the EEG segment length; ITR dependency on the threshold d^* is illustrated by curves in Figure 4.3**.** Albeit ITR accounts for both accuracy and selection speed in a unique indicator, it is worth remarking again how, for the targeted application, selection accuracy is actually rather more relevant than speed itself, given the limited amount of user interactions involved.

Hence, in Figure 4.4**,** accuracy as a function of *d** is also explicitly illustrated. Unlike the error plot, this function can also show a non-monotonic trend, since the relative weight of errors located in the high-*d* tail increases while reducing the "valid" epoch subset. In this case, given a target accuracy, the best algorithm is the one which guarantees a lower percentage of epochs rejected from classification. As we can observe, tCCA and maxDeltaVar are good candidates, especially for shorter EEG windows. Also fCCA shows a good performance, and achieves high accuracies rejecting less epochs with respect to AMCC and MEC.

On the whole, Figure 4.2**,** Figure 4.3**,** and Figure 4.4 make it evident that a practical range of *d** exists: at lower neutralization rates, appreciable accuracy improvements are obtained, without implying too relevant data loss and thus not jeopardizing speed performance.

4.1.2 An adaptive EEG window length choice

The neutralization strategy described above provides a quality metric than can be exploited also to introduce some adaptivity in the SSVEP classification stage. In particular, as shown above, using shorter timeframes allows for reducing latency, to the potential detriment of informative content. We can check the quality of the current classification at runtime by looking at the indicator *d* again; we start with a short time window length, to be increased whenever *d* does not exceed a given threshold. Such mechanism should also improve the BCI flexibility and, in particular, its responsiveness towards the user.

A simple proof-of-concept test has been carried out: just a couple of window lengths were exploited here, switching from 2 s to 3 s whenever the *d* threshold test fails. Of course, a more flexible scheme can be implemented, accounting for parametrized window lengths and increments. The accuracy we obtained with such an adaptive method with tCCA, fCCA and maxDeltaVar are reported in Table 4.1.

Table 4.1 Performance of the adaptive window mechanism: average (std. dev.) accuracy and neutralization rate.

	Accuracy	Neutralization rate
tCCA (2 s)	96.0 % (1.5)	16.6 % (5.4)
tCCA (3 s)	95.6 % (0.6)	19.6 % (6.3)
tCCA (adapt.)	**95.3 % (0.7)**	**11.8 % (4.0)**
fCCA (2 s)	94.5 % (0.9)	23.9 % (6.7)
fCCA (3 s)	94.3 % (1.5)	14.7 % (4.8)
fCCA (adapt.)	**93.8 % (1.0)**	**10.0 % (3.2)**
maxDeltaVar (2 s)	95.9 % (2.5)	16.0 % (6.0)
maxDeltaVar (3 s)	93.6 % (1.7)	13.2 % (4.3)
maxDeltaVar (adapt.)	**94.7 % (1.9)**	**7.0 % (3.1)**

Even though the gathered data do not allow to draw a statistically significant conclusion, mainly due to the limited available data (due to time constraints), still, some promising signals that the adaptive mechanism could reduce the neutralization rate while retaining comparable accuracy were noticed. Lower neutralization rate, in turn, implies better efficiency in data exploitation and allows to improve the overall responsiveness of the system. In the future, more data will be collected to allow a more thorough analysis. Nonetheless, the major factor for a smooth online, self-paced operation is still represented by the *neutralization* mechanism described in §4.1.1.

4.2 Going *online*

Having discussed the core adaptation to the online, self-paced case (i.e. the neutralization mechanism), we are ready to describe this operating scenario.

We will use, as an example, the tCCA algorithm; the signal acquisition and processing chain is the following:

- By default, the EEG module sends a new data packet every 200 ms, which is the main refresh cycle.
- After conversion and vectorization, data enter the main processing buffer, in the last position.
- The length of the processing buffer is such that it can accommodate the largest window length of interest (typically, 4 s), plus a couple of seconds of older entries, left for initializing the temporal filters.
- Data is pre-processed by applying a low-pass filter (f_{cut}=46 Hz, with a 60 dB attenuation at 50 Hz), and the average is then removed.
- The last 5 s of EEG waveforms are displayed in real-time in the GUI.
- The last 3 s of EEG waveforms are used to calculate a PSD using Welch's method (resolution = 1 Hz, 50% overlap between sub-windows), and the result is displayed in real-time in a GUI sub-plot.
- The EEG signal is standardized and fed to the classification algorithm.
- The classification algorithm (e.g. tCCA) attempts classification with the minimum window length. If the confidence indicator meets a minimum threshold requirement (as it was shown earlier in §4.1.1), classification is validated and passed on. Otherwise, the EEG window is dynamically expanded until a maximum value is reached. If none of the attempted classification yielded a valid result, the epoch is neutralized.
- Before issuing a command, classification is further processed and smoothed. In particular, a post-smoother averages the last 5 classification outputs for each class (the 4 targets plus the neutral state): if the average for a class exceeds a given threshold, the choice

is validated, otherwise a null output is assumed. This further step contributes in lowering false positive events.

4.3 Results

As previously stated, in order to provide smoother operation in BCI-enabled control applications, we are primarily concerned with maximizing the accuracy (i.e. correctly classifying the command when the user is trying to issue one) and, at the same time, minimizing the false positives, which requires to be able to discern when the user is actively controlling the device, or is just resting or performing other tasks.

Furthermore, we would like to adopt a general approach, in which the BCI is robust against changes in the user's features, as well as against user changes (i.e. subject independence).

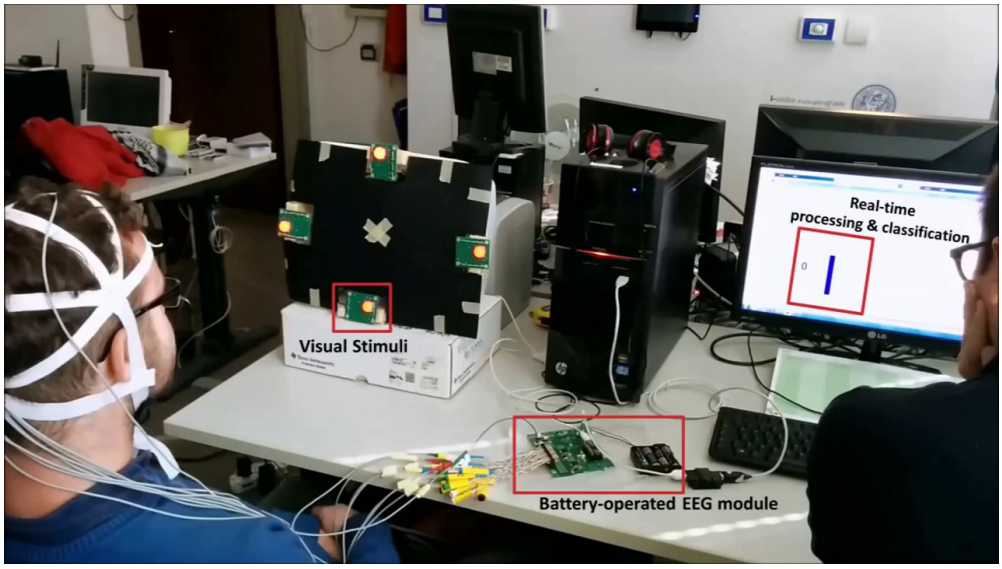

Figure 4.5 Photo of the experimental setup in the online, self-paced SSVEP-BCI experiment.

Table 4.2 Online, self-paced performance of the 4 class SSVEP-BCI: mean (std. deviation) of *True Positive Rate* (TPR), *False Negative Rate* (FNR), *False Positive Rate* (FPR).

	TPR	FNR	FPR [min^{-1}]
No smoother	96.44% (0.77)	3.56% (0.77)	0.74 (0.08)
With smoother	94.62% (0.83)	5.38% (0.83)	0.26 (0.03)

The experimental setup is similar to that in §3.4 (4 targets blinking at 16, 18, 20 22 Hz, 6 passive Ag/AgCl electrodes, now located over Pz, P3, P4, POz, O1, O2 positions); this time, though, the subject autonomously decides when to attend to visual stimuli and when to rest. A photograph of the experimental setup is shown in Figure 4.5.

In order to assess the stability in terms of low false positive events, long, inactive NIC periods are introduced on purpose in each run, during which the subject could also talk and move.

A total of 6 healthy volunteers (age 24-61) participated in this study.

Table 4.2 reports the online experiment results (mean and standard deviation), in terms of true positive, false negative and false positive rates.

A very good performance is achieved, both in terms of true positive and false positive rates. In Table 4.2, influence of the optional post-smoothing step is also accounted for: when no smoothing is accounted for, the "raw" performance of the neutralization mechanism can be assessed. In this case, false positives are kept to a very small amount (0.74 min^{-1} on average), in line with literature data [122],[123]. Such performance is further boosted by switching on the smoother stage: a 0.26 min^{-1} false positive rate is achieved, significantly improving over the state of the art (0.8 min^{-1}). Inserting a smoothing stage comes at the expense of an increase in latency time (due to the summing stages of the smoother, which introduce an additional 1 s delay) and of an almost negligible decrease in the true positive rate (-1.82%); however, this does not jeopardize the user ability to effectively control the BCI.

In evaluating such results, it is worth remarking that the parameters for the neutralization mechanism and the post-smoother are kept constant across all users and that no user-specific setup adjustment was made. Results therefore show that the signal processing chain is quite stable with respect to user variations, supporting the aimed "plug & play" vision.

The BCI was also displayed during the *Handimatica 2014* exhibition, held in Bologna from November 27th to November 29th. A colleague performed two interactive demo sessions per day, approximately 30 min. each. The experimental setup was the same as above, in terms of EEG acquisition. Four commands allowed to switch on and off a desk lamp, as well as to open or close a motorized rolling shutter.

Environmental conditions were far from the usual, lab-controlled ones; examples of non-idealities are: very high ambient luminosity (high-power spotlights), EM interference (air-conditioning motors, WiFi access points nearby, mobile phones), loud acoustic noise, necessity to move (partially) and interact with the audience. A picture from the exhibition is shown in Figure 4.6.

Even though results apply to just one user (for organizational and insurance reasons), a remarkably low false positive rate was recorded, approximately 0.15 min^{-1}. This is an encouraging signal of possible applications outside lab environments for the realized device.

Figure 4.6 Photo of the experimental setup at the *Handimatica 2014* exhibition.

Conclusions and future developments

The aim of this work was to develop a compact, yet flexible BCI platform, which, when compared to most commercially-available solutions, can offer an optimal tradeoff within the following boundary conditions:

- minimal, compact, and easy experimental setup;
- flexibility, allowing simultaneous studies of other bio-potentials (e.g. EMG);
- contained costs (e.g. < 1000 €);
- robust design, operation outside controlled lab environments;

We then identified and discussed a possible application target for the realized BCI, i.e. Ambient Assisted Living system control. However, the adopted design methodologies, actually, make our approach more general. Nonetheless, considering a practical problem, such as the one indicated, allows us to better visualize and focus on other additional requirements. In particular, given the nature and dynamics of system interaction of our application (limited and sparse in time), the following characteristics are highly desirable:

- online, self-paced BCI operation (i.e., the BCI monitors the EEG in real-time and must discern between intentional control periods, and non-intentional, rest ones, interpreting the user's intent only in the first case);
- calibration-free approach ("ready-to-use", "Plug&Play");
- subject-independent (general approach).

Given these requirements, the choice for the operating protocol fell on Steady State Visual Evoked Potentials (SSVEP).

The development flow of the present work started from the ground, electrical level with the realization of a suitable bio-potential acquisition platform. Then, we built our entire platform on top of it, addressing all the related aspects of storing the data, processing it in real-time, and delivering meaningful output. Such pervasive customization allowed us to fine-tune each step of this design, allowing us to craft each time the optimal solution for the specific needs, from the hardware level up to the software/processing one.

From the hardware point of view, two hardware platforms for bio-potentials acquisitions were realized. Both designs achieve good results in terms of noise performance and costs. In particular, with reference on the latest release, the following results were achieved:

- Possibility of simultaneously acquiring 16 channels with a small 10x13 cm form factor. The module can be powered via 4xAA alkaline batteries, thanks to its reduced power consumption (≈162 mW). Price range in large scale is within 300 €.
- Wide input dynamic range (±188 mV min.), allowing to acquire different bio-potentials at high resolution (24 bit, with the LSB being as low as, approximately, 22 nV)
- Superior noise performance (< 1.3 μV_{pp} over the whole signal bandwidth).
- Static and dynamic performance were positively compared against a commercial *g.tec USBamp* device (§2.5.2 for the details).
- The module was also successfully integrated within the standard TOBI platform.

In this state of the research, the platform is based on MATLAB (for faster research and prototyping purposes) and is able to run on commercial laptops. It can acquire, store and process data in real-time; moreover, it features a GUI which can continuously display the temporal and time-frequency evolution of the EEG signals. Update frequency was tested up to 10 Hz, successfully, and it is usually set for 5 Hz operation.

From the signal processing point of view, the following results were achieved:

- popular calibration-less SSVEP processing from the literature were studied and re-implemented inside our platform.
- Two novel methods for *offline* SSVEP classification were proposed and favorably compared to the state of the art.
- A methodology for improving SSVEP classification accuracy was presented. It is suitable for online, self-paced operation, as, it allows to discern between active, intentional control periods and inactive ones, where the user rests or is engaged in other tasks. Classification is attempted only in the former case, when the estimated prediction confidence exceeds a given value.
- A method for dynamically scaling the observed EEG window was devised, allowing to improve BCI responsiveness with respect to fixed-length designs.
- Performance of the 4 class, SSVEP-based BCI was tested in an online, self-paced experiment. The achieved sensitivity results are in line with the state of the art (> 95%).
- Even more remarkably, significant improvements over the state of the art were achieved in False Positive Rate minimization: an average 0.26 min^{-1} ($\sigma = 0.03$) rate was achieved, with respect to the 0.8 min^{-1} best value found in literature.
- In addition, such results were achieved without any parameter fitting on each user: they were shared among all. This is a major step in looking towards "Plug&Play" approaches.
- System performed consistently even in a relatively "harsh" scenario as in the *Handimatica 2014* exhibition (§4.3).

Open questions and room for improvements still remain, for example:

- How does the system perform in mobility scenarios?

- Should the system include active electrodes (partially covered in §2.6) for reducing the impact of motion artifacts or is the signal processing able to compensate for that? From our experience in SSVEP-based BCI, where the subject somehow free to move, within certain limits, the latter point seems more likely. Nonetheless, this is not the general case: other factors, such as the particular BCI paradigm choice, could also call for technological improvements.
- How can current SSVEP-based signal processing be improved, in terms of further false positives minimization and speed-up?
- Which signals (even from other bio-potentials) could be aggregated to improve the BCI performance, realizing a hybrid-BCI? We are currently studying the integration of EMG signals to allow for a hybrid control, e.g. by providing an *on*/*off* switch.
- Other BCI operating paradigms (e.g. motor imagery) could be integrated in our current platform as well, in the form of signal processing module plugins.
- Also, it is possible to realize plugins and drivers for integrating our platform/hardware module into existing BCI software, such as BCI2000[12], BCILAB[13] or OpenVibe[14].

[12] http://www.schalklab.org/research/bci2000
[13] http://sccn.ucsd.edu/wiki/BCILAB
[14] http://openvibe.inria.fr/

Appendix

EEG module (rel. 2): schematics and gerber files

In the following pages, the schematics and Gerber (PCB production) files for the EEG module – release 2 are presented. Some notes:

- Gerber files for PCB production were exported in RS-274X format.
- The PCB was produced by EuroCircuits GmbH[15] using a standard pool process
- Technological parameters: 4 layer buildup, 1.55 mm thickness, 0.15/0.15 mm track/clearance, 0.25 mm minimum via diameter, HAL lead-free surface finishing.
- Final board dimensions: 10x13 cm.
- Components are mounted mainly on the top layer; for space constraints, some passive components are mounted on the bottom layer as well.
- Due to the presence of fine-pitch components (pin-to-pin distance less than 0.65 mm), PCB mounting was performed by Elit Snc[16] using a standard reflow process.
- M3-compatible screw holes allow PCB mounting in plastic enclosures.

[15] http://www.eurocircuits.com/
[16] http://www.elitparma.it/

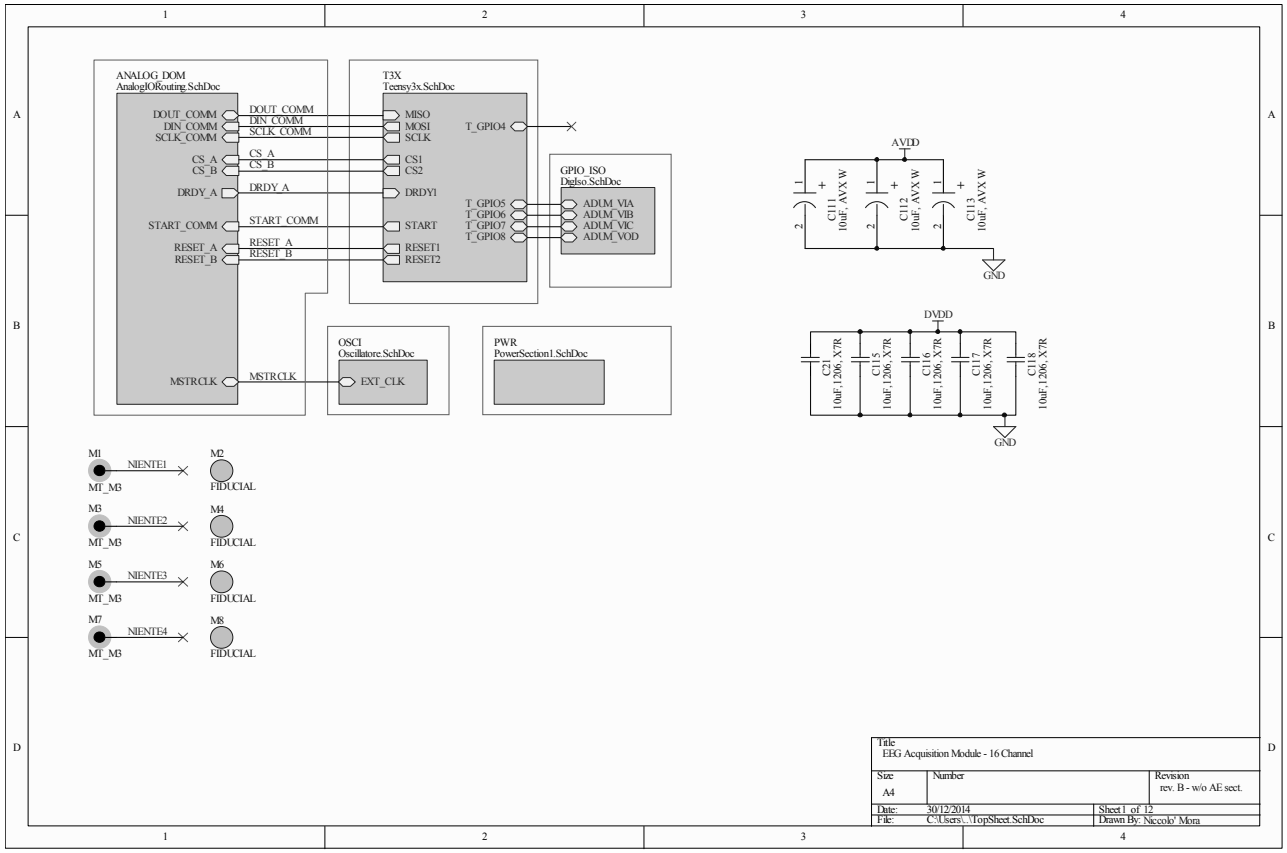

Title: EEG Acquisition Module - 16 Channel		
Size: A4	Number	Revision: rev. B - w/o AE sect.
Date: 30/12/2014		Sheet 1 of 12
File: C:\Users\...\TopSheet.SchDoc		Drawn By: Niccolo' Mora

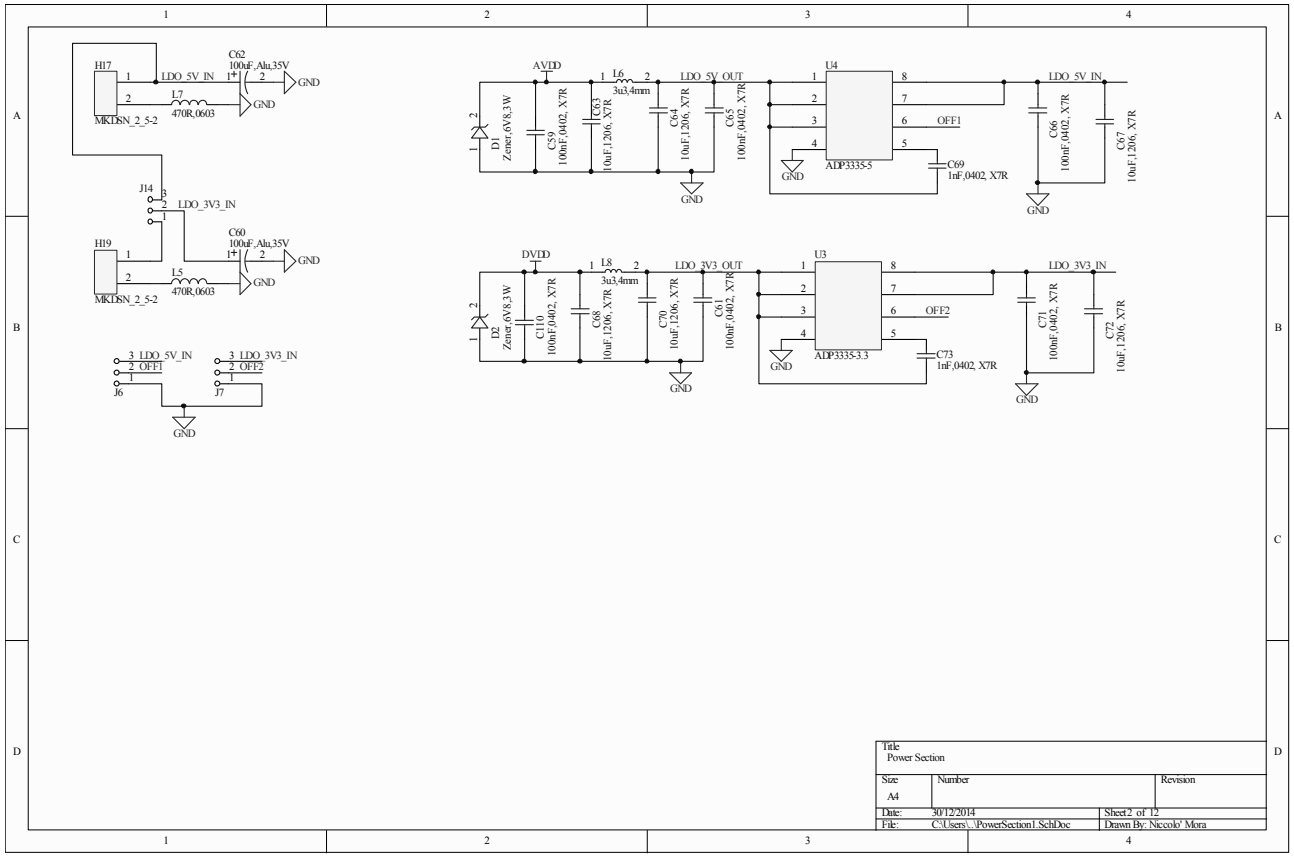

Title: Power Section		
Size: A4	Number:	Revision:
Date: 30/12/2014		Sheet 2 of 12
File: C:\Users\..\PowerSection1.SchDoc		Drawn By: Niccolo' Mora

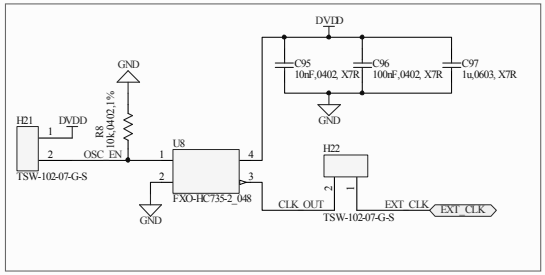

Title: External clock generation		
Size: A4	Number:	Revision:
Date: 30/12/2014		Sheet 3 of 12
File: C:\Users\...\Oscillatore.SchDoc		Drawn By: Niccolo' Mora

ISOLATION WAS REMOVED due to space contraints. Only the connectors are left.
Isolation must be provided externally. Possible chip choice: ADI i-Coupler (ADUM family)

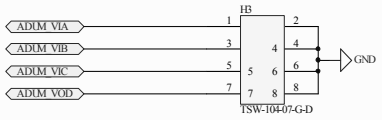

Title: Digital I/O isolation		
Size: A4	Number	Revision
Date: 30/12/2014		Sheet 4 of 12
File: C:\Users\...\DigIso.SchDoc		Drawn By: Niccolo' Mora

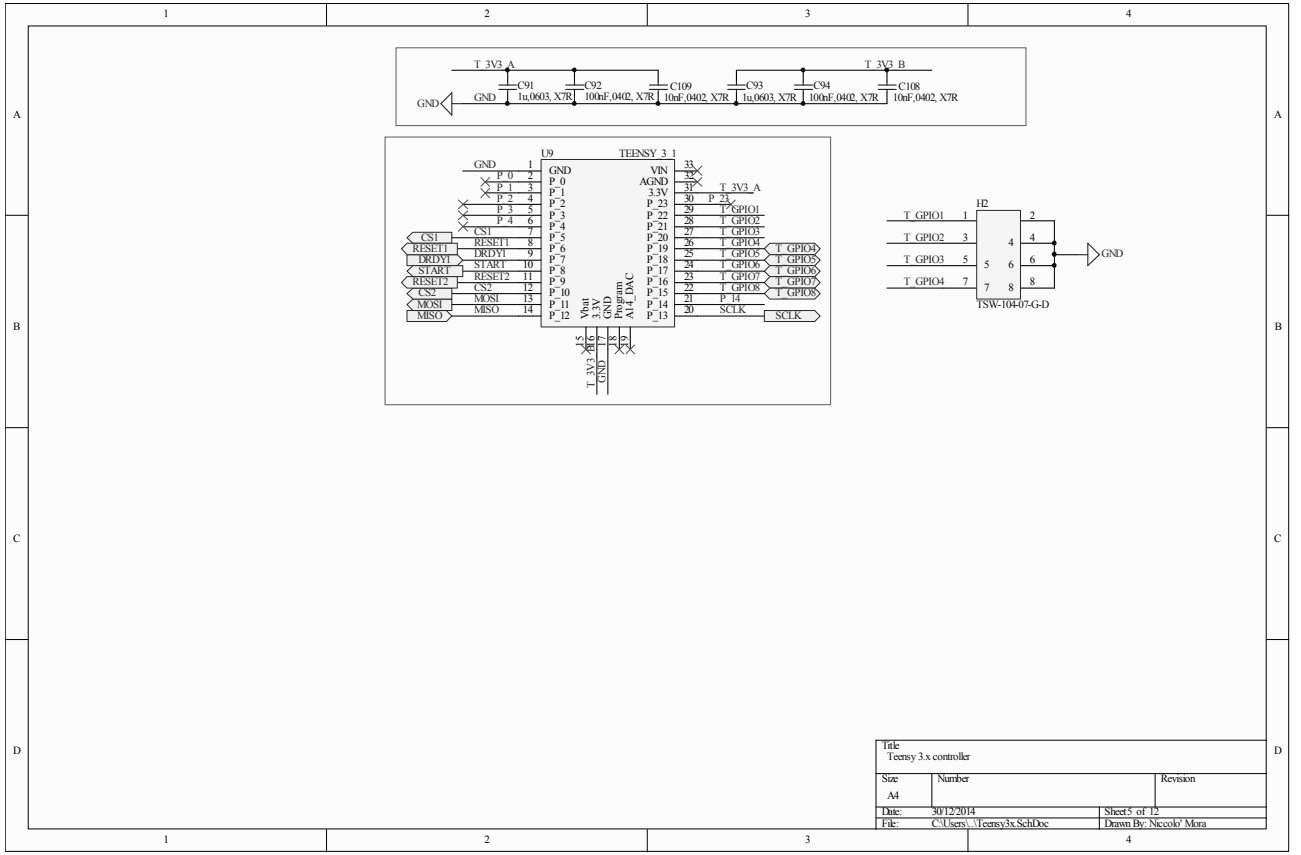

Title: Teensy 3.x controller		
Size: A4	Number	Revision
Date: 30/12/2014		Sheet 5 of 12
File: C:\Users\...\Teensy3x.SchDoc		Drawn By: Niccolo' Mora

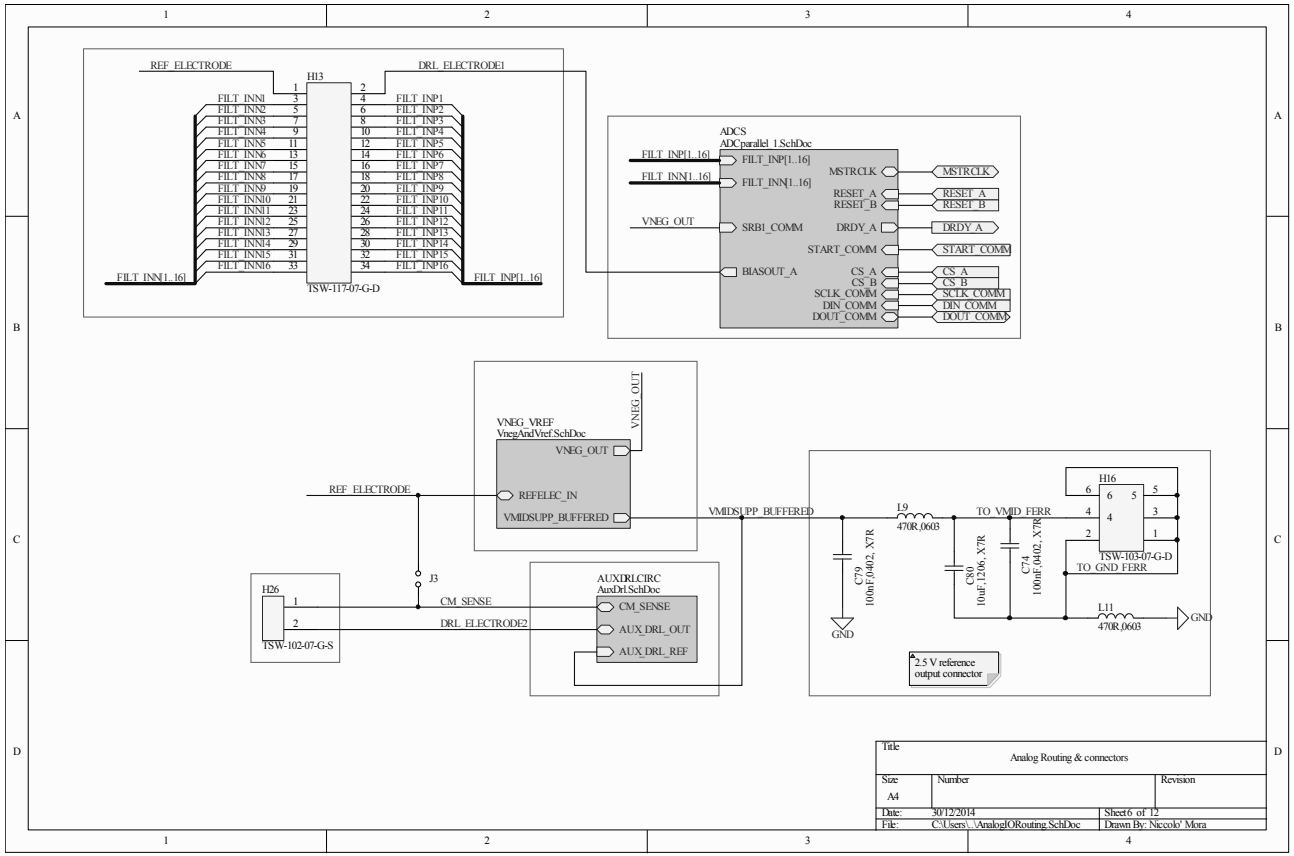
REF_ELECTRODE
DRL_ELECTRODE1
H13
FILT_INN1 3
FILT_INN2 5
FILT_INN3 7
FILT_INN4 9
FILT_INN5 11
FILT_INN6 13
FILT_INN7 15
FILT_INN8 17
FILT_INN9 19
FILT_INN10 21
FILT_INN11 23
FILT_INN12 25
FILT_INN13 27
FILT_INN14 29
FILT_INN15 31
FILT_INN16 33
FILT_INP1 4
FILT_INP2 6
FILT_INP3 8
FILT_INP4 10
FILT_INP5 12
FILT_INP6 14
FILT_INP7 16
FILT_INP8 18
FILT_INP9 20
FILT_INP10 22
FILT_INP11 24
FILT_INP12 26
FILT_INP13 28
FILT_INP14 30
FILT_INP15 32
FILT_INP16 34
FILT_INN[1..16]
FILT_INP[1..16]
TSW-117-07-G-D
ADCS
ADCparallel 1.SchDoc
FILT_INP[1..16]
FILT_INN[1..16]
VNEG_OUT
FILT_INP[1..16]
FILT_INN[1..16]
SRB1_COMM
BIASOUT_A
MSTRCLK
RESET_A
RESET_B
DRDY_A
START_COMM
CS_A
CS_B
SCLK_COMM
DIN_COMM
DOUT_COMM
MSTRCLK
RESET_A
RESET_B
DRDY_A
START_COMM
CS_A
CS_B
SCLK_COMM
DIN_COMM
DOUT_COMM
VNEG_VREF
VnegAndVref.SchDoc
VNEG_OUT
REFELEC_IN
VMIDSUPP_BUFFERED
VNEG_OUT
REF_ELECTRODE
VMIDSUPP_BUFFERED
L9
470R,0603
TO_VMID_FERR
H16
TSW-103-07-G-D
TO_GND_FERR
C79
100nF,0402, X7R
C80
10uF,1206, X7R
C74
100nF,0402, X7R
L11
470R,0603
GND
GND
2.5 V reference output connector
J3
H26
1
2
TSW-102-07-G-S
CM_SENSE
DRL_ELECTRODE2
AUXDRLCIRC
AuxDrl.SchDoc
CM_SENSE
AUX_DRL_OUT
AUX_DRL_REF
Title
Analog Routing & connectors
Size
A4
Number
Revision
Date:
30/12/2014
Sheet 6 of 12
File:
C:\Users\...\AnalogIORouting.SchDoc
Drawn By:
Niccolo' Mora

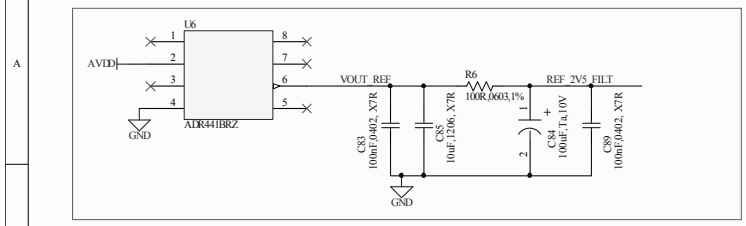

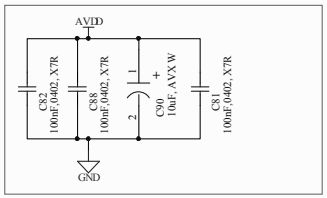

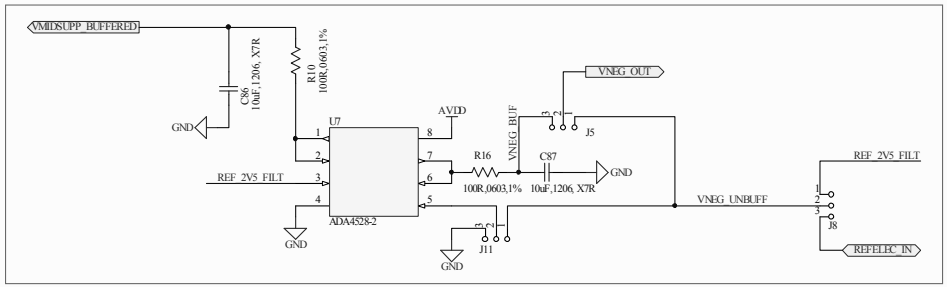

Title: Vmidsupply generation & Vneg selection			
Size: A4	Number		Revision
Date: 30/12/2014		Sheet 7 of 12	
File: C:\Users\...\VnegAndVref.SchDoc		Drawn By: Niccolo' Mora	

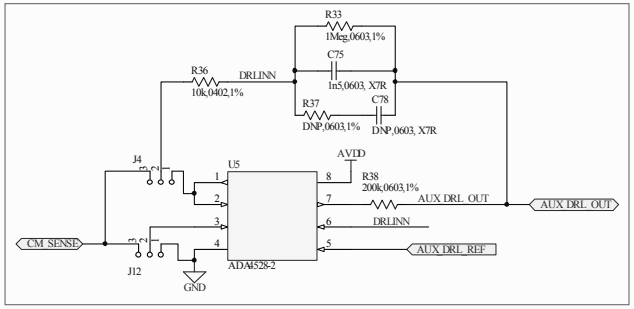

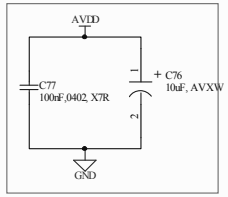

Title: Aux DRL circuit		
Size: A4	Number	Revision
Date: 30/12/2014		Sheet8 of 12
File: C:\Users\...\AuxDrl.SchDoc		Drawn By: Niccolo' Mora

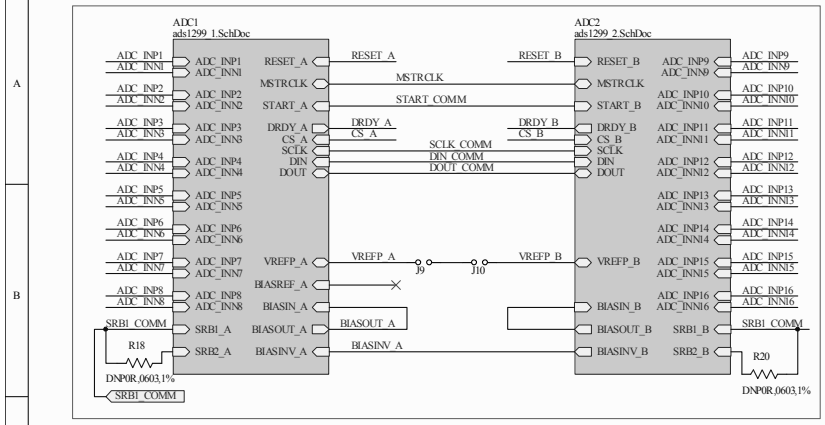

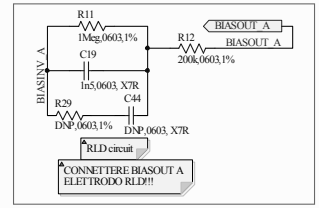

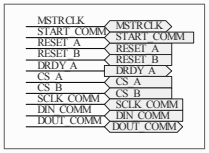

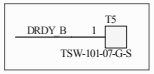

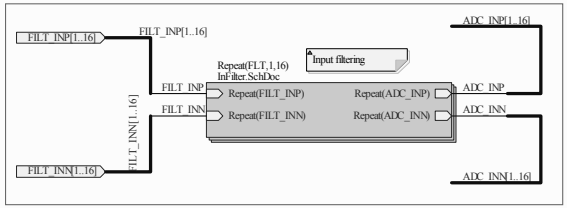

Title: ADS1299 paralleling			
Size: A4	Number:	Revision:	
Date: 30/12/2014		Sheet 9 of 12	
File: C:\Users\...\ADC\parallel_1.SchDoc		Drawn By: Niccolo' Mora	

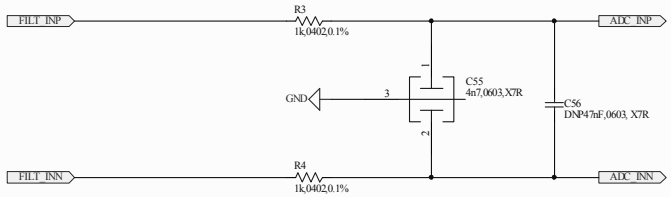

Title: EEG Acquisition Module - 16 Channel			
Size: A4	Number		Revision
Date: 30/12/2014		Sheet 10of 12	
File: C:\Users\...\InFilter.SchDoc		Drawn By: Niccolo' Mora	

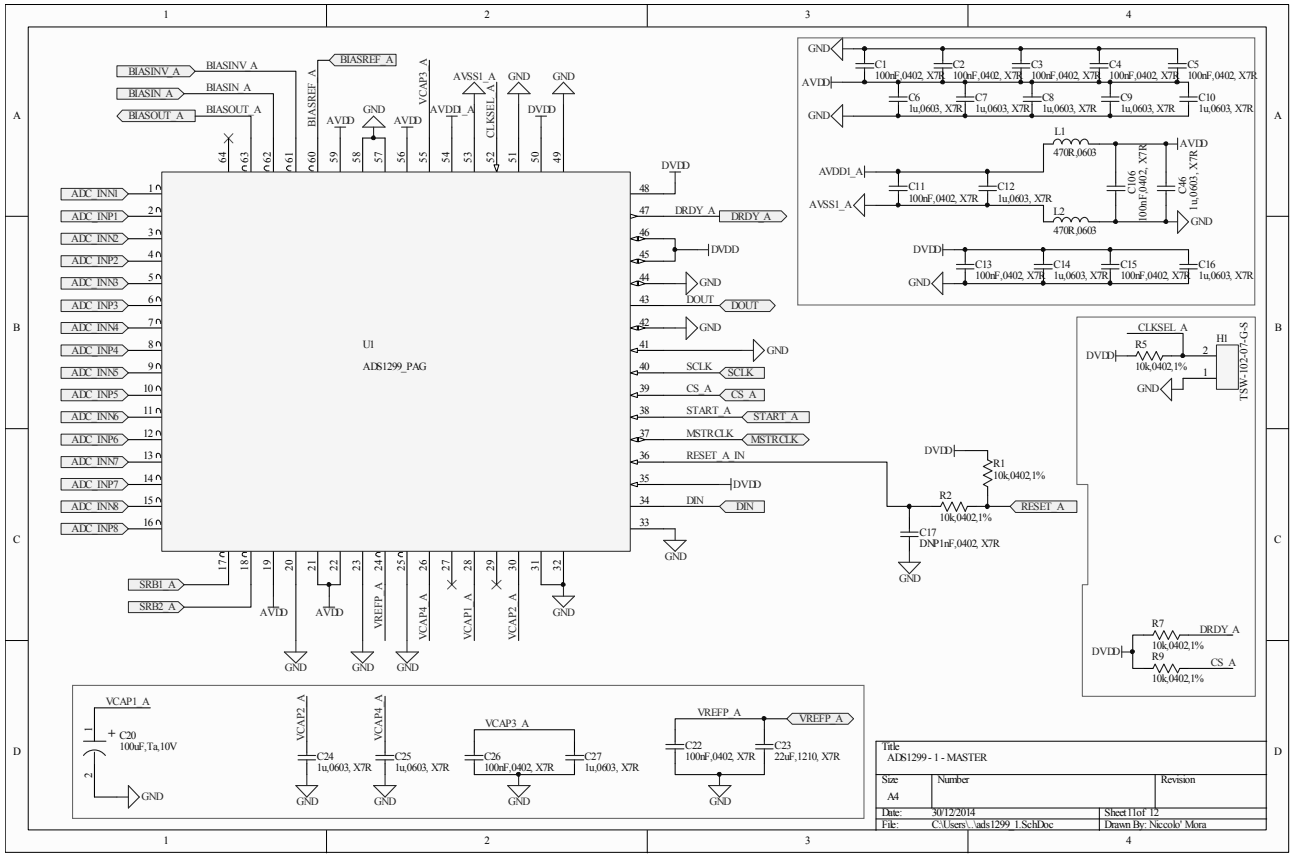
BIASINV_A
BIASIN_A
BIASOUT_A
BIASREF_A
VCAP3_A
AVSS1_A
GND
GND
AVDD
GND
AVDD
AVDD1_A
CLKSEL_A
DVDD
DVDD
ADC_INN1
ADC_INP1
ADC_INN2
ADC_INP2
ADC_INN3
ADC_INP3
ADC_INN4
ADC_INP4
ADC_INN5
ADC_INP5
ADC_INN6
ADC_INP6
ADC_INN7
ADC_INP7
ADC_INN8
ADC_INP8
U1
ADS1299_PAG
DRDY_A
DVDD
GND
DOUT
GND
GND
SCLK
CS_A
START_A
MSTRCLK
RESET_A_IN
DVDD
DIN
GND
SRB1_A
SRB2_A
AVDD
AVDD
VREFP_A
VCAP4_A
VCAP1_A
VCAP2_A
GND
GND
GND
GND
GND
C1 100nF,0402,X7R
C2 100nF,0402,X7R
C3 100nF,0402,X7R
C4 100nF,0402,X7R
C5 100nF,0402,X7R
C6 1u,0603,X7R
C7 1u,0603,X7R
C8 1u,0603,X7R
C9 1u,0603,X7R
C10 1u,0603,X7R
L1 470R,0603
L2 470R,0603
C11 100nF,0402,X7R
C12 1u,0603,X7R
C106 100nF,0402,X7R
C46 1u,0603,X7R
C13 100nF,0402,X7R
C14 1u,0603,X7R
C15 100nF,0402,X7R
C16 1u,0603,X7R
CLKSEL_A
R5 10k,0402,1%
H1 TSW-102-07-G-S
R1 10k,0402,1%
R2 10k,0402,1%
C17 DNP1nF,0402,X7R
R7 10k,0402,1%
R9 10k,0402,1%
C20 100uF,Ta,10V
C24 1u,0603,X7R
C25 1u,0603,X7R
C26 100nF,0402,X7R
C27 1u,0603,X7R
C22 100nF,0402,X7R
C23 22uF,1210,X7R
Title
ADS1299 - 1 - MASTER
Size
A4
Number
Revision
Date: 30/12/2014
Sheet 1 of 12
File: C:\Users\...\ads1299_1.SchDoc
Drawn By: Niccolo' Mora

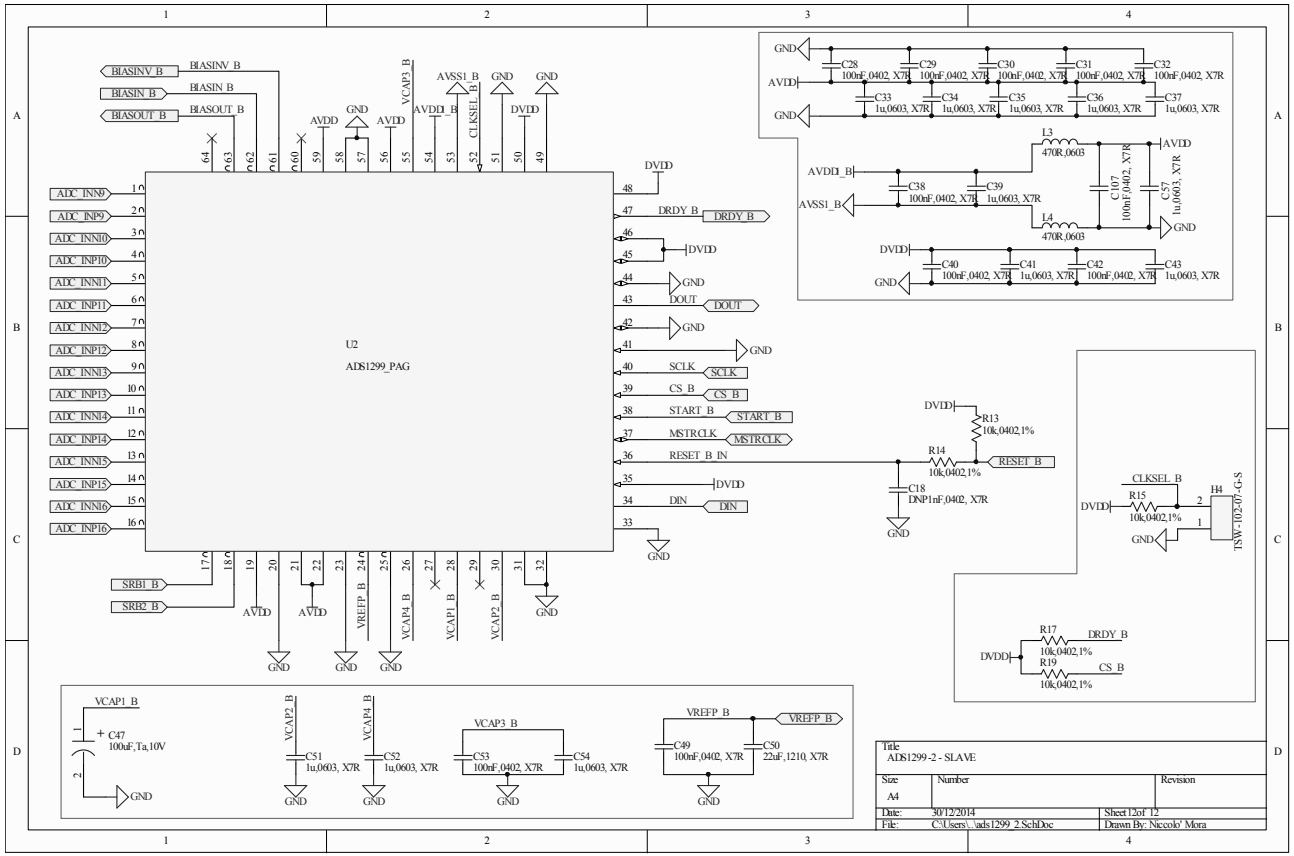

Title: ADS1299-2 - SLAVE		
Size: A4	Number	Revision
Date: 30/12/2014		Sheet 12of 12
File: C:\Users\...\ads1299_2.SchDoc		Drawn By: Niccolo' Mora

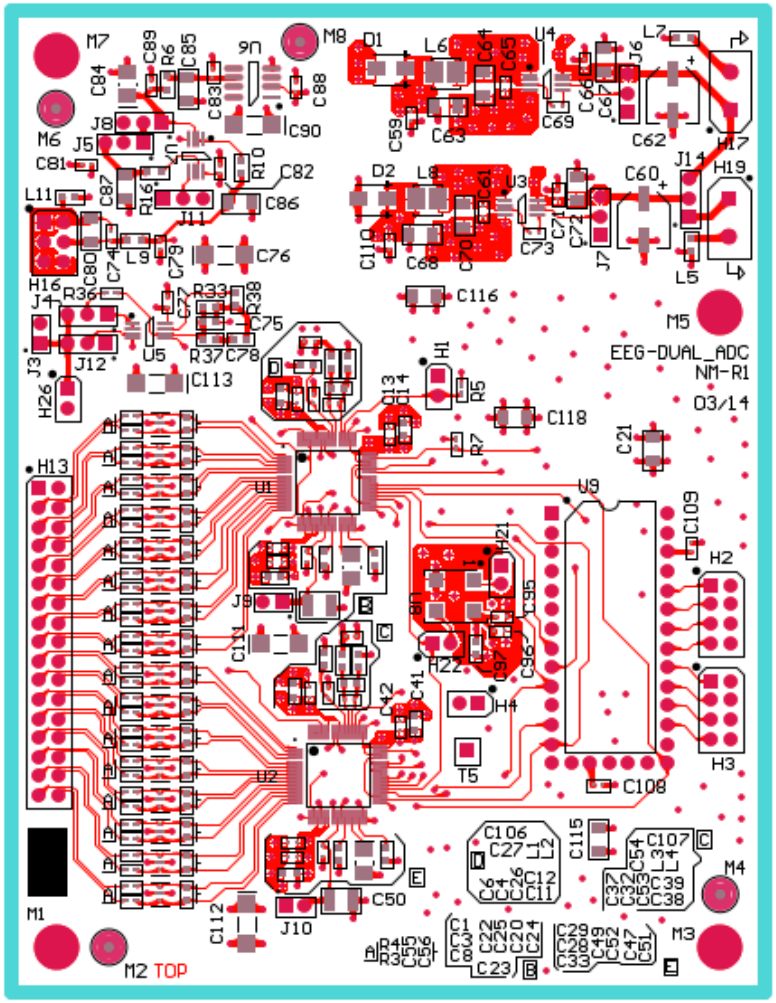

Figure i: Top layer Gerber files

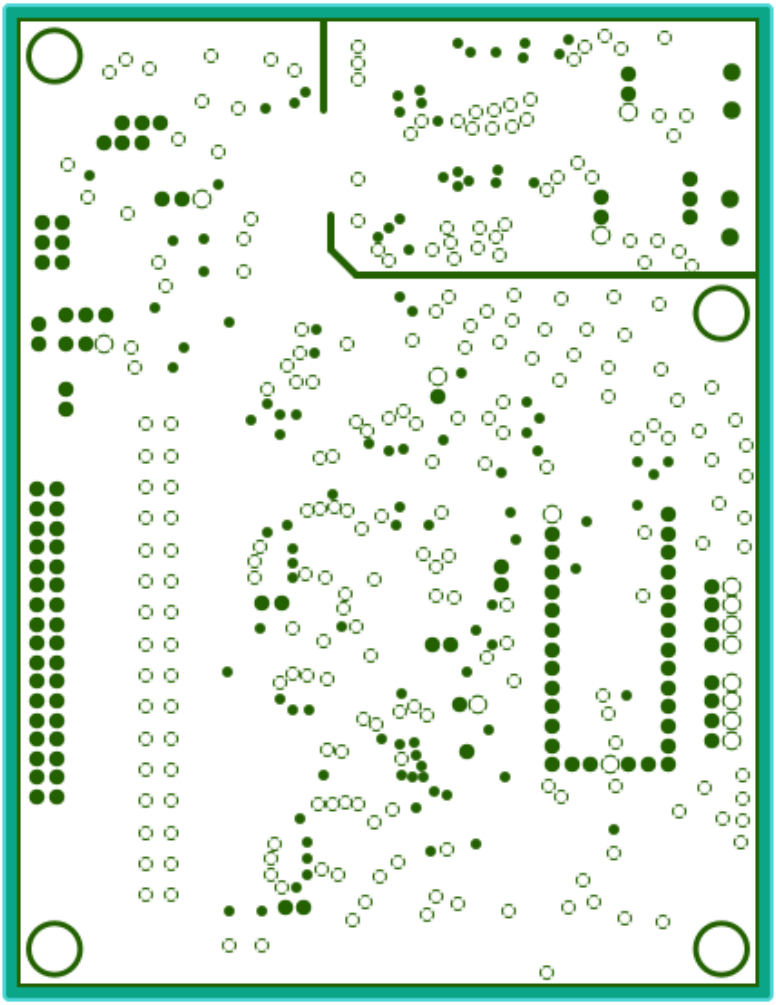

Figure ii: Ground plane Gerber file

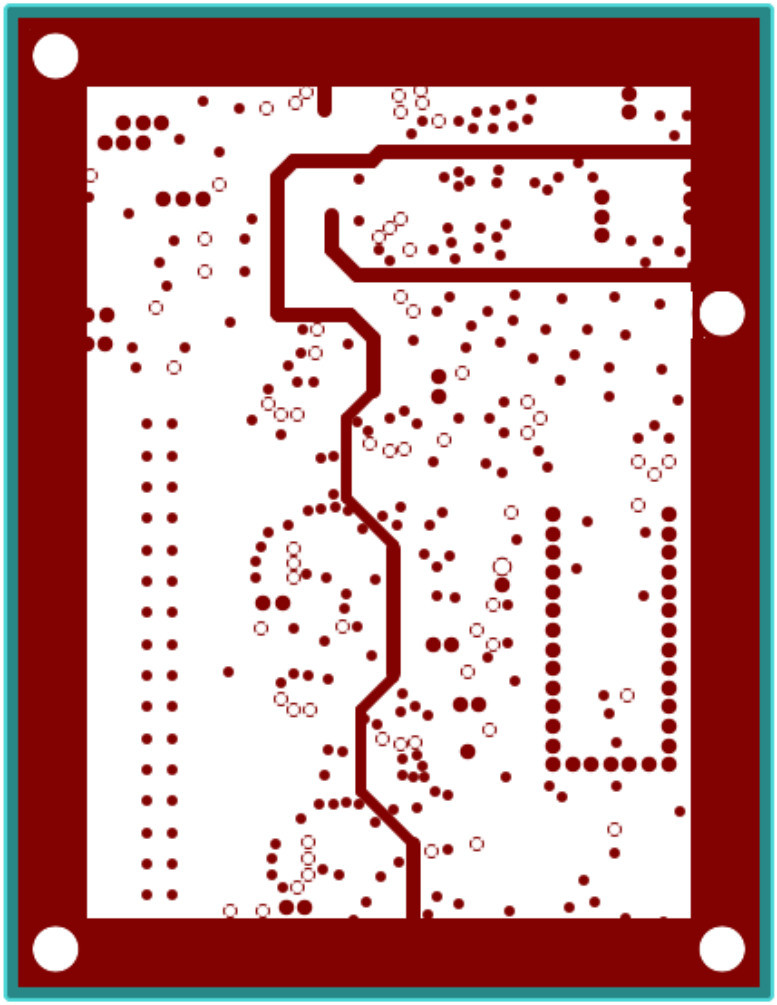

Figure iii: Supply plane Gerber file

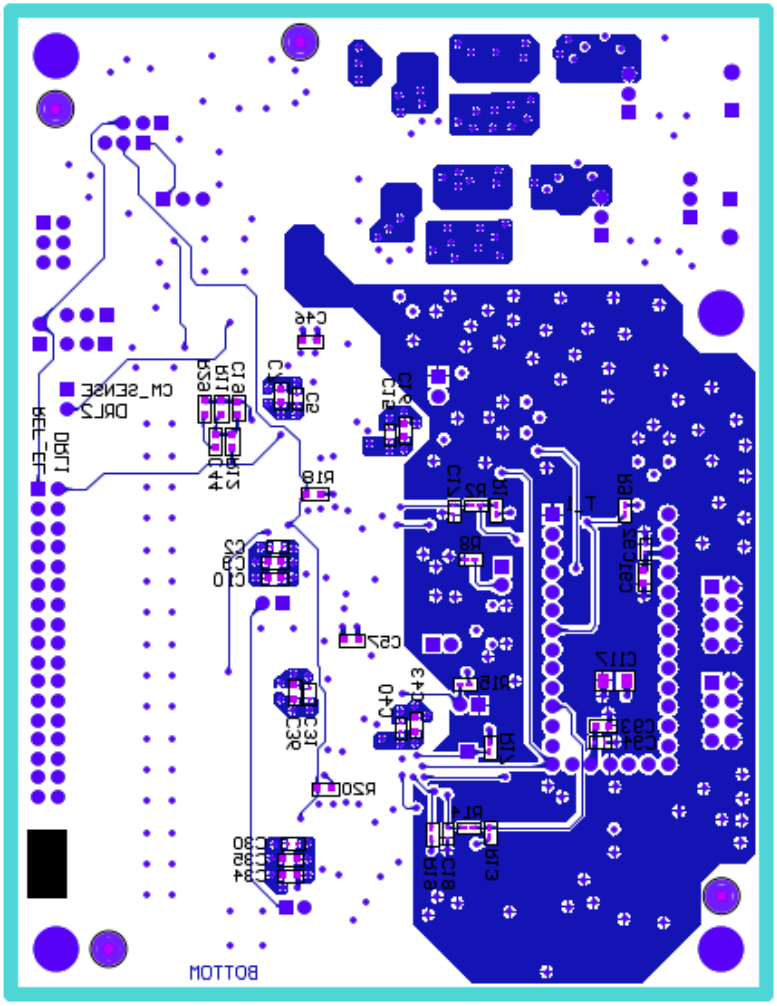

Figure iv: Bottom layer Gerber files

References

[1] J.R. Wolpaw, N. Birbaumer, D.J. McFarland, G. Pfurtscheller, T.M. Vaughan, "Brain-computer interfaces for communication and control," in *Clin. Neurophysiol.*, vol.113, no.6, pp.767-91, Jan. 2002.

[2] G. Dornhege, J.d.R. Millán, T. Hinterberger, D.J. McFarland, K.R. Müller, "Toward Brain-Computer Interfacing," *MIT press*, 2007.

[3] C. Stephanidis, G. Salvendy, et al., "Toward an information society for all: HCI challenges and R&D recommendations," in *International Journal of Human-Computer Interaction*, vol.11, no.1, pp.1-28, 1999.

[4] H. Cecotti, "A Self-Paced and Calibration-Less SSVEP-Based Brain–Computer Interface Speller," in *IEEE Trans. Neural Syst. Rehabil. Eng.*, vol.18, no.2, pp.127-133, Apr. 2010.

[5] G. Pfurtscheller, T. Solis-Escalante, R. Ortner, P. Linortner, G. R. Muller-Putz, "Self-paced operation of an SSVEP-Based orthosis with and without an imagery-based "brain switch:" a feasibility study towards a hybrid BCI," in *IEEE Trans. on Neural Systems and Rehabilitation Engineering*, vol. 18, no.4, pp.409-414, 2010.

[6] R. Ortner, B.Z. Allison, G. Korisek, H. Gaggl, G. Pfurtscheller, "An SSVEP BCI to Control a Hand Orthosis for Persons With Tetraplegia," in *IEEE Trans. on Neural Systems and Rehabilitation Engineering*, vol.19, no.1, pp.1,5, 2011.

[7] C. E. King, P. T. Wang, M. Mizuta, D. J. Reinkensmeyer, A. H. Do, S. Moromugi, Z. Nenadic, "Noninvasive brain-computer interface driven hand orthosis," in *Engineering in Medicine and Biology Society, EMBC, 2011 Annual International Conference of the IEEE*, pp. 5786-5789, 2011.

[8] A. H. Do, P. T. Wang, C. E. King, A. Abiri, Z. Nenadic, "Brain-Computer Interface Controlled Functional Electrical Stimulation System for Ankle Movement," in *Journal of NeuroEngineering and Rehabilitation*, vol.8, no.49, Aug. 2011.

[9] A. Biasiucci, R. Leeb, A. Al-Khodairy, V. Buhlmann, J.d.R. Millán, "Brain Controlled Functional Electrical Stimulation for Motor Recovery after Stroke," in *Proceedings of TOBI Workshop IV*, 2013.

[10] A. Biasiucci, R. Chavarriaga, B. Hamner, R. Leeb, F. Pichiorri, F. De Vico Fallani, D. Mattia, J. d. R. Millan, "Combining discriminant and topographic information in BCI: Preliminary results on stroke patients," in *Neural Engineering (NER), 2011 5th International IEEE/EMBS Conference on*, pp.290,293, 2011.

[11] T. Carlson, J. del R Millan, "Brain-Controlled Wheelchairs: A Robotic Architecture," in *IEEE Robotics & Automation Magazine*, vol.20, no.1, pp.65,73, March 2013.

[12] J. del R. Millan, F. Renkens, J. Mourino, W. Gerstner, "Noninvasive brain-actuated control of a mobile robot by human EEG," in *IEEE Transactions on Biomedical Engineering*, vol.51, no.6, pp.1026-1033, June 2004.

[13] L. Bi, X. Fan, Y. Liu, "EEG-Based Brain-Controlled Mobile Robots: A Survey," in *IEEE Transactions on Human-Machine Systems*, vol.43, no.2, pp.161-176, March 2013.

[14] A. Losardo, F. Grossi, G. Matrella, I. De Munari, P. Ciampolini, "Exploiting AAL environment for behavioral analysis," in Assistive Technology: From Research to Practice - Assistive Technology Research Series, vol.33, pp.1121-1125, 2013.

[15] F. Grossi, V. Bianchi, G. Matrella, I. De Munari, P. Ciampolini, "Internet-based home monitoring and control," In *AAATE'09 Conference Proceedings*, pp.309-313, 2009.

[16] F. Grossi, G. Matrella, I. De Munari, P. Ciampolini, "A flexible home automation system applied to elderly care," in *Consumer Electronics, ICCE'07*, 2007.

[17] R. Leeb, S. Perdikis, L. Tonin, A. Biasiucci, M. Tavella, M. Creatura, A. Molina, A. Al-Khodairy, T. Carlson, J.D.R. Millán, "Transferring brain–computer interfaces beyond the laboratory: Successful application control for motor-disabled users," in *Artificial intelligence in medicine*, vol.59, no.2, pp.121-32, Oct. 2013.

[18] Fabien Lotte, Florian Larrue, Martin Hachet, "BCI Research at Inria Bordeaux: making BCI designs usable outside the lab," in *International BCI meeting*, Asilomar, United States, 2013.

[19] T.H. Falk, M. Guirgis, S. Power, T. Chau, "Taking NIRS-BCIs Outside the Lab: Towards Achieving Robustness Against Environment Noise," in *IEEE Transactions on Neural Systems and Rehabilitation Engineering*, vol.19, no.2, pp.136,146, April 2011.

[20] N. Mora, V. Bianchi, I. De Munari, P. Ciampolini, "A BCI platform supporting AAL applications," in *Conf. Proc. HCI'14*, 2014.

[21] N. Mora, V. Bianchi, I. De Munari, P. Ciampolini, "A Low Cost Brain Computer Interface Platform for AAL Applications," in *Conf. Proc. AAATE'13*, 2013.

[22] N. Mora, V. Bianchi, I. De Munari, P. Ciampolini, "Controlling AAL environments through BCI," in *IEEE/ASME 10th International Conference on Mechatronic and Embedded Systems and Applications (MESA), 2014*, pp.1-6, 2014.

[23] N. Mora, V. Bianchi, I. De Munari, P. Ciampolini, "Brain.me: Low-Cost Brain Computer Interface methods for AAL scenarios," in *Ambient Assisted Living: Italian Forum 2014*, Springer, 2015.

[24] N. Mora, V. Bianchi, I. De Munari, P. Ciampolini, "Brain.me : a Low-Cost Brain Computer Interface for AAL Applications," in Ambient Assisted Living: Italian Forum 2013, Springer, 2014.

[25] G. Pfurtscheller, C. Neuper, G.R. Müller, B. Obermaier, G. Krausz, A. Schlögl, R. Scherer, B. Graimann, C. Keinrath, D.

Skliris, M. Wörtz, G. Supp, C. Schrank, "Graz-BCI: state of the art and clinical applications," in *IEEE Trans Neural Syst Rehabil Eng*., vol. 11, no.2, pp.177-180, 2003.

[26] R. Scherer, A. Schloegl, F. Lee, H. Bischof, J. Janša, G. Pfurtscheller, "The Self-Paced Graz Brain-Computer Interface: Methods and Applications," in *Computational Intelligence and Neuroscience*, vol. 2007, no. 79826, 2007.

[27] R. Leeb, D. Friedman, G. R. Müller-Putz, R. Scherer, M. Slater, G. Pfurtscheller, "Self-Paced (Asynchronous) BCI Control of a Wheelchair in Virtual Environments: A Case Study with a Tetraplegic," in *Computational Intelligence and Neuroscience*, vol. 2007, no. 79642, 2007.

[28] R. Scherer, F. Lee, A. Schlogl, R. Leeb, H. Bischof, G. Pfurtscheller, "Toward Self-Paced Brain–Computer Communication: Navigation Through Virtual Worlds," in *IEEE Transactions on Biomedical Engineering*, vol.55, no.2, pp.675-682, 2008.

[29] A. Satti, D. Coyle, G. Prasad, "Continuous EEG classification for a self-paced BCI," in *NER '09, 4th International IEEE/EMBS Conference on*, pp.315,318, 2009.

[30] G. Pfurtscheller, T. Solis-Escalante, R. Ortner, P. Linortner, G. R. Muller-Putz, "Self-paced operation of an SSVEP-Based orthosis with and without an imagery-based "brain switch:" a feasibility study towards a hybrid BCI," in *IEEE Transactions on Neural Systems and Rehabilitation Engineering*, , vol. 18, no.4, pp.409-414, 2010.

[31] G. R. Mueller-Putz, C. Breitwieser, F. Cincotti, R. Leeb, M. Schreuder, F. Leotta, M. Tavella, L. Bianchi, A. Kreilinger, A. Ramsay, M. Rohm, M. Sagebaum, L. Tonin, C. Neuper, J. del R. Millán, "Tools for Brain-Computer Interaction: a general concept for a hybrid BCI (hBCI)," in *Frontiers in Neuroinformatics*, vol.5, no.30, 2011.

[32] R. Leeb, H. Sagha, R. Chavarriaga, J. del R. Millán, "A hybrid brain–computer interface based on the fusion of electroencephalographic and electromyographic activities," in *Journal of neural engineering*, vol.8, no.2, 2011.

[33] J. Webster, "Medical Instrumentation", *4th ed.*, *Wiley*, 2009.

[34] M. Ahn, S. Ahn, J. H. Hong, *et al*., "Gamma band activity associated with BCI performance: simultaneous MEG/EEG study," in *Frontiers in Human Neuroscience*, 2013, 7 pp.848.

[35] P. T. Lin, K. Sharma, T. Holroyd, H. Battapady, D. Y. Fei, O. Bai, "A High Performance MEG Based BCI Using Single Trial Detection of Human Movement Intention, " Functional Brain Mapping and the Endeavor to Understand the Working Brain, ISBN: 978-953-51-1160-3, InTech, 2013.

[36] J. Mellinger, G. Schalk, C. Braun, H. Preissl, W. Rosenstiel, N. Birbaumer, A. Kübler, "An MEG-based brain–computer interface (BCI)," in *NeuroImage*, vol. 36, no. 3, pp.581-593, 2007.

[37] P. Andersson; M. A. Viergever, J. Pluim, N. F. Ramsey, J. Siero, "fMRI based BCI control using spatial visual attention at 7T," in *Neural Engineering, 2009. NER '09. 4th International IEEE/EMBS Conference on*, pp.444-446, 2009.

[38] R. Sitaram, S. Lee, S. Ruiz, and N. Birbaumer. "Real-Time Regulation and Detection of Brain States from fMRI Signals," in *Neurofeedback and Neuromodulation Techniques*, Elsevier 2011.

[39] N. Weiskopf, R. Veit, M. Erb, K. Mathiak, W. Grodd, R. Goebel, N. Birbaumer, "Physiological self-regulation of regional brain activity using real-time functional magnetic resonance imaging (fMRI): methodology and exemplary data," in *Neuroimage*, vol.19, no.3, pp.577-586, 2003.

[40] S. M. Coyle, T. E. Ward, C. M. Markham, "Brain-computer interface using a simplified functional near-infrared spectroscopy system," in *J. Neural Eng.*, vol.4, no.3, pp.219-26, 2007.

[41] G. Pfurtscheller, B. Z. Allison, C. Brunner, G. Bauernfeind, T. Solis-Escalante, R. Scherer, T. O. Zander, G. Mueller-Putz, C.

Neuper, N. Birbaumer, "The hybrid BCI," in *Frontiers in neuroscience,* vol.4, 2010.

[42] S. D. Power, A. Kushki, T. Chau, "Automatic single-trial discrimination of mental arithmetic, mental singing and the no-control state from prefrontal activity: toward a three-state NIRS-BCI," in *BMC research notes*, vol.5, no.1, 2012.

[43] S. E. Kober, G. Wood, J. Kurzmann, E. V. C. Friedrich, M. Stangl, T. Wippel, A. Väljamäe, C. Neuper, "Near-infrared spectroscopy based neurofeedback training increases specific motor imagery related cortical activation compared to sham feedback," in *Biological Psychology*, vol.95, pp.21-30, 2014.

[44] D. K. Su, J. G. Ojemann, "Electrocorticographic sensorimotor mapping," in Clinical neurophysiology: official journal of the International Federation of Clinical Neurophysiology, vol.124, no.6, 2013.

[45] S. Martin, P. Brunner, C. Holdgraf, H. J. Heinze, N. E. Crone, J. Rieger, G. Schalk, R. T. Knight, B. N. Pasley, "Decoding spectrotemporal features of overt and covert speech from the human cortex," in *Frontiers in Neuroengineering*, vol.7, 2014.

[46] E. C. Leuthardt, J. Cunningham, D. Barbour, "Towards a Speech BCI Using ECoG," in *Brain-Computer Interface Research*, Springer Berlin Heidelberg, pp. 93-110, 2013.

[47] S. Martin, P. Brunner, C. Holdgraf, H. J. Heinze, N. E. Crone, J. Rieger, G. Schalk, R. T. Knight, B. N. Pasley, "Decoding spectrotemporal features of overt and covert speech from the human cortex," in *Frontiers in Neuroengineering*, vol.7, 2014.

[48] G. Dornhege, B. Blankertz, G. Curio, "Speeding up classification of multi-channel brain-computer interfaces: Common spatial patterns for slow cortical potentials," in *First International IEEE EMBS Conference on Neural Engineering*, pp.595-598, 2003.

[49] T. Hinterberger, S. Schmidt, N. Neumann, J. Mellinger, B. Blankertz, G. Curio, N. Birbaumer, "Brain-computer communication and slow cortical potentials," in *IEEE*

Transactions on Biomedical Engineering, vol.51, no.6, pp.1011-1018, 2004.

[50] N. Birbaumer, N. Ghanayim, T. Hinterberger, I. Iversen, B. Kotchoubey, A. Kubler, J. Perelmouter, E. Taub, H. Flor, "A spelling device for the paralysed," in *Nature*, vol.398, no.6725, pp.297-298, 1999.

[51] N. Neumann, A. Kübler, J. Kaiser, T. Hinterberger, N. Birbaumer, "Conscious perception of brain states: mental strategies for brain–computer communication," in Neuropsychologia, vol.41, no.8, pp.1028-1036, 2003.

[52] G. Pfurtscheller and F. H. Lopes da Silva, "Event-related EEG/MEG synchronization and desynchronization: Basic principles," in *Clin. Neurophysiol.*, vol.110, pp.1842–1857, 1999.

[53] H. Yuan, B. He, "Brain–Computer Interfaces Using Sensorimotor Rhythms: Current State and Future Perspectives," in *IEEE Transactions on Biomedical Engineering*, vol.61, no.5, pp.1425-1435, 2014.

[54] A. S. Royer, A. J. Doud, M. L. Rose, and B. He, "EEG control of a virtual helicopter in 3-dimensional space using intelligent control strategies," in *IEEE Trans. Neural Syst. Rehabil. Eng.*, vol.18, no.6, pp. 581–589, 2010.

[55] J. R. Wolpaw and D. J. McFarland, "Control of a two-dimensionalmovement signal by a noninvasive brain-computer interface in humans," in *Proc. Nat. Acad. Sci. USA*., vol.101, pp.17849–17854, 2004.

[56] L.A. Farwell, E. Donchin, "Talking off the top of your head: toward a mental prosthesis utilizing event-related brain potentials," in *Electroencephalogr Clin Neurophysiol*, vol.70, pp.510–23, 1988.

[57] F. Aloise , P. Aricò , F. Schettini , A. Riccio , S. Salinari , D. Mattia , F. Babiloni , F. Cincotti, "A covert attention P300-based brain–computer interface: Geospell," in *Ergonomics*, vol.55, no.5, pp.538-551, 2012.

[58] Y. Liu, Z. Zhou, D. Hu, "Gaze independent brain–computer speller with covert visual search tasks," in *Clinical Neurophysiology*, vol.122, no.6, pp.1127-1136, 2011.

[59] T. Kaufmann, S. M. Schulz, C. Grünzinger, A. Kübler, "Flashing characters with famous faces improves ERP-based brain–computer interface performance," in *Journal of neural engineering*, vol.8, no.5, 2011.

[60] Q. Zhao, Y. Zhang, A. Onishi, A. Cichocki, "An affective BCI using multiple ERP components associated to facial emotion processing," in *Brain-Computer Interface Research*, Springer Berlin Heidelberg, pp.61-72, 2013.

[61] J. N. Mak, Y. Arbel, J. W. Minett, L. M. McCane, B. Yuksel, D. Ryan, D. Thompson, L. Bianchi, D. Erdogmus, "Optimizing the P300-based brain-computer interface: current status, limitations and future," in *Journal of Neural Engineering*, vol.8, no.2, 2011.

[62] E. W. Sellers, E. Donchin, "A P300-based brain–computer interface: initial tests by ALS patients," in *Clinical neurophysiology*, vol.117, no.3, pp.538-548, 2006.

[63] H. Bakardjian, T. Tanaka, A. Cichocki, "Optimization of SSVEP brain responses with application to eight-command Brain–Computer Interface," in *Neuroscience Letters*, vol. 469, no.1, pp.34-38, 2010.

[64] D. Regan, "Human Brain Electrophysiology: Evoked Potentials and Evoked Magnetic Fields in Science and Medicine," *Elsevier*, 1989.

[65] J. J. Wilson, R. Palaniappan, "Augmenting a SSVEP BCI through single cycle analysis and phase weighting," in *Neural Engineering, 2009. NER '09. 4th International IEEE/EMBS Conference on*, pp.371-374, 2009.

[66] P. L. Lee, J. J. Sie, Y. J. Liu, C. H. Wu, M. H. Lee, C. H. Shu, P. H. Li, C. W. Sun, K. K. Shyu, "An SSVEP-actuated brain computer interface using phase-tagged flickering sequences: a

cursor system," in *Annals of Biomedical Engineering*, vol.38, no.7, pp.2383-2397, 2010.

[67] K. K. Shyu, P. L. Lee, M. H. Lee, M. H. Lin, R. J. Lai, Y. J. Chiu, "Development of a Low-Cost FPGA-Based SSVEP BCI Multimedia Control System," in *IEEE Transactions on Biomedical Circuits and Systems*, vol.4, no.2, pp.125-132, April 2010.

[68] C. Jia, X. Gao, B. Hong, S. Gao, "Frequency and Phase Mixed Coding in SSVEP-Based Brain--Computer Interface," in *IEEE Transactions on Biomedical Engineering*, vol.58, no.1, pp.200-206, 2011.

[69] D. Zhu, J. Bieger, G. G. Molina, R. M. Aarts, "A survey of stimulation methods used in SSVEP-based BCIs," in *Computational intelligence and neuroscience*, 2010.

[70] X. Gao, D. Xu, M. Cheng, S. Gao, "A BCI-based environmental controller for the motion-disabled," in *IEEE Trans Neural Syst Rehabil Eng*, vol.11, no.2, pp. 137–140, 2003.

[71] B. Allison, I. Sugiarto, B. Graimann, A. Gräser, "Display Optimization in SSVEP BCIs," in *Computer-Human Interaction 2008*, 2008.

[72] H. Bakardjian, T. Tanaka, A. Cichocki, "Emotional faces boost up steady-state visual responses for brain–computer interface," in *Neuroreport*, vol.22, no.3,pp.121-125, 2011.

[73] M. S. Treder, N. M. Schmidt, B. Blankertz, "Gaze-independent brain–computer interfaces based on covert attention and feature attention," in *Journal of neural engineering*, vol.8, no.6, 2011.

[74] S. Walter, C. Quigley, S. K. Andersen, M. M. Mueller, "Effects of overt and covert attention on the steady-state visual evoked potential," in *Neuroscience letters*, vol.519, no.1, pp.37-41, 2012.

[75] M. Ordikhani-Seyedlar, H. B. Sorensen, T. W. Kjaer, H. R. Siebner, S. Puthusserypady, "SSVEP-modulation by covert and overt attention: Novel features for BCI in attention neuro-rehabilitation," in *Engineering in Medicine and Biology Society*

(EMBC), 2014 36th IEEE Annual International Conference, pp.5462-5465, 2014.

[76] R. Chavarriaga, A. Sobolewski, J. del R. Millán, "Errare machinale est: The use of error-related potentials in brain-machine interfaces," in *Frontiers in Neuroscience*, vol.8, 2014.

[77] M. Falkenstein, J. Hohnsbein, S. Christ, J. Hohnsbein, "ERP components on reaction errors and their functional significance: A tutorial," in *Biol. Psychol.*, vol.51, no.2, pp.87–107, 2000.

[78] M. X. Cohen, C. E. Elger, C. Ranganath, "Reward expectation modulates feedback-related negativity and EEG spectra," in *Neuroimage*, vol.35, no.2, pp.968–978, 2007.

[79] R. Chavarriaga, J. d. R. Millán, "Learning from EEG error-related potentials in noninvasive brain-computer interfaces," in *IEEE Trans. Neural. Syst. Rehabil. Eng.*, vol.18, no.4, pp.381–388, 2010.

[80] P. W. Ferrez, J. d. R. Millán, "Error-related EEG potentials generated during simulated brain-computer interaction," in *IEEE Trans. Biomed. Eng.*, vol.55, no.3, pp.923–929, 2008.

[81] N. M. Schmidt, B. Blankertz, M. S. Treder, "Online detection of error-related potentials boosts the performance of mental typewriters," in *BMC Neurosci.*, vol.13, no.19, 2012.

[82] S. Roset, H. Gonzalez, J. and Sanchez, "Development of an EEG based reinforcement learning brain-computer interface system for rehabilitation," in *Conference of the IEEE Engineering in Medicine and Biology Society (Osaka 2013)*, pp.1563–1566, 2013.

[83] H. Cecotti, "A Self-Paced and Calibration-Less SSVEP-Based Brain–Computer Interface Speller," in *IEEE Trans. Neural Syst. Rehabil. Eng.*, vol.18, no.2, pp.127-133, Apr. 2010.

[84] V. Bostanov, "BCI competition 2003-data sets Ib and IIb: feature extraction from event-related brain potentials with the continuous wavelet transform and the t-value scalogram," in *IEEE*

Transactions on Biomedical Engineering, vol.51, no.6, pp.1057-1061, 2004.

[85] W. Ting, Y. Guo-Zheng, Y. Bang-Hua, S. Hong, "EEG feature extraction based on wavelet packet decomposition for brain computer interface," in *Measurement*, vol.41, no.6, pp.618-625, 2008.

[86] B. Schölkopf, A. Smola, K. R. Müller, "Nonlinear component analysis as a kernel eigenvalue problem," in *Neural computation*, vol.10, no.5, pp.1299-1319, 1998.

[87] A. Kachenoura, L. Albera, L. Senhadji, P. Comon, "ICA: a potential tool for BCI systems," in *Signal Processing Magazine, IEEE*, vol.25, no.1, pp.57-68, 2008.

[88] S. Lemm, B. Blankertz, G. Curio, K. Muller, "Spatio-spectral filters for improving the classification of single trial EEG," in *IEEE Transactions on Biomedical Engineering*, vol.52, no.9, pp.1541-1548, 2005.

[89] B. Blankertz, R. Tomioka, S. Lemm, M. Kawanabe, K. R. Muller, "Optimizing Spatial filters for Robust EEG Single-Trial Analysis," in *Signal Processing Magazine, IEEE*, vol.25, no.1, pp.41-56, 2008.

[90] F. Lotte, C. Guan, "Regularizing common spatial patterns to improve BCI designs: unified theory and new algorithms," in *IEEE Transactions on Biomedical Engineering*, vol.58, no.2, pp.355-362, 2011.

[91] G. Townsend, B. Graimann, G. Pfurtscheller, "Continuous EEG classification during motor imagery-simulation of an asynchronous BCI," in *IEEE Transactions on Neural Systems and Rehabilitation Engineering*, vol.12, no.2, pp.258-265, 2004.

[92] Y. Wang, S. Gao, X. Gao, "Common spatial pattern method for channel selection in motor imagery based brain-computer interface," in *IEEE-EMBS 2005, 27th Annual International Conference*, pp.5392-5395, 2006.

[93] S. Lemm, B. Blankertz, G. Curio, K. R. Müller, "Spatio-spectral filters for improving classification of single trial EEG," in *IEEE Trans. Biomed. Eng.*, vol. 52, no. 9, pp. 1541–1548, 2005.

[94] G. Dornhege, B. Blankertz, G. Curio, K. R. Müller, "Increase information transfer rates in BCI by CSP extension to multi-class," in *Advances in neural information processing systems*, 2003.

[95] D. J. McFarland, J. R. Wolpaw, "Sensorimotor rhythm-based brain–computer interface (BCI): model order selection for autoregressive spectral analysis," in *Journal of neural engineering*, vol.5, no.2, 2008.

[96] L. Citi, R. Poli, C. Cinel, F. Sepulveda, "P300-based BCI mouse with genetically-optimized analogue control," in *IEEE Transactions on Neural Systems and Rehabilitation Engineering*, vol.16, no.1, pp.51-61, 2008.

[97] M. Grosse-Wentrup, M. Buss, "Multiclass common spatial patterns and information theoretic feature extraction," in *IEEE Transactions on Biomedical Engineering*, vol.55, no.8, pp.1991-2000, 2008.

[98] Y. Shahriari, A. Erfanian, "A mutual information based channel selection scheme for P300-based brain computer interface," in Neural Engineering, 5th International IEEE/EMBS Conference on, pp.434-437, 2011.

[99] K. Van Leemput, F. Maes, D. Vandermeulen, and P. Suetens, "A unifying framework for partial volume segmentation of brain MR images," in *IEEE Trans. Med. Imag.*, vol.22, no.1, pp.105–119, 2003.

[100] S. Marcel, J. del R. Millán, "Person authentication using brainwaves (EEG) and maximum a posteriori model adaptation," in *IEEE Transactions on Pattern Analysis and Machine Intelligence*, vol.29, no.4, pp.743-752, 2007.

[101] J. del R. Millán, "On the need for on-line learning in brain-computer interfaces," in *Conf. Proc. Neural Networks, 2004*, vol.4, pp.2877-2882, 2004.

[102] T. Kohonen, "Self-Organizing Maps, 2nd ed.," *Springer-Verlag*, 1997.

[103] A. Buttfield, P. W. Ferrez, J. del R. Millán, "Towards a robust BCI: error potentials and online learning," in *IEEE Transactions on Neural Systems and Rehabilitation Engineering*, vol.14, no.2, pp.164-168, 2006.

[104] C. Cortes, V. Vapnik, "Support-vector networks," in *Machine learning*, vol.20, no.3, pp.273-297, 1995.

[105] A. B. Gardner, A. M. Krieger, G. Vachtsevanos, B. Litt, "One-class novelty detection for seizure analysis from intracranial EEG," in *The Journal of Machine Learning Research*, vol.7, pp.1025-1044, 2006.

[106] G. R. Mueller-Putz, C. Breitwieser, F. Cincotti, R. Leeb, M. Schreuder, F. Leotta, M. Tavella, L. Bianchi, A. Kreilinger, A. Ramsay, M. Rohm, M. Sagebaum, L. Tonin, C. Neuper, J. del R. Millán, "Tools for Brain-Computer Interaction: a general concept for a hybrid BCI (hBCI)," in *Frontiers in Neuroinformatics*, vol.5, no.30, 2011.

[107] Analog Devices, "In-Amp Input RFI Protection," in *MT-070*.

[108] A. Nonclercq, P. Mathys, "Reduction of power line interference using active electrodes and a driven-right-leg circuit in electroencephalographic recording with a minimum number of electrodes," in *Conf. Proc. IEEE Eng. Med. Biol. Soc.*, vol.3, pp.2247-50, 2004.

[109] E. M. Spinelli, R. Pallas-Areny, M. A. Mayosky, "AC-coupled front-end for biopotential measurements," in *IEEE Trans. Biomed. Eng.*, vol.50, no.3, pp.391-395, 2003.

[110] N. Bermúdez, E. M. Spinelli and C. H. Muravchik, "Bio-potential amplifier for potential gradient measurements," in *J. Phys.: Conf. Ser.*, vol.90, no.1, 2007.

[111] Analog Devices, "AD8221 Precision Instrumentation Amplifier Datasheet".

[112] Texas Instruments, "Analysis of the Sallen-Key Architecture," in Application Report SLOA024B, 2002.

[113] M. A. Haberman, E. M. Spinelli, "A Multichannel EEG Acquisition Scheme Based on Single Ended Amplifiers and Digital DRL," in *IEEE Trans. Biomed. Circuits Syst.*, vol.6, no.6, pp.614-618, 2012.

[114] H. W. Johnson, M. Graham, "High-speed digital design: a handbook of black magic," *Prentice Hall*, 1993.

[115] W. Kester, J. Bryant, M. Byrne, "Grounding Data Converters and Solving the Mystery of "AGND" and "DGND"," in *Analog Devices Application Note MT-031*, 2006.

[116] T. Degen, S. Torrent, H. Jackel, "Low-noise two-wired buffer electrodes for bioelectric amplifiers," in *IEEE Transactions on Biomedical Engineering*, vol.54, no.7, pp.1328-1332, 2007.

[117] I. Volosyak, "SSVEP-based Bremen-BCI interface - boosting information transfer rates," in *J. Neural Eng.*, vol.8, no.3, 2011.

[118] G. Garcia-Molina, D. Zhu, "Optimal spatial filtering for the steady state visual evoked potential: BCI application," in *Neur. Eng., 5th International IEEE/EMBS Conf. on*, pp.156-160, 2011.

[119] Z. Lin, C. Zhang, W. Wu, X. Gao, "Frequency recognition based on canonical correlation analysis for SSVEP-based BCIs," in *IEEE Trans. Biomed. Eng.*, vol.54, pp.1172–1176, 2007.

[120] N. Mora, V. Bianchi, I. De Munari, P. Ciampolini, "Simple and Efficient Methods for Steady State Visual Evoked Potential Detection in BCI Embedded System," in *Conf. Proc. IEEE ICASSP'14*, 2014.

[121] J. del R.Millan, J. Mourino, "Asynchronous BCI and local neural classifiers: an overview of the adaptive brain interface project," in *IEEE Trans. on Neural Systems and Rehabilitation Engineering*, vol.11, no.2, pp.159-161, 2003.

[122] G. Pfurtscheller, T. Solis-Escalante, R. Ortner, P. Linortner, G. R. Muller-Putz, "Self-Paced Operation of an SSVEP-Based Orthosis With and Without an Imagery-Based "Brain Switch:" A Feasibility Study Towards a Hybrid BCI," in *IEEE Trans. Neur. Sys. and Rehab. Eng.*, vol.18, no.4, pp.409-414, 2010.

[123] J. Pan, Y. Li, R. Zhang, Z. Gu, F. Li, "Discrimination Between Control and Idle States in Asynchronous SSVEP-Based Brain Switches: A Pseudo-Key-Based Approach," in IEEE Trans. Neur. Sys. and Rehab. Eng., vol.21, no.3, pp.435-443, 2013.

Acknowledgements/Ringraziamenti

Not only is this thesis multidisciplinary, but also bilingual, at least in this section. You will excuse me for the Italian, but certain concepts are better expressed in the default, own language .

So let's start from the English part, for international as well as English speaking friends and colleagues.

Well, I could not start without infinitely thanking my Professors, Ilaria De Munari and Paolo Ciampolini for their appreciable (and huge) efforts in guiding, helping and constantly encouraging me to explore different ideas, as well as alternative perspectives. I believe I owe them a lot, especially in terms of patience!

Also, I would like to personally thank Prof. Millán: four months spent in his *dream lab* have taught me a lot! I thank him for the opportunity, his availability and openness. Also, his students and colleagues were very kind and made me immediately feel part of the team (thanks!). My hope is to have returned something, for all I could have taken during such a wonderful experience!

And, with a little, tiny hint of *captatio benevolentiae*, I also thank the reviewers for their time in evaluating this work ☺

Let's now switch to Italian, I still have a lot to go...

Essendo questa la terza tesi che scrivo, il rischio di ripetersi nei ringraziamenti è alto, ma che ci posso fare se ho la fortuna di avere una famiglia così eccezionale? Non ripeto anche questa volta le motivazioni, comunque troppe per essere esaustivo; mi limito a ringraziarli collettivamente (*urbi et orbi*, anche nelle varie recenti acquisizioni ☺): GRAZIE!

Cari amici, per voi la stessa sorte, sapete che il merito di affrontare con un generoso pizzico di ironia le sfide (e sfighe) in questi anni è anche vostro.

Ho poi la fortuna di poter includere il capitolo colleghi di lavoro in quello precedente degli amici: la serenità nell'ambiente lavorativo è un valore aggiunto (anche un lusso, dai!) senza prezzo.

Non fare nomi espliciti può sembrare… come dire… ai sensi di legge… *paraculistico* ☺ In realtà: *(i)* spero di dimostrare quanto scritto più con i fatti che con una citazione, *(ii)* in realtà mentre scrivevo pensavo proprio a tutti voi, e nel mentre ho pure registrato il mio EEG: lascio, a richiesta, il dump dei dati per verificare voi stessi la presenza dei vostri nomi ☺

Non mi sono nemmeno scordato degli amici di ABB, con cui ho ancora la fortuna di essere in contatto e, occasionalmente, pure di collaborare! L'essere *multivariate* in termini di interessi mi gratifica molto, professionalmente, e devo loro questa possibilità.

Infine, un ringraziamento veramente sentito anche a (*cognome e nome*) _____, per la sua (*specificare motivazioni*) _____, _____, _____ e, non ultima, la sua _____. Questo serva a parziale risarcimento di chi non abbia ringraziato o non si ritrovi nel mio tracciato EEG.

Parma, Gennaio 2015 (appena in tempo ☺)

Niccolò Mora, interista.